8-1996

The petrogenesis of andesites produced during regional extension: examples from the northern McCullough Range, NV and Xitle Volcano, Mexico

Kelly Ann Boland
University of Nevada, Las Vegas

The Petrogenesis of Andesites Produced During Regional Extension: Examples from the Northern McCullough Range, NV and Xitle Volcano, Mexico

by

Kelly Ann Boland

A thesis submitted in partial fulfillment
of the requirements for the degree of

Master of Science

in

Geology

Department of Geoscience
University of Nevada, Las Vegas
August, 1996

This thesis of Kelly Ann Boland for the degree of Master of Science in Geology is approved.

[redacted] 6/10/96

Chairperson, Eugene I. Smith, Ph.D.

[redacted] 10 June 1996

Examining Committee Member, Rodney V. Metcalf, Ph.D.

[redacted] 6/10/96

Examining Committee Member, Wanda J. Taylor, Ph.D.

[redacted] 10 June 96

Graduate Faculty Representative, Peter L. Starkweather, Ph.D.

Graduate Dean, Ronald W. Smith, Ph.D.

University of Nevada, Las Vegas
August, 1996

Abstract

Andesite dominated volcanic systems produced during regional crustal extension remain a relatively unexplored aspect of andesite petrogenesis. In the southern Basin and Range province, thick sections of andesite and basaltic andesite have been documented in areas including the Piute Range, California, the Eldorado Range, Nevada, and the McCullough Range, Nevada. The northern McCullough Range, located 20 miles south-southeast of Las Vegas, is an ideal place to study the petrogenesis of an andesite dominated system. This area contains a mid-Miocene stratocone composed mainly of a 1200 m thick section of andesite flows that formed synchronous with regional extension.

The northern McCullough Range andesites are calc-alkaline and contain phenocrysts of olivine, clinopyroxene, and plagioclase. Although the andesites are similar in major element chemistry, they exhibit wide variations in trace element chemistry. Resulting trace element Harker diagrams show considerable scatter and no discernible petrogenetic trends. On $^{87}Sr/^{86}Sr$ and ε_{Nd} isotope plots, however, andesites fall into 3 distinct groups: group A ($^{87}Sr/^{86}Sr$=0.70758 to 0.7077; ε_{Nd}=-6.2 to -6.9), group B ($^{87}Sr/^{86}Sr$=0.7081 to 0.7083; ε_{Nd}=-6.7 to -7.4), and group C ($^{87}Sr/^{86}Sr$=0.70897 to 0.70904; ε_{Nd}=-8.8 to -9.8). Chemical variations and petrogenesis were assessed using fractional crystallization, assimilation and fractional crystallization, magma recharge, and magma mixing models. Geochemical variations, isotopic data and petrogenetic modeling suggest that the andesites in the northern McCullough Range formed primarily

from mixing together several different andesitic sources (represented by isotope groups A, B, and C) that are similar in chemistry but isotopically distinct. This proposed model involving mixing of different andesitic end members explains the andesite dominated section observed in the McCullough Range and provides an alternative explanation for andesite petrogenesis in extensional terranes. A preliminary study of Xitle volcano in central Mexico shows similarities to the McCullough Range results. It is possible, therefore, that the petrogenetic model developed in the northern McCullough Range may be applied to extensional environments in other areas of the world.

Table of Contents

Abstract iii

List of Figures vii

Acknowledgments ix

CHAPTER 1 INTRODUCTION 1

CHAPTER 2 GEOLOGIC BACKGROUND AND REGIONAL GEOLOGY 8
- The McCullough Range 8
- Other Nearby Volcanoes and Plutons 11

CHAPTER 3 STRATIGRAPHY AND STRUCTURAL GEOLOGY OF THE NORTHERN MCCULLOUGH RANGE 14
- Stratigraphy 14
  - Introduction 14
  - Precambrian basement 16
  - Ivan Canyon andesite 16
  - Colony dacite 16
  - Lower member of the Farmer Canyon andesite 18
  - Upper member of the Farmer Canyon andesite 19
    - Dikes 20
- Fog Ridge andesite 20
- Discussion-Stratocone facies and vent locations 21
- Structural Geology 23

CHAPTER 4 GEOCHEMISTRY OF THE VOLCANIC ROCKS OF THE NORTHERN MCCULLOUGH RANGE 28
- Analytical Techniques 28
  - Major and trace element analysis 29
  - Trace and rare-earth element analysis 29
  - Isotope analysis 30
- Major Elements 30

Alteration and contamination 31
Metasomatism 31
Incompatible Trace Elements 32
Large Ion Lithophile (LIL) and High Field Strength Elements (HFSE) 32
REE 33
Compatible Trace Elements 33
Isotopes 33

CHAPTER 5 GEOCHEMICAL MODELS 45
Introduction 45
Petrogenetic Models (Stage 3) 47
Fractional crystallization 47
Table 1. Distribution coefficients 49
Assimilation and fractional crystallization (AFC) 50
Magma mixing/commingling 52
Table 2. Summary of models 56
Discussion 57
Conclusions of modeling 57
Mixing styles in volcanic systems in the southern Basin and Range 58
Source and Evolution of Andesitic Magma Types (Stages 1 and 2) 60
Stage1 60
Stage 2 62

CHAPTER 6 XITLE VOLCANO, MEXICO 75
Geologic Background 75
Geochemical Descriptions and Petrography 77
Major elements 77
Trace elements 77
Petrography 78
Geochemical Modeling 79
Recharge 79
Fractional crystallization 79
Group 1 80
Group 2 80
Mixing 81
Discussion 82
Stratigraphic implications 82
Comparisons to the northern McCullough Range 82
Tectonic setting 82

Petrogenesis..... 83

CHAPTER 7 Conclusions..... 93

Appendix I Point Count Data..... 95

Appendix II Regional Structure and Tectonics..... 96

Appendix III Geochemical Data..... 101

Appendix IV Analytical Techniques: Data Precision and Accuracy.... 114

References..... 119

List of Figures

Figure 1. Location map of thesis area..... 6
Figure 2. Photo of the Tertiary volcanic section in the study area 7
Figure 3. Stratigraphic column of the central McCullough Range..... 12
Figure 4. Map of field area with sample locations and specific areas discussed in text..... 13
Figure 5. Stratigraphic column of the northern McCullough Range..... 25
Figure 6. Photos of contact between the Ivan Canyon andesite and Precambrian basement and contact between the Colony dactie and Fog Ridge andesite..... 26
Figure 7. Map showing faults and dip reversals..... 27
Figure 8. Rock classification diagrams of volcanic rocks in the northern McCullough Range..... 36
Figure 9. SiO2 vs. MgO and Na2O vs. K2O- unmetasomatized fields..... 37
Figure 10. Harker diagrams of SiO2 vs. incompatible trace elements Nb, Sm, and La..... 38
Figure 11. McCullough Range rocks normalized to primitive mantle..... 39
Figure 12. McCullough Range rocks normalized to OIB..... 40
Figure 13. SiO2 vs. compatible trace elements Cr and Ni..... 41
Figure 14. Isotope plots of the northern McCullough Range rocks..... 42
Figure 15. Isotopic data for the River Mountains-Wilson Ridge system from Feuerbach et al. (1993)..... 43

Acknowledgments

There are many people I would like to thank for their help, influence, and support. I would first like to thank my advisor Dr. Gene Smith for his constant patience, encouragement, enthusiasm, and support. I have learned immensely under his advisement and thoroughly enjoyed it. A sincere thank you goes out to my committee members, Dr. Wanda Taylor, Dr. Rod Metcalf, and Dr. Peter Starkweather for their advice, support, constructive editing, and time.

I am grateful to many organizations that provided financial support for this project including: Dr. E.I. Smith and the Center for Volcanic and Tectonic Studies; the Lipman Research Award from the Geological Society of America; the Nevada EPSCoR, Women in Science and Engineering fund, UNLV; the Graduate Student Association, UNLV; and the Bernada E. French scholarship from the Department of Geoscience, UNLV.

Thank you to the exceptional geoscience teachers, faculty and staff who have always been supportive, friendly, and willing to help. Thank you to all my fellow graduate students and friends for their help, support, advice, and friendship, especially Carole Farr, Alex Sanchez, Joe Blaylock, Rhonda Knupp, Kelly Rash, Holly Langrock, Jodi Zuckerman, Shirley Morikawa, Jason Herrmann, and Jason Johnson.

I would like to thank my field assistants Jason Herrmann, Gary Gin, Martin Braun, Kelly Rash, Alex Sanchez, and Gene Smith.

A huge thank you to my roommate, best friend, counselor, advisor, and partner in crime Gary Gin. Thank you for teaching me about trench fill, cooking, cliches, and life in general.

Thank you to Martin Braun for his love, friendship, incredible support, motivation and computer expertise. Thank you for the laughs, smiles, letters, inspiration, and helping me keep things in perspective.

Thank you to my family, especially my parents Jake and Isabelle Boland who have always encouraged and supported me and made me believe I could accomplish just about anything. Thank you Jeanne Marie, Debra, Stacey, and Erik.

A sincere and heartfelt thanks to all of you who helped make the past two and a half years in graduate school at UNLV a positive and rewarding experience.

Chapter 1

Introduction

Calc-alkaline andesites* are a common rock type in continental arcs, such as the Andes and the eastern Aleutians, and in continental regions that have undergone regional extension such as the Basin and Range province of the southwestern United States. Previous research on andesite petrogenesis focused on volcanic fields in magmatic arcs associated with subduction processes; this literature is extensive (Gill, 1981; Luhr and Carmichael, 1985; Grove and Kinzler, 1986; Kay et al., 1993; Yogodzinski et. al., 1994). Few authors, however, specifically addressed the origin and evolution of calc-alkaline andesites produced during regional continental extension, although some noted the formation of calc-alkaline rocks during extension in magmatic arcs and back-arc basins (Hughes, 1990; Lange and Carmichael, 1991). The origin of andesitic magma produced during continental extension, therefore, remains a relatively unexplored topic.

Volcanic sections in extended terranes that are dominated by calc-alkaline andesite are relatively common. In the southern Basin and Range, for example,

*For clarity of discussion throughout this thesis, andesite will be used in the broad sense and includes high silica basalt, basaltic andesite, and andesite, all within a silica range of 50 to 60 wt. %.

nearly 6000 meters of andesite crop out in the Eldorado Range, Nevada (Anderson, 1971); 1200 m in the Piute Range, California (Nielson et al., 1993); and 1200 m in the northern McCullough Range, Nevada (Hewitt, 1956; Bridwell, 1991). However, these andesite sections have not been studied in detail. The assumption that the mineralogy and chemistry of the andesites are not sufficiently variable to model petrogenetic processes may have discouraged studies on these andesite dominated sections. Instead, studies have emphasized the more compositionally variable volcanic systems where andesites contribute only a small volume to the whole volcanic section (McMillan, 1986; Smith et al. 1990, Metcalf et al., 1993b).

This thesis evaluates and develops models to explain the andesite dominated sections produced during extension in the southern Basin and Range province. It also determines the applicability of these models to other extensional settings. Four existing models have traditionally been used to explain the petrogenesis of calc-alkaline andesites:

(1) Crustal contamination: Many workers call upon contamination of mantle derived mafic magmas by crustal material to explain the geochemical signatures of calc-alkaline rocks. Crustal contamination is the traditional model used to explain andesite production in continental arcs (Gill, 1981). DePaolo (1981) suggested that the latent heat released by simultaneous crystallization may provide much of the large input of heat required to assimilate crustal material in a magma. Grove and Kinzler (1986), however, use thermodynamic calculations to suggest that the amount of crustal material and thermal energy needed to produce significant volumes of rocks with andesitic composition from a basaltic

magma by contamination or assimilation violates simple heat budget calculations.

(2) Magma mixing: Koyaguchi (1986) suggested mixing of mantle and crustal derived magmas as a mechanism for the production of intermediate calc-alkaline rocks. More specifically, studies in the Basin and Range province focused on the evolution of calc-alkaline magmatism in extensional tectonic settings and demonstrate the importance of magma mixing in the petrogenetic process (Gans et. al, 1989; Larsen, 1989; Glazner, 1990; Smith et al., 1990; Metcalf et al., 1993b; Metcalf et al., 1995). Magma mixing explains some compositionally variable magmatic systems, but it may not be reasonable to apply this process to systems of compositionally similar magmas.

(3) Direct melting of the mantle: Calc-alkaline andesites may also form directly from the mantle in a two step process (Grove and Kinzler, 1986). The first step involves partially melting mantle peridotite to produce tholeiitic basaltic magmas. In the second step, crustal-level fractional crystallization of the basaltic magma under high pressure conditions results in andesite formation (This process is discussed in detail in Chapter 5).

(4) Magma recharge: Reagan et al. (1987) proposed a model involving magma recharge to explain the generation of andesite. Monitoring of open-system differentiation at Arenal volcano in Costa Rica suggested that continuously erupting andesitic volcanoes directly tapped middle to lower crustal chambers that were replenished periodically by new magma. Recharge models may provide an explanation for the production of thick sections of andesite flows.

Testing the models required the selection of two areas for study; one in the Northern Colorado River Extensional Corridor (northern McCullough Range) and the other in central Mexico (Xitle volcano). Andesite lavas of the

northern McCullough Range are well exposed, relatively unaltered, and were chosen as the prime study area for this project. The 48 km^2 field area in the northern McCullough Range is 32 km south-southeast of Las Vegas and contains a stratocone composed of thick sections of andesite flows that are locally overlain by dacite and rhyolite flows and domes (Hewett, 1956; Smith et al., 1986; Smith et al., 1988) (Figure 1). A steep, east facing escarpment provides an excellent exposure of the Tertiary volcanic section (Figure 2). The stratocone is Miocene in age (between 16.7 and 13 Ma, P.B. Gans and J.E. Faulds, unpublished $^{40}Ar/^{39}Ar$ dates on biotite) and evolved during a time of regional extension (Weber and Smith, 1987).

The study of Xitle volcano compares petrogenetic processes and helps test the global applicability of the models. Located in the central Trans-Mexican Volcanic Belt (TMVB), Xitle volcano is a cinder cone composed mainly of andesite. The cone is approximately 2000 years old (H. Delgado, ^{14}C dates, personal commun.) and formed in an area of the TMVB that is simultaneously undergoing extension and subduction (Allan, 1981; Sheridan and Macias, 1992).

Evaluation and development of models in the northern McCullough Range field area involved two steps: mapping the area to establish the stratigraphy and framework for geochemical sampling and conducting a geochemical study. Although controversial, a stratigraphy of Xitle volcano is established, so this study only involved sampling and geochemical analysis.

The major contributions of this thesis are: (1) the determination of the stratigraphy in the northern McCullough Range (Chapter 3), (2) the construction of a model for the petrogenesis of the andesites and related rocks in the northern McCullough Range (Chapters 4 and 5), and (3) a comparison of processes that

form andesites in the northern McCullough Range with those associated with Xitle volcano (Chapter 6).

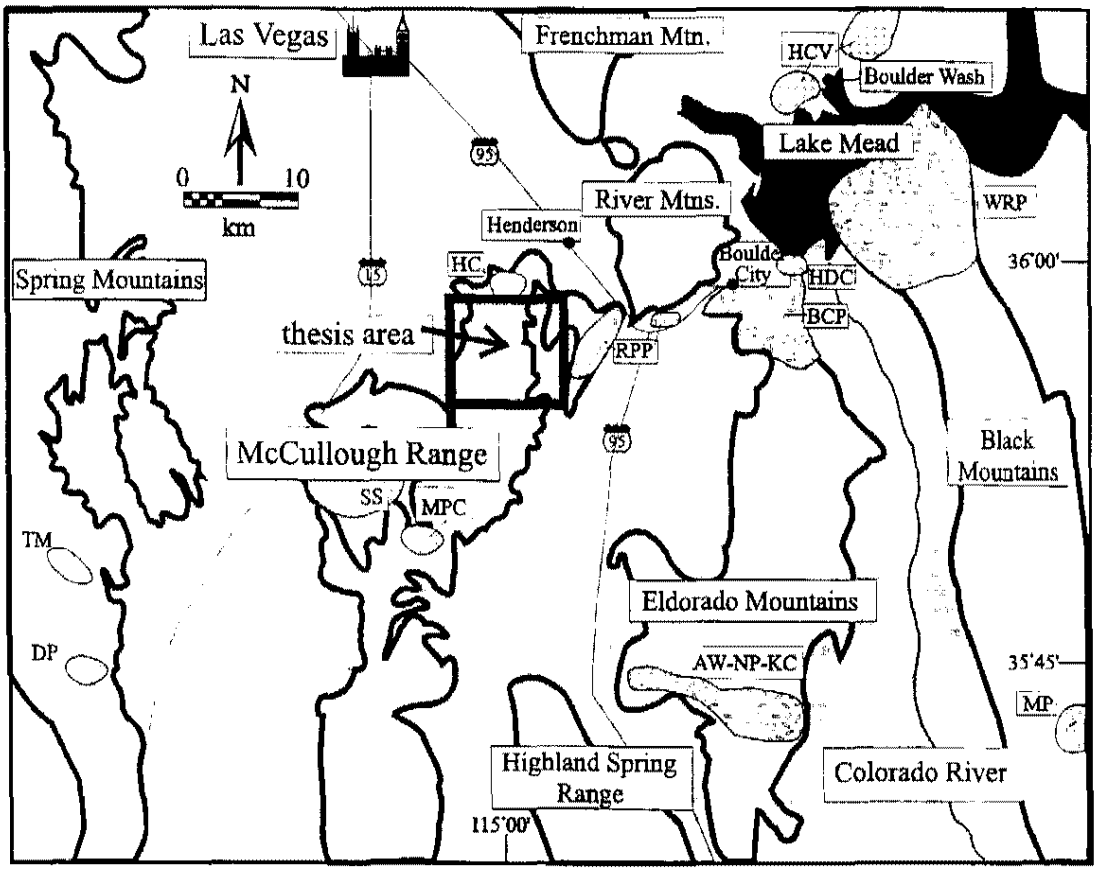

Figure 1. Location map of the thesis area in the northern McCullough Range and selected calderas, plutons, and other volcanic centers in the Las Vegas-Lake Mead area. AW-NP-KC= Aztec Wash, Nelson, and Keyhole Canyon plutons; BCP=Boulder City pluton; DP=Devil's Peak; HCV=Hamblin-Cleopatra volcano; HC=Henderson caldera; HDC=Hoover Dam caldera; MPC=McCullough Pass caldera; MP=Mt. Perkins pluton; RPP=Railroad Pass pluton; SS=Sloan Sag; TM=Table Mountain; WRP=Wilson Ridge pluton. The Dolan Springs volcanic field referred to in the text is located in the southern White Hills, northwestern Arizona approximately 15 km east of the Mt. Perkins pluton. Senator Mountain is located approximately 15 km north of the Dolan Springs volcanic field. References for locations in text.

Figure 2. East-facing escarpment of the Tertiary volcanic section in the northern McCullough Range. The break in slope represents the contact between two andesite units. In the past, flows in the lower section were correlated with the Eldorado Valley Volcanics while flows in the upper section were correlated with the Hidden Valley Volcanics (Refer to stratigraphic section of the central McCullough Range, Figure 3).

Chapter 2

Geologic Background and Regional Geology

The McCullough Range

The McCullough Range lies in the southern Basin and Range province near the western border of the northern Colorado River extensional corridor (NCREC) (Howard and John, 1987; Faulds et al., 1990). The McCullough Range trends north-south and extends from the New York Mountains in California to the city of Henderson in the Las Vegas Valley (Figure 1). Hewett (1956) and Longwell et al. (1965) first described the geology of the McCullough Range. The southern part of the McCullough Range consists of Precambrian igneous and metamorphic rocks. A Tertiary volcanic section in the central part of the range overlies Precambrian basement. The northern part of the range consists primarily of Tertiary volcanic rocks exposed on a prominent 600 to 1,000 m high east-facing escarpment (Figure 2).

The Tertiary volcanic section in the northern part of the McCullough Range comprises andesite flows which are overlain by dacite domes and flows in some areas, and in turn, overlie an older section of dacite domes, flows and andesite flows in other localities. Andesite flows are potentially correlative with

both the Eldorado Valley Volcanics * (Patsy Mine equivalent; 18.5-15.2 Ma), and the Hidden Valley Volcanics that crop out in the central McCullough Range (Mount Davis equivalent; 15.2-12 Ma) (Schmidt, 1987) (Figure 3). In the central part of the McCullough Range, it is easy to distinguish these units because the Tuff of Bridge Spring (TBS), a distinctive marker unit dated at 15.23 Ma, separates the units (Bridwell, 1991). The TBS, does not extend into the northern McCullough Range, so it is difficult to identify the contact between the Eldorado Valley and Hidden Valley Volcanics and even to determine whether both units crop out in the northern McCullough Range. In the past, however, both units were assumed to be present. The contact between them was placed at a prominent break in slope that lies about two-thirds of the way up from the base of the slope, and the units were distinguished by differences in the degree of alteration (Figure 2). Highly altered andesite flows in the lower part of the section were correlated with the Eldorado Valley Volcanics. The upper part of the section is relatively unaltered and was correlated with the Hidden Valley andesites (E.I. Smith, person. commun.).

Dikes that vary in composition from dacite to andesite intrude the lower two thirds of northern McCullough Range volcanic section, but are not present in the upper third of the section. The dikes are generally thin (<10 m) and fine grained. In the northeastern part of the field area, numerous dikes cut the lower part of the section, but because of the high density of dikes, the host rock is difficult to identify (Location A, Figure 4 and Plate 1). The Boulder City-Railroad Pass Pluton crops out east of the dike swarm (Longwell et al., 1974; Smith, 1982).

---

*Although the use of volcanics in this sense is grammatically incorrect, the Eldorado Valley Volcanics and the Hidden Valley Volcanics are the formal names for these units (Anderson, 1971).

The possible petrogenetic relationship of the dike swarm and pluton to the volcanic section is unknown. Hydrothermal fluids related to the emplacement of this pluton and dike swarm possibly caused the heavy alteration of the andesites, particularly in the lower part of the section.

Previous workers identified volcanic source areas in the McCullough Range to the north, south, and southwest of the field area (Figure 1). The Henderson Caldera to the north is superimposed on tilted and eroded andesite flows (Smith et al., 1993). The McCullough Pass caldera to the south is the source of the McCullough Pass ash-flow tuff (Schmidt, 1987). The McCullough Pass tuff is dated at 14.00 $\pm$ 0.02 Ma (P.B Gans and J.E. Faulds, $^{40}Ar/^{39}Ar$ on sanidine, unpublished data). Andesite and dacite domes and flows fill the Sloan Sag located to the southwest in the Hidden Valley area (Bridwell, 1991) (Figure 1). The Sloan Sag dacite was dated at 13.07 $\pm$ 0.02 Ma (P.B Gans and J.E. Faulds, $^{40}Ar/^{39}Ar$ on biotite, unpublished data).

Faulting and upper crustal extension occurred in the northern McCullough Range from about 14.5 Ma until about 13 Ma (Smith et al., 1988). The first evidence of extension in the area is a set of faults that cut and tilt the 15.55 Ma Eldorado Valley volcanic rocks, but do not extend upward into the overlying McCullough Pass volcanic section dated at 14-13.95 Ma (P.B Gans and J.E. Faulds, $^{40}Ar/^{39}Ar$ whole rock on andesite and sanidine, unpublished data). Another faulting event occurred during and after the eruption of the McCullough Pass volcanic section and the Hidden Valley section (13.07 to 13.95 Ma). However, dacites dated at 13.07 Ma (P.B Gans and J.E. Faulds, unpublished data) are untilted and unfaulted. These observations suggest that faulting began after the eruption of the Eldorado Valley volcanic rocks (14-15.55 Ma) and ceased by about 13 Ma (E.I. Smith, person. commun.; Smith et al., 1988). Smith et al.

(1988) noted that stratigraphic separation on individual faults is small in the northern part of the range (less than 20 m) but increases in the southern part of the McCullough range to 100 m. Although faults crop out in the McCullough Range, it is significantly less extended than nearby ranges (Weber and Smith, 1987).

Other Nearby Volcanoes and Plutons

Other volcanic centers within close proximity to the thesis area are the Hamblin-Cleopatra stratocone (Anderson, 1973; Thompson, 1985), the Callville Mesa basalt field (Feuerbach, 1993), the River Mountains stratovolcano complex (Smith,1982), the Hoover Dam caldera (Mills, 1985), the Eldorado Mountains basaltic-andesite stratovolcano complex (Anderson, 1971), the Devil Peak intrusive rhyolite plug in the southern Spring Mountains (Walker et al., 1981), and Table Mountain, a dacitic eruptive center about 10 km north of Devil Peak (E.I. Smith, personal commun.) (Figure 1). Plutons in the area include: the Nelson, Aztec Wash, Keyhole Canyon plutons (Anderson, 1971; Faulkner et al., 1995); the Mt. Perkins pluton (Faulds, 1995; Metcalf et al., 1995); the Boulder City pluton (Longwell et al., 1974); and the Wilson Ridge pluton (Larsen and Smith, 1990; Metcalf et al., 1993b) (Figure 1).

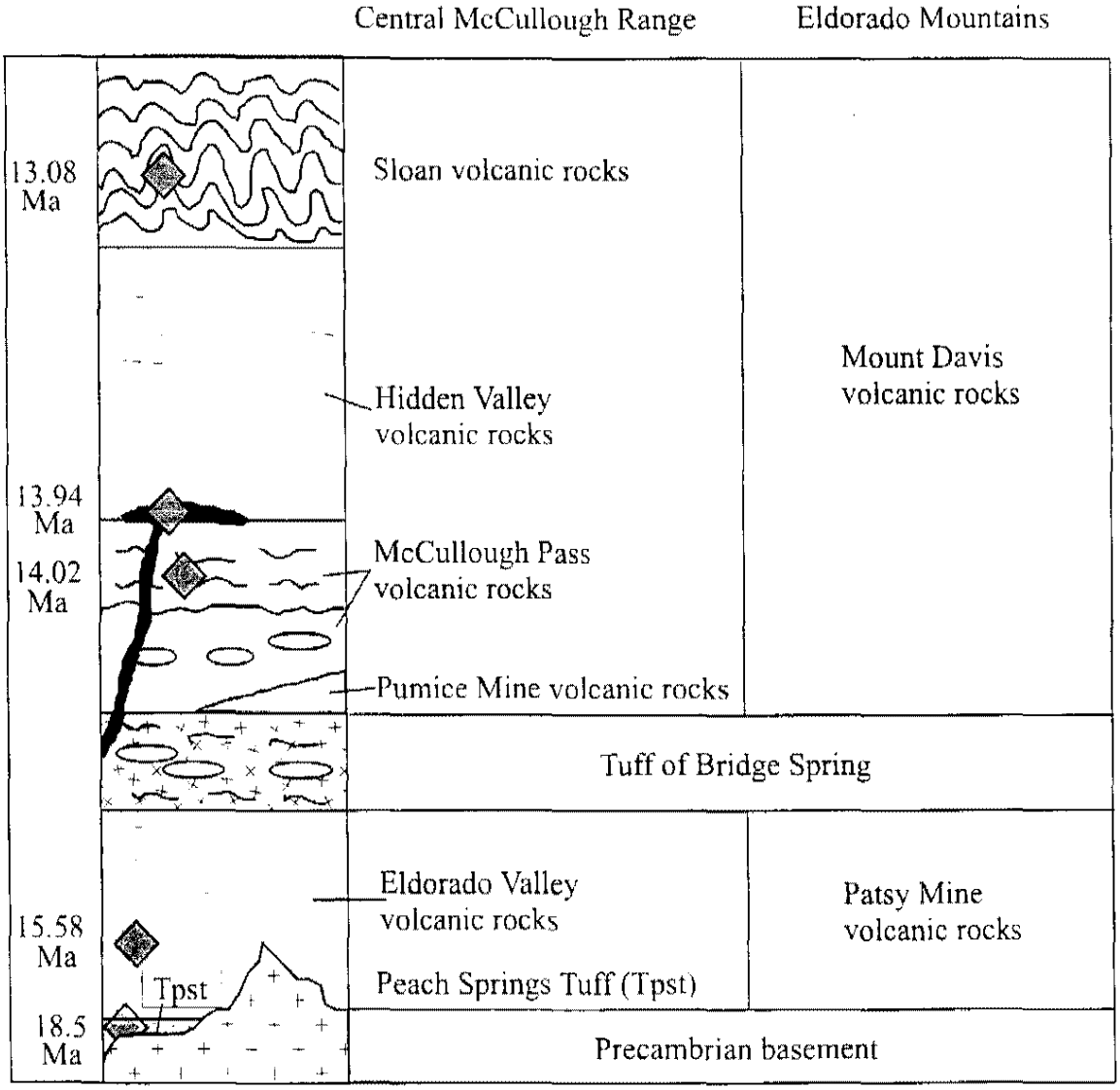

Figure 3. Stratigraphic column of the central McCullough Range from Schmidt (1987) and Bridwell (1991). Equivalent stratigraphy in the Eldorado Mountains from Anderson (1971). $^{40}Ar/^{39}Ar$ dates (gray diamonds) on whole rock, sanidine, and biotite from P.B Gans and J.E. Faulds, unpublished data. Column modified from Smith and Faulds (1994).

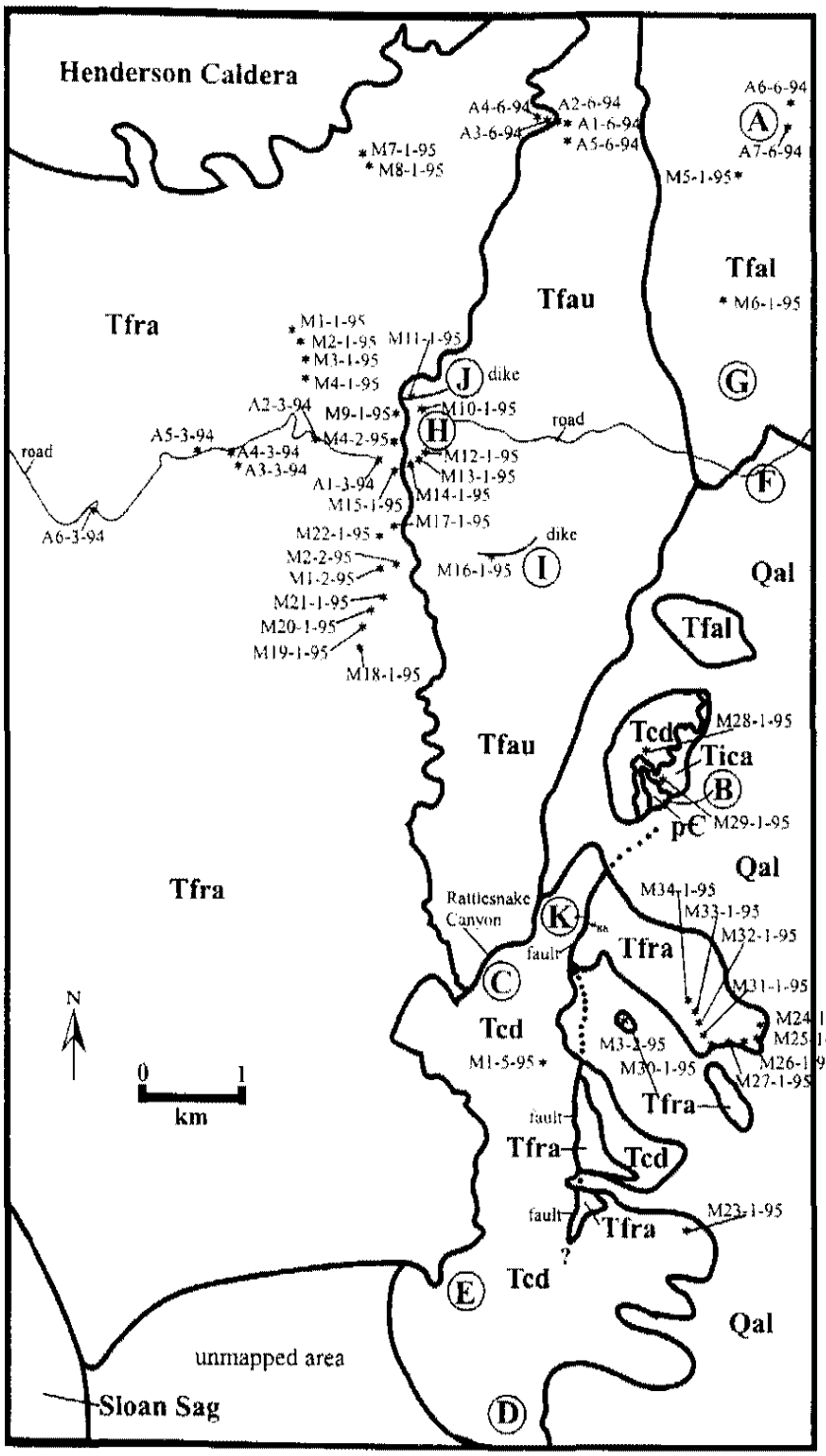

Figure 4. Simplified geologic map of the field area in the northern McCullough Range containing specific locations discussed in text (bold letters enclosed in circles). Black stars show rock sample locations for geochemical analyses (e.g. A1-3-94; M1-1-95). Qal=alluvium; Tfra=Fog Ridge andesite; Tfau=Farmer Canyon andesite (upper member); Tfal=Farmer Canyon andesite (lower member); Tcd=Colony dacite; Tica= Ivan Canyon andesite; pC=Precambrian basement. See Plate 1 for more detail.

Chapter 3

Stratigraphy and Structural Geology of the Northern McCullough Range

Stratigraphy

Introduction

Correlating volcanic units in the northern McCullough Range with previously named units in the central and southern part of the range is problematic due to a lack of marker beds, dated units, and isotopic data. Although identification of the vent areas for most lava flows is difficult, andesite and dacite flows are not regionally extensive and probably erupted from local vents. Thus it is unlikely that volcanic units in the study area will correlate with other units in the region. Volcanic vents in the study area, however, may be age equivalent to other units in the region. For these reasons, I will apply new names to units in the northern McCullough Range.

In the central and southern part of the field area, the oldest Tertiary unit in the stratigraphic section consists of andesite flows that lie on the Precambrian basement (Figure 5). This andesite unit may be age equivalent to the Eldorado Valley Volcanics in the central and southern McCullough Range and the Patsy

Mine Volcanics in the Eldorado Range and is here named informally the Ivan Canyon andesite. A thick section of dacite domes and flows and high-silica andesite flows overlies the Ivan Canyon andesite. This volcanic section was previously unrecognized and is here informally named the Colony dacite. The Ivan Canyon andesite and Colony dacite only crop out in the central and southern parts of the field area (Figure 4 and Plate 1). A thick section of andesite, debris flow deposits, and breccia makes up the lowest part of the volcanic section in the northern part of the field area and is here named informally the Farmer Canyon andesite. The Farmer Canyon andesite is broken into two members based on changes in flow morphology, differences in phenocryst content, and differences in dike concentration. The members are referred to as the lower member of the Farmer Canyon andesite and the upper member of the Farmer Canyon andesite. Throughout the field area, a younger andesite section lies on both the upper member of the Farmer Canyon andesite and the Colony dacite. This section may be age equivalent to the Hidden Valley Volcanics in the McCullough Range and the Mt. Davis Volcanics in the Eldorado Range and is here informally named the Fog Ridge andesite (Figure 5). The unit names Fog Ridge andesite, Farmer Canyon andesite, Colony dacite, and Ivan Canyon andesite are all informal names used in this thesis. The following section contains a description of the units in the stratigraphic section in the northern McCullough Range from oldest to youngest. Point counts of representative samples determined modal mineral percentages (Appendix I).

Precambrian basement

Precambrian basement rock in the area is a coarse-grained red granitic rock containing large (up to 3 cm) potassium feldspar crystals and a biotite

gneiss. The granitic rock appears to be intruding the biotite gneiss. Ivan Canyon contains the best exposure of basement rock (Location B, Figure 4). Coarse-grained "Rapakivi" granites occur to the southwest of the thesis area near Beer Bottle Pass in the Lucy Gray Range and the central McCullough Range (Duebendorfer and Christensen, 1995). It is unclear whether the granite in Ivan Canyon is equivalent to the granite at Beer Bottle Pass.

Ivan Canyon andesite

The Ivan Canyon andesite consists of 5-10 massive andesite flows containing phenocrysts (21%) of plagioclase (50%; up to 1.5 mm), clinopyroxene (47%; up to 2 mm), and Fe-Ti minerals (3%; up to 0.25 mm). Weathered and fresh surfaces of the unit are dark gray in color. In Ivan Canyon (Location B, Figure 4), the andesite lies nonconformably on Precambrian basement. The contact zone between the Precambrian rock and the Ivan Canyon andesite is a 15 cm thick zone of cemented granite grus. Above this zone, the basal part of an Ivan Canyon andesite flow contains xenoliths of the Precambrian granite (Figure 6a). The Ivan Canyon andesite lies beneath the Colony dacite and increases in thickness from north to south (approximately 20 m to 50 m).

Colony dacite

The Colony dacite contains rhyolite to dacite flows and domes and high-silica andesite flows, but it is predominantly dacite. Dacites and andesites contain phenocrysts (20-26%) of plagioclase (70-75%; up to 5 mm), biotite (13-26%; up to 2.5 mm), Fe-Ti minerals (<3%), and clinopyroxene (0-<5%). Rhyolite (M23-1-95) contains phenocrysts (21%) of sanidine (71%; up to 6 mm), plagioclase (16%; up to 5 mm), Fe-Ti minerals (7%; up to 2 mm), biotite (5%; up to 2.5 mm),

and clinopyroxene (1%; up to 1.5 mm). The presence of large and abundant biotite phenocrysts easily distinguishes the Colony rocks from other volcanic units in the section. One dacite flow (M1-5-95) contains several basaltic xenoliths up to 8 mm in size, but generally xenoliths are rare.

Colony andesite and dacite flows are pink to dark gray on weathered surfaces; fresh surfaces are slightly darker in color. Flows are thick (up to 100 m), platy, and locally flow banded and autobrecciated. Colony dacite domes are platy, pink to light gray in color on fresh and weathered surfaces, and slightly coarser grained than Colony flows. It is difficult to distinguish between flows and domes because Colony flows are so coarse-grained and structureless. The opposing dips of flow banding, however, allowed identification of one dacite dome (Location C, Figure 4).

Some dacite flows are interbedded with dacite breccias and/or debris flow deposits. . Some breccia units in the field area are interpreted as debris flow deposits based on poor sorting, lack of internal layering, and wide range of clast sizes (clay to boulders) supported in an open framework of a finer-grained matrix (Boggs, 1987; Cas and Wright, 1988). In the southern part of the field area, (location D, Figure 4), a thin (7 m) red to gray debris flow contains angular dacite clasts (average size-5 cm). Farther west towards the range (Location E, Figure 4) debris flow deposits are thicker (35-40 m), weather to a tannish-yellow color, and have large blocky clasts ranging in size from a few cm's to 1 m in a sand matrix.

Paleohills of Colony dacite acted as a topographic barrier to the emplacement of flows of the upper member of the Farmer Canyon andesite (Location C, Figure 4). A surface of high relief developed on eroded Colony dacite domes and flows and the upper member of the Farmer Canyon andesite

was deposited on it. The contact between the Colony dacite and the overlying Fog Ridge andesite is an unconformity (Figure 6b).

Lower member of the Farmer Canyon andesite

The lower member of the Farmer Canyon andesite consists of massive, porphyritic andesite flows containing abundant phenocrysts (24%) of large (up to 5 mm) plagioclase (85%), Fe-Ti minerals (9%), clinopyroxene (5%; up to 3 mm) phenocrysts and smaller (<1.5 mm) phenocrysts of biotite and oxyhornblende (<1%). The clinopyroxene phenocrysts are highly altered and corroded. Fresh and weathered surfaces of flows are dark pink to red in color. Unlike the rest of the volcanic section in the area, the flows of the lower member of the Farmer Canyon andesite are not interbedded with breccia units.

Many andesitic and dacitic dikes that are finer grained and more resistant to erosion than the host rock intrude the section. The density of dikes is considerably greater in the lower member of the Farmer Canyon section than in the Colony dacite just to the south. Highly weathered and altered andesite flows and dikes of the lower member of the Farmer Canyon contain fractures filled with secondary calcite. Many exposures are so highly fractured and altered it is difficult to distinguish host rock from dike.

One outcrop of the andesite lies on a poorly exposed, course grained plutonic rock with a distinctive red color (Location F, Figure 4). This rock may be Precambrian basement. To the north, dikes with a similar composition to the andesite intrude highly altered, dark gray plutonic rock (Location G, Figure 4) that may also be Precambrian basement. The lower Farmer Canyon andesite, therefore, may lie on Precambrian basement.

Upper member of the Farmer Canyon andesite

The flows of the upper member of the Farmer Canyon andesite are porphyritic and fine grained with phenocrysts (15-45%) of sub-euhedral plagioclase up to 1.75 mm in size (42-91%), subhedral clinopyroxene up to 0.75 mm (5-17%), subhedral olivine up to 0.75 mm (0-14%), and Fe-Ti minerals up to 0.5 mm (<5%). Plagioclase laths, clinopyroxene and olivine crystals, devitrified glass, and Fe-Ti minerals compose the groundmass. Many plagioclase grains are zoned. In some samples, several plagioclase grains exhibit wavy extinction; these grains may be xenocrysts. Olivine crystals, where present, are altered to iddingsite. Fresh and weathered color of flows is dark gray or red. Altered Farmer Canyon andesite flows of the upper member contain secondary calcite, quartz, and zeolite minerals.

Andesite flows make up only a small volume of the upper member of the Farmer Canyon andesite section. The section consists primarily of a thick section of andesite breccia. The breccia is clast supported, red to dark green in color with angular clasts composed of andesite and/or basalt. About 145 m up in the section, thin andesite flows are interbedded with autobrecciated flows and debris flow deposits. About 300 m below the radio towers (Location H, Figure 4), breccia units are interbedded with platy andesite flows which exhibit prominent flow banding. Near vertical contacts between breccia units and flows possibly indicate periods of erosion between erupting flows and the development of significant topography. A tannish-yellow debris flow that causes a dramatic change in slope separates the upper member of the Farmer Canyon and younger Fog Ridge andesite sections (Figure 2). This debris flow deposit is about 50 m thick, poorly sorted, and contains angular clasts which range in size from 1 cm to a few meters. The average clast size is about 7 cm. Clasts are andesitic to

basaltic, vary in color from red to green to black, and are fine-grained to porphyritic. No grading or stratification is visible.

Dikes

Dikes that vary in composition from dacite to andesite intrude the andesite and debris flow deposits of the upper member of the Farmer Canyon section. One andesite dike (M16-1-95; Location I, Figure 4) is about 14 m thick and contains phenocrysts (20%) of plagioclase (80%) and clinopyroxene (20%). Another andesite dike (M11-1-95; Location J, Figure 4) is about 3 m thick and contains phenocrysts (34%) of plagioclase (59%), clinopyroxene (38%), and Fe-Ti oxides (3%). This dike cuts several andesite flows and the uppermost debris flow deposit in the section; it is a prominent topographic feature in the area. Dikes are prevalent throughout the upper member of the Farmer Canyon andesite, but no dikes intrude the younger Fog Ridge andesite. The Fog Ridge andesite flows lie directly on truncated dikes that are intruding the upper member of the Farmer Canyon andesite (Location J, Figure 4). This relationship suggests that there was a period of erosion between the deposition of the upper member of the Farmer Canyon and Fog Ridge andesite sections.

Fog Ridge andesite

The Fog Ridge andesite consists of thin basaltic-andesite and andesite flows interbedded with breccia units. Flows are porphyritic and contain 20-40% phenocrysts of sub-euhedral plagioclase up to 2.5 mm in size (14-61%), sub-euhedral olivine up to 2.25 mm (3-46%), and sub-euhedral clinopyroxene up to 2.5 mm (10-40%). Plagioclase laths, olivine and clinopyroxene crystals, devitrified glass, and Fe-Ti oxides compose the groundmass. Some vesicles are

present. Many plagioclase grains are zoned. Sample A1-3-94 contains several plagioclase phenocrysts that exhibit wavy extinction and have a sieve texture suggesting strain and disequilibrium (see Figure 4 and Plate 1 for sample locations). These plagioclase grains are probably xenocrysts. Clinopyroxene phenocrysts have polysynthetic twinning and zoning. Olivine crystals are altered to iddingsite. Glomerocrysts consisting of plagioclase, olivine, clinopyroxene, and Fe-Ti oxides are present in many samples. Weathered surfaces of Fog Ridge flows are dark gray with fresh surfaces dark gray to black. Altered Fog Ridge flows contain secondary calcite, quartz, and zeolite minerals in vesicles and fractures. Breccias is clast supported, red to dark gray in color with angular clasts composed of andesite and/or basalt.

In contrast to the upper member of the Farmer Canyon andesite, Fog Ridge andesite breccias are generally thinner and lava flows are thicker (~3 m) and more numerous. The flows become progressively thicker and the breccias thinner upward within the section. Agglomerate zones are common between flows.

Discussion of Stratocone facies and vent locations

Weber and Smith (1987) suggested that the northern McCullough Range contains a stratocone composed of andesite flows (upper member of the Farmer Canyon andesite and the Fog Ridge andesite) interlayered with volcaniclastic units. Mapping and field relationships from this study suggest that there is indeed a stratocone in the northern part of the field area, and possibly other vent locations. Flows in the field area are not regionally extensive and most likely erupted from local volcanoes. Other evidence suggesting a nearby vent includes: thick debris flows, volcaniclastic breccias, and nearby dike swarms. These

that the Fog Ridge section erupted from a different and more distal vent area than the upper member of the Farmer Canyon section, or that a change in eruptive style occurred from Plinian/Vulcanian (Farmer Canyon) to a more Hawaiian type (Fog Ridge).

The east side of the range may expose a separate vent area that produced the Colony dacite and possibly the lower member of the Farmer Canyon andesite (Location E, Figure 4). Massive dacite flows, local and thick dacite debris flows, and numerous dikes suggest a possible a vent area for these units based on the general stratocone facies model presented above.

Structural Geology

The McCullough Range is relatively unextended compared to neighboring ranges (see Appendix II for details). Andesite flows of the Fog Ridge and Farmer Canyon andesite sections, however, dip 15-25° to the west. Weber and Smith (1987) thought that this dip represented the flanks of a stratocone. Tilting related to faulting, however, may be responsible for the observed dips. Mapping revealed that all units in the area, including the older Colony dacite and Ivan Canyon andesite, dip west (Plate 1). The Colony dacite erupted prior to the formation of the stratocone suggested to exist by Weber and Smith (1987). The consistent dips observed throughout the field area regardless of the age of the unit, therefore, are most likely due to structural tilting. In addition, the dips of flows within the Fog Ridge andesite progressively decrease up section and eventually reach horizontal at the top of the section. A fanning dip pattern is an indicator of synextensional volcanism (Faulds et al., 1995), and thus, normal faulting probably caused the structural tilt. Although faults are rare in the field

area, a major normal fault places the Fog Ridge andesite against Colony dacite flows and has about 400 meters of stratigraphic separation (Location K, Figure 4 and Plate 1). The Fog Ridge andesite flows in the hangingwall of this fault dip between 20 and 35° to the west while Colony dacite flows in the footwall dip between 10 and 20° to the west.

Rocks dip east in the central McCullough Range north to the latitude of McCullough Pass. Rocks in the northern part of the range and to the east of Hidden Valley dip west (Figure 7). If the dips are due to structural tilting, the northern McCullough Range may contain a dip reversal. The geometry of this dip change in the McCullough Range, however, is synformal rather than antiformal as described in the Black Mountains accommodation zone; a major axis dip reversal that projects toward the McCullough Range (Figure 7) (Faulds et al. 1990; Faulds et al., 1995). Dip reversals help facilitate strain release in structurally complex accommodation zones that separate major fault domains with opposing tilt directions. The Black Mountains accommodation zone contains several such dip reversals (Faulds et al., 1990; Faulds, 1994; Olsen and Faulds, 1995; Varga and Faulds, 1995). In the McCullough Range, the McCullough Pass Caldera, the Sloan Sag, and the Henderson Caldera all occur near or on the axis of a dip reversal (Figure 7). The close association of volcanic centers and the axis of dip reversal suggests a possible volcanic control on structural geometry (J.E. Faulds, personal commun.). Alternatively, the location of volcanoes may be controlled by the structures.

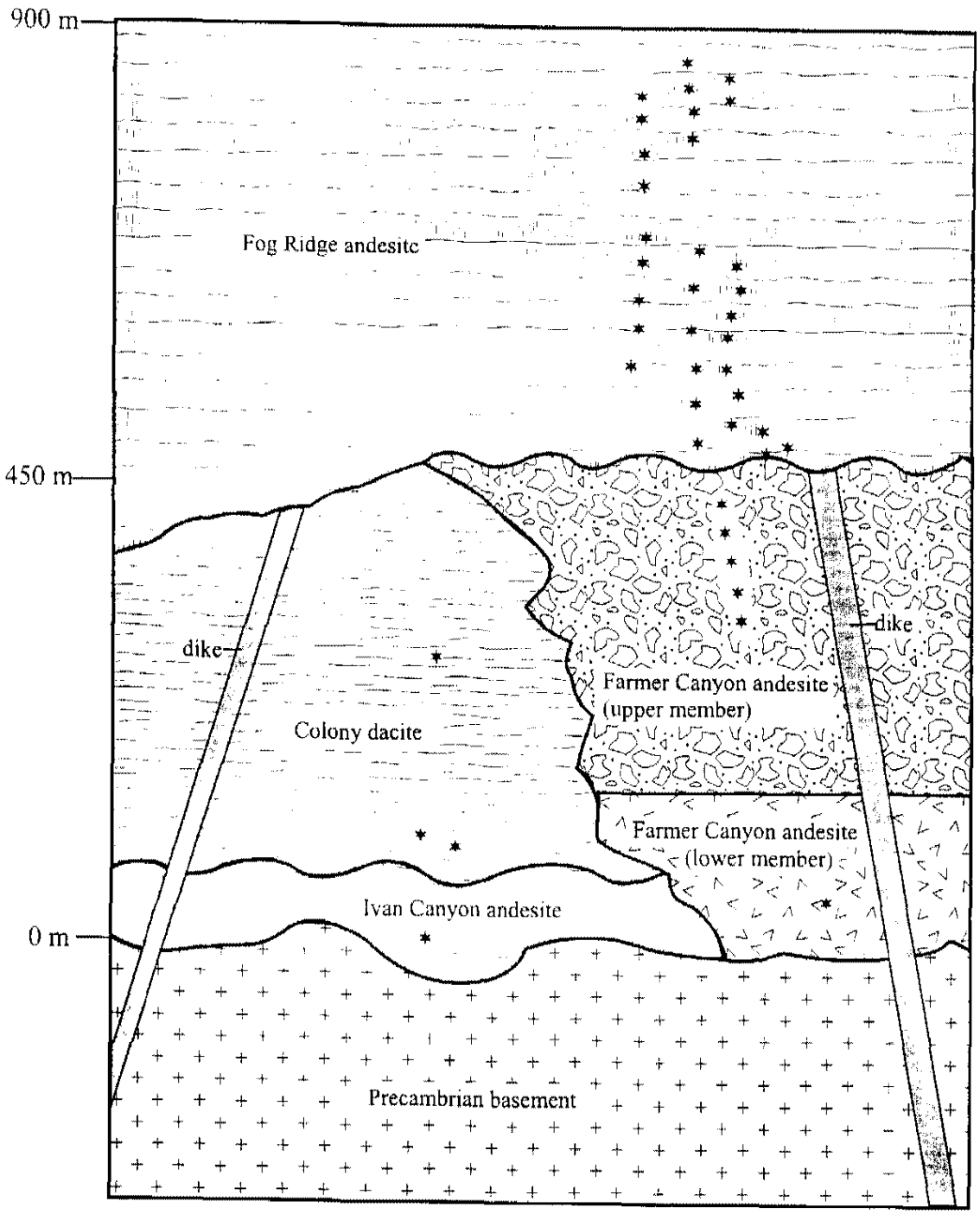

Figure 5. Diagrammatic stratigraphic column of the northern McCullough Range. Unit thicknesses are variable and estimated from calculations on map (see Plate 1). Black stars represent approximate location of rock samples within the section. Dikes shown are diagrammatic and do not represent true orientation.

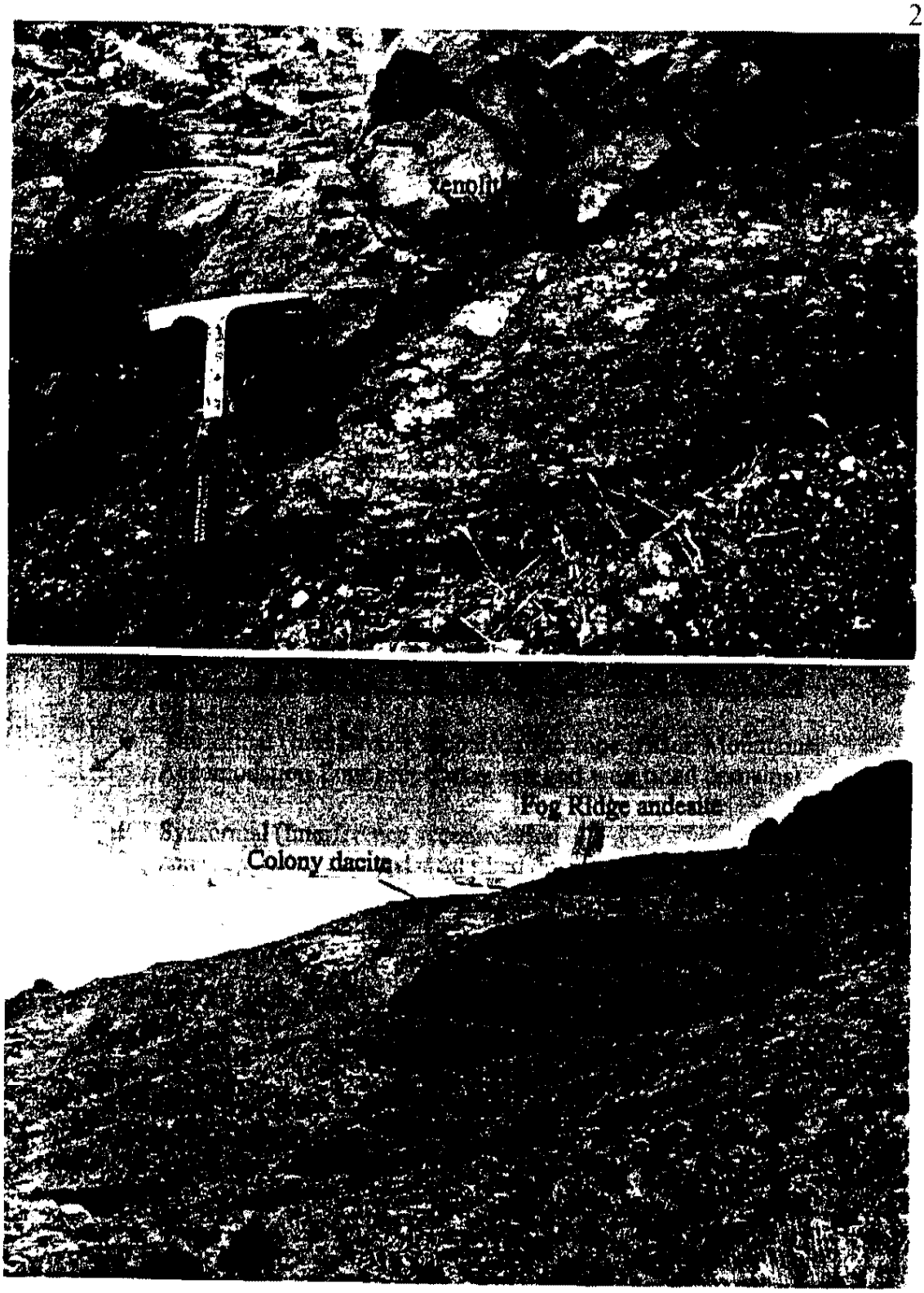

Figure 6. (Top) Contact between the Ivan Canyon andesite and Precambrian basement from Ivan Canyon (Location B, Figure 4; Plate 1). Note the Precambrian xenolith contained in the base of the overlying Ivan Canyon andesite flow. (Bottom) Contact between the Colony dacite and overlying Fog Ridge andesite. View is looking south from Rattlesnake Canyon (Plate 1).

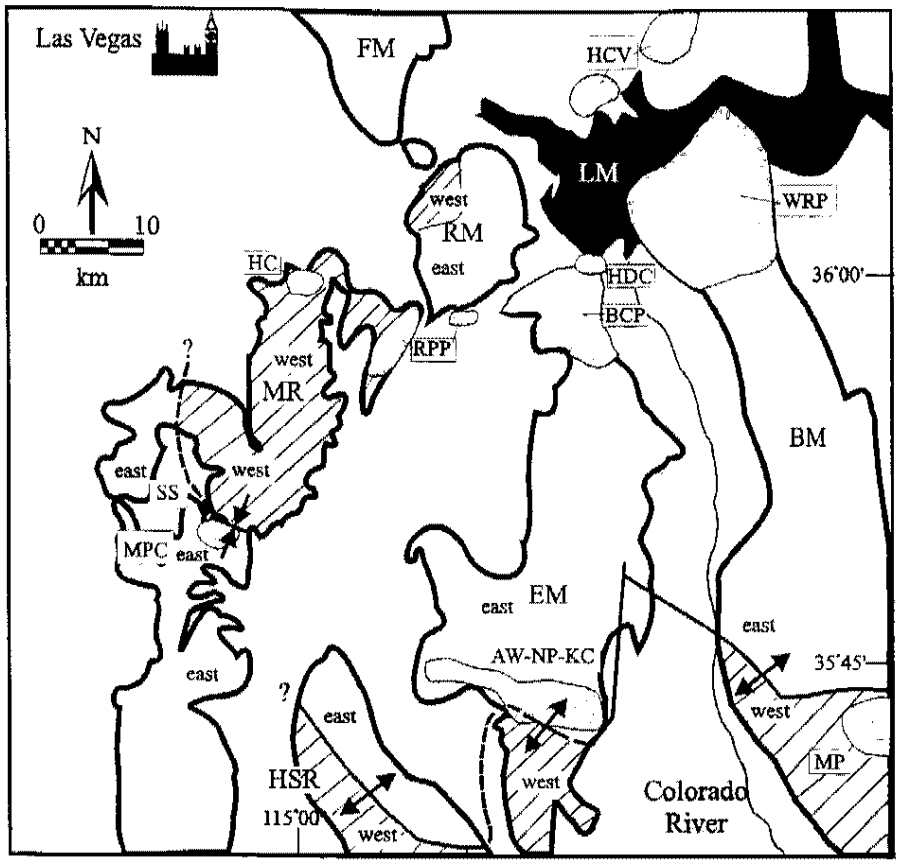

Antiformal (Interference accomodation zone (Black Mountains. Accomodation Zone) separating east and west tilted domains).

Synformal (Interference accomodation zone separating east and west tilted domains).

east — east tilted domain

west — west tilted domain

=volcanic centers

=plutons

Figure 7. Simplified geologic map showing location of axis of dip reversals in the NCREC. The central McCullough Range may contain a synformal dip reversal separating east and west tilted domains similar to but in an opposite sense to the dip reversal structures described by Faulds et al. (1990), Faulds (1994), Olsen and Faulds (1995), and Varga and Faulds (1995). See Plate 1 for structure data from this study. AW-NP-KC= Aztec Wash, Nelson, and Keyhole Canyon plutons; BM=Black Mountains; BCP=Boulder City pluton; EM=Eldorado Mountains; FM=Frenchmen Mountain; HCV=Hamblin-Cleopatra volcano; HC=Henderson caldera; HSR=Highland Spring Range; HDC=Hoover Dam caldera; LM=Lake Mead; MPC=McCullough Pass caldera; MR=McCullough Range; MP=Mt. Perkins pluton; RPP=Railroad Pass pluton; RM=River Mountains; SS=Sloan Sag; WRP=Wilson Ridge pluton.

Chapter 4

Geochemistry of the Volcanic Rocks of the Northern McCullough Range

Analytical Techniques

Sixty-eight rock samples were collected from field locations in Nevada and Mexico and analyzed for chemistry. Fifty-one samples were collected from the northern McCullough Range and are representative of the thick sequence of andesite flows, as well as dacite domes and flows, dikes, and the pluton (see Figure 4 and Plate 1 for sample locations). Although many lava flows in the section have heavy calcite and zeolite alteration, careful sampling avoided these localities. A few samples contained vesicles filled with calcite crystals. These samples were broken apart in the lab and the crystals removed before being crushed for chemical analysis. In addition, 17 samples of basaltic-andesite were collected from Xitle volcano in Mexico to compare chemistry and test models of andesite petrogenesis. All samples were stored in resealable plastic bags. Whole rock samples were used for geochemical analysis.

All samples were analyzed for major, trace, and rare-earth elements (REE) (see Appendix III for geochemical data of all samples). The Braun "chipmunk" crushed half of each sample to pea size pieces, then the Bico "shatterbox" further

crushed the sample to <300 mesh. Appendix IV reports standards used for machine calibration, and accuracy and precision of all analyses.

Major and trace element analyses

For major element analysis, samples were prepared as fused glass disks. Heating 9.0 g lithium tetraborate, 0.16 g ammonium nitrate, and 1.0 g of sample at 1100°C in gold-platinum crucibles produced a melt that was then poured into gold-platinum molds (Noorish and Hutton, 1969). For trace element analysis, samples were prepared as pressed pellets by mixing 3.0 g of sample with 0.6 g of methyl cellulose and compressing to 3,000 psi in an Ashcroft hydraulic pellet press. Major and trace elements were analyzed by a Rigaku 3030 XRF spectrometer. Sample discs and pellets were stored in a dessicator and run within several days of preparation.

Trace and rare-earth element analyses

Fourteen samples were analyzed for REE and Cr, V, Sc, Co, Ta, Hf, and Th by Instrumental Neutron Activation Analysis (INAA) at the Phoenix Memorial Laboratory, University of Michigan. Approximately 0.200 g of sample powder was placed in clean, 8 cm long, sealed Suprasil silica tubes. The tubing was sealed by heating each end with a natural gas/oxygen mixture. A standard sample was also prepared from sample #78-220, an andesite collected from the River Mountains, Clark County, Nevada (Smith and others, 1990). Appendix IV reports accuracy and precision for these analyses.

Fifty-four samples were analyzed for REE and Ba, Th, Nb, Y, Hf, Ta, U, Pb, Rb, Cs by the Sciex inductively coupled plasma mass spectrometer (ICP-MS) at the GeoAnalytical Laboratory, Washington State University (WSU). Researchers

at WSU completed sample preparation and digestion techniques adapted from experiments conducted in the WSU lab.

Isotope analyses

Fourteen samples were analyzed for isotopes (Sr, Nd, and Pb) by thermal ionization mass spectrometry (TIMS) using the VG Sector 54 mass spectrometer at the University of Kansas, Lawrence. Feuerbach et al. (1993) described this technique in detail. Reproducibility of Sr concentrations is +/-0.000020 and Nd is within 0.25 epsilon units (Feuerbach et al., 1993). Nine additional samples were analyzed for Sr and Nd isotopes at the Massachusetts Institute of Technology (MIT) geochemistry lab. Precision and accuracy for $^{87}Sr/^{86}Sr$ are based on the National Bureau of Standards (NBS) sample 987 and reported as 0.0004% and 0.0034%, respectively. Precision and accuracy for $^{143}Nd/^{144}Nd$ are based on the sample La Jolla and reported as 0.0005% and 0.0004%, respectively.

Major elements

Calc-alkaline andesite, basaltic-andesite, dacite and rhyolite compose the northern McCullough Range volcanic section (Figure 8a, b, and c). The sample from the Railroad Pass pluton is a granodiorite. Refer to Appendix III for the complete geochemical database.

Northern McCullough Range andesites do not vary significantly in major element chemistry. Andesites range in SiO_2 content from 50.2 to 58.9 wt. % and MgO from 1.7 to 7.2 wt. % (Figure 9a). Mg numbers [((Mg/(Mg + Fe)) x 100] of the andesites range from 36.6 to 61.1. In comparison, volcanic rocks with Mg #'s > 71 are considered primary magmas produced by partial melting of mantle

peridotite (Green et al., 1974). Harker diagrams show a decrease in TiO_2, FeO, CaO, MnO, P_2O_5, and MgO with increasing SiO_2, while Al_2O_3, K_2O, and Na_2O slightly increase with increasing SiO_2 (figures not shown).

Dacites and rhyolites vary in SiO_2 content from 63.2 to 70.7 wt. % and in MgO from 0.18 to 1.6 wt. % (Figure 9a).

Alteration and Contamination

A few samples, such as A2-6-94 from the upper member of the Farmer Canyon andesite, have significantly higher SiO_2 contents (up to 58 wt. %) than the rest of the upper member of the Farmer Canyon section. Thin section data suggest that the higher SiO_2 content may be a result of alteration and/or secondary mineral growth. For example, sample A3-6-94 from the Fog Ridge andesite contains secondary quartz in small vesicles. The secondary quartz is most likely responsible for the higher SiO_2 of this sample. Contamination is also evident in a few samples. For example, sample A2-6-94 contains crystals of hornblende with embayed edges and rims of Fe-Ti oxide. Such crystals are most likely xenocrysts. Although these hornblende crystals would not increase the SiO_2 content in these andesites, their occurrence suggests that the rock is contaminated.

Metasomatism

Although some rocks in the field area contain secondary quartz, calcite, or zeolite minerals, potassium metasomatism does not appear to have significantly affected the chemistry of the samples. Potassium metasomatism tends to decrease sodium and increase potassium contents. For example, K_2O contents > 10 wt. % accompanied by Na_2O < 1 wt. % are not uncommon in potassium

metasomatized rocks (Chapin and Glazner, 1983). However, the andesite samples from the northern McCullough Range have K_2O (2.5-5.0 wt. %) and Na_2O (2.4-3.8 wt. %) concentrations that fall within the range of unmetasomatized rocks according to fields defined by Carmichael et al. (1974) and Wilson (1989) (Figure 9b). Colony dacite samples are more variable with K_2O up to 8.6 wt. % and Na_2O up to 5.2 wt. %.

Incompatible trace elements

Andesites in the northern McCullough Range show wide variations in trace element chemistry. In general, incompatible trace elements (e.g., Nb, Sm, La) tend to cluster or decrease in abundance when plotted against an index of differentiation like wt. % SiO_2 (Figure 10). Rocks of the northern McCullough Range have similar chemical signatures on spider diagrams normalized to either primitive mantle (Sun and McDonough, 1989) or ocean island basalt (OIB) (Fitton et al., 1991) (Figures 11 and 12).

Large Ion Lithophile (LIL) and High Field Strength Elements (HFSE)

When normalized to primitive mantle abundances, northern McCullough Range samples are enriched in the large ion lithophile elements (LIL), such as Rb, Th, U, and Ba, relative to high field strength elements (HFSE) and heavy rare earth (HREE) elements (Figure 11a and b). Sr values range from 722 to 2005 ppm in the andesites and from 130 to 776 ppm in the dacites. Andesites are similar to OIB except for troughs at Nb and variable depletion of P and Ti with respect to either OIB or mid-ocean ridge basalt (MORB) (Figure 12a). The Colony rhyolite (M23-1-95) differs from all other rocks in the northern McCullough Range in that

it is more enriched in Rb, Th, U, Nb, and K, depleted in Ba, and more strongly depleted in Sr, P and Ti (Figures 11b and 12b).

Rare-earth elements

Light rare earth elements (LREE) are enriched in the rocks in the northern McCullough Range relative to heavy rare earth elements (HREE) and HFSE (Figure 11a and b). Also, note that Yb and Lu are > 10 x chondrite abundance (chondrite normalized plots are not shown).

Compatible trace elements

In these andesites, Cr decreases as SiO_2 increases; Ni data is more scattered but also shows a decrease in concentration with increasing SiO_2 (Figure 13a and b). Cr and Ni vary from < 5 ppm to 242 ppm and 157 ppm respectively. Sample A5-3-94 from the Fog Ridge andesite contains the highest values of both Cr and Ni. Ni and Cr contents in the dacites are <5 ppm.

Isotopes

Sr and Nd isotopes were obtained for 21 samples from the northern McCullough Range. The overall range in ε_{Nd} is from -6 to -10, and initial $^{87}Sr/^{86}Sr$ varies from 0.7076 to 0.7098 (Figure 14a). These values are typical of >9 Ma mafic volcanic rocks in the NCREC (Feuerbach et al., 1993). Although andesites show scatter and wide variations in trace element chemistry, Sr and Nd data reveal four isotopic groups. The first isotopic group, type A ($^{87}Sr/^{86}Sr$ ~0.7077; ε_{Nd} ~-6.6), is defined by two samples; A5-3-94, the most mafic sample of the Fog Ridge andesite and A2-3-94, also from the Fog Ridge andesite. The

second group, type B ($^{87}Sr/^{86}Sr$ ~0.7082; ε Nd ~-7.1), is defined by nine samples from the Fog Ridge (6), Farmer Canyon (2), and Ivan Canyon (1) andesite sections. The third group, type C ($^{87}Sr/^{86}Sr$ ~0.7090; ε_{Nd} ~-9.4), is defined by three samples of the Farmer Canyon andesite and one Colony andesite sample. The fourth group, type D ($^{87}Sr/^{86}Sr$ ~0.7093; ε_{Nd} ~-8.7), is defined by two Colony dacites and two dacite dikes sampled from the dike swarm area (Figure 14a).

On an ε_{Nd} vs. $^{87}Sr/^{86}Sr$ diagram, there are gaps between groups. From group A to B, $^{87}Sr/^{86}Sr$ steps from 0.7077 to 0.7081 and ε_{Nd} slightly decreases. From group C to D, $^{87}Sr/^{86}Sr$ differs by 0.0003 and ε_{Nd} also differs slightly. The most significant jump in both $^{87}Sr/^{86}Sr$ and ε Nd is between groups B and C. A jump in ε_{Nd} from 7.5 to 9 defines this gap. The $^{87}Sr/^{86}Sr$ jump across the gap is about 0.0007 (Figure 14a). Although small, these gaps are larger than can be explained by analytical error (see Feuerbach et al., 1993).

Pb isotopes were obtained for 14 samples. $^{206}Pb/^{204}Pb$ varies from 17.977-18.496, $^{207}Pb/^{204}Pb$ varies from 15.522-15.589, and $^{208}Pb/^{204}Pb$ varies from 38.665-39.263. The samples plot above the Northern Hemisphere Reference Line (NHRL) and have ratios typical of pre-9 Ma volcanic rocks in the NCREC (Smith, unpublished data) (Figure 14b).

The River Mountains-Wilson Ridge magmatic system in southern Nevada just northeast of the field area displays an isotopic trend similar to the McCullough Range isotope array (Figure 15a). In the River Mountains and Wilson Ridge pluton, a mafic mantle component may have mixed with a crustal component to form a linear data array between the two end members (Feuerbach et al., 1993). The River Mountains isotope data exhibits an increase in SiO_2 with increasing $^{87}Sr/^{86}Sr$ and decreasing ε_{Nd} reflecting the addition of a crustal

component (Figure 15b). In contrast, SiO_2 contents of isotope groups A, B, and C from the northern McCullough Range are very similar to each other (Figure 14a). Isotopic ratios do not correlate with increasing SiO_2 or any other index of differentiation.

Correlation of isotope groups to stratigraphy

The isotope groups temporally and spatially correlate with position in the volcanic section (Figure 16). The Ivan Canyon andesite is the oldest unit and corresponds to isotope group B. The next unit above the Ivan Canyon andesite, the Colony dacite, corresponds to groups C and D. The Farmer Canyon andesite belongs to group C, but the top of the upper member of the Farmer Canyon section is isotope group B. Dikes cutting the lower member of the Farmer Canyon unit belong to group D. Most of the samples collected are andesites from the Fog Ridge andesite section where isotope groups A and B are prevalent. Samples of the Fog Ridge andesite that lack isotope data, therefore, most likely belong to isotopic groups A and B.

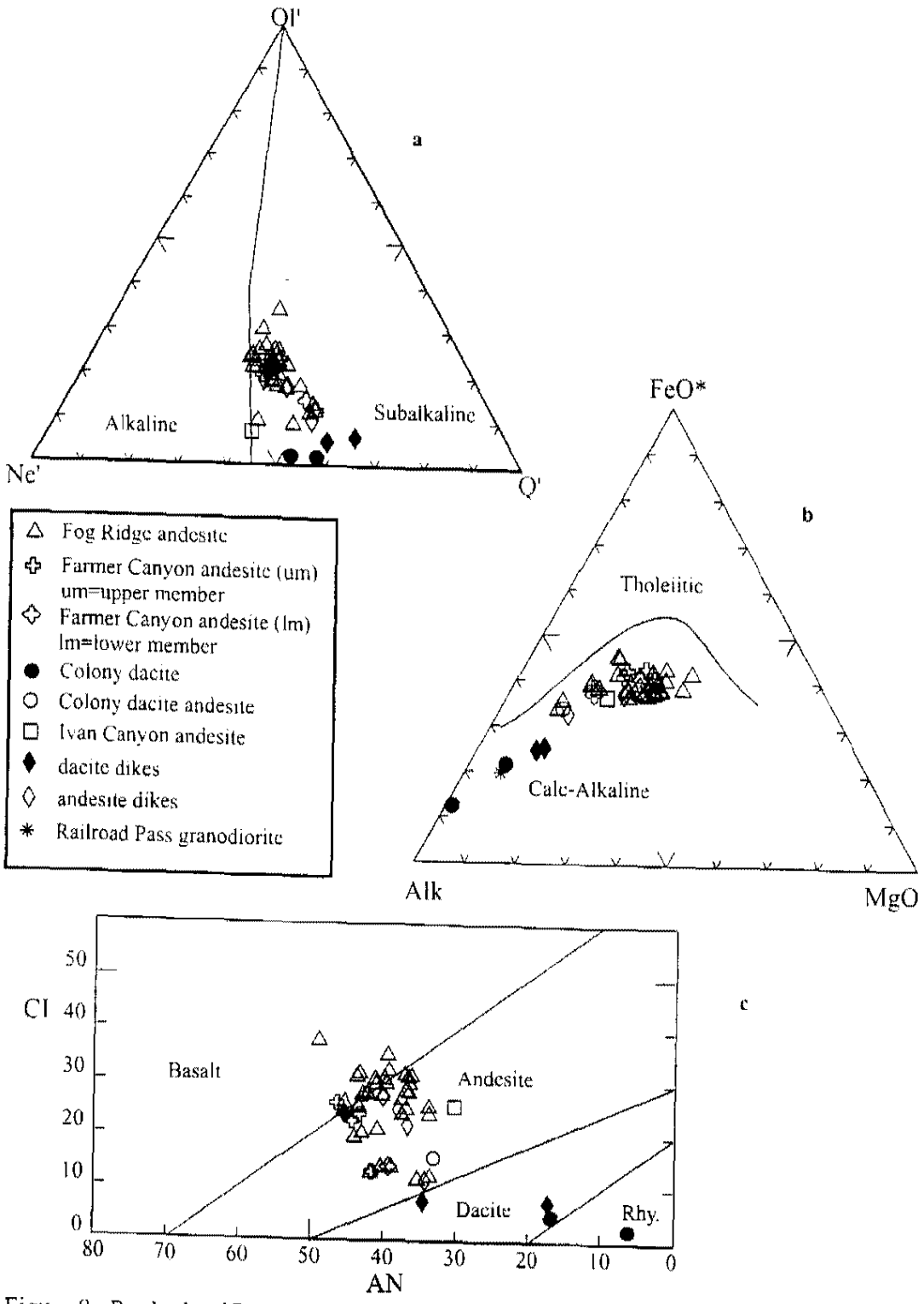

Figure 8. Rock classification diagrams of the volcanic rocks in the northern McCullough Range (Irvine and Baragar, 1971). (a) Alkaline vs. subalkaline. (b) Tholeiitic vs. calc-alkaline. (c) AN vs. CI. AN= 100 An/(An+Ab+(5/3Ne)), CI-Color Index=normative ol+cpx+mt+il+hm in wt. %, Ne'=Ne+3/5 Ab, Ol'=Ol+3/4 Opx, Q'=Q+2/5 Ab+1/4 Opx.

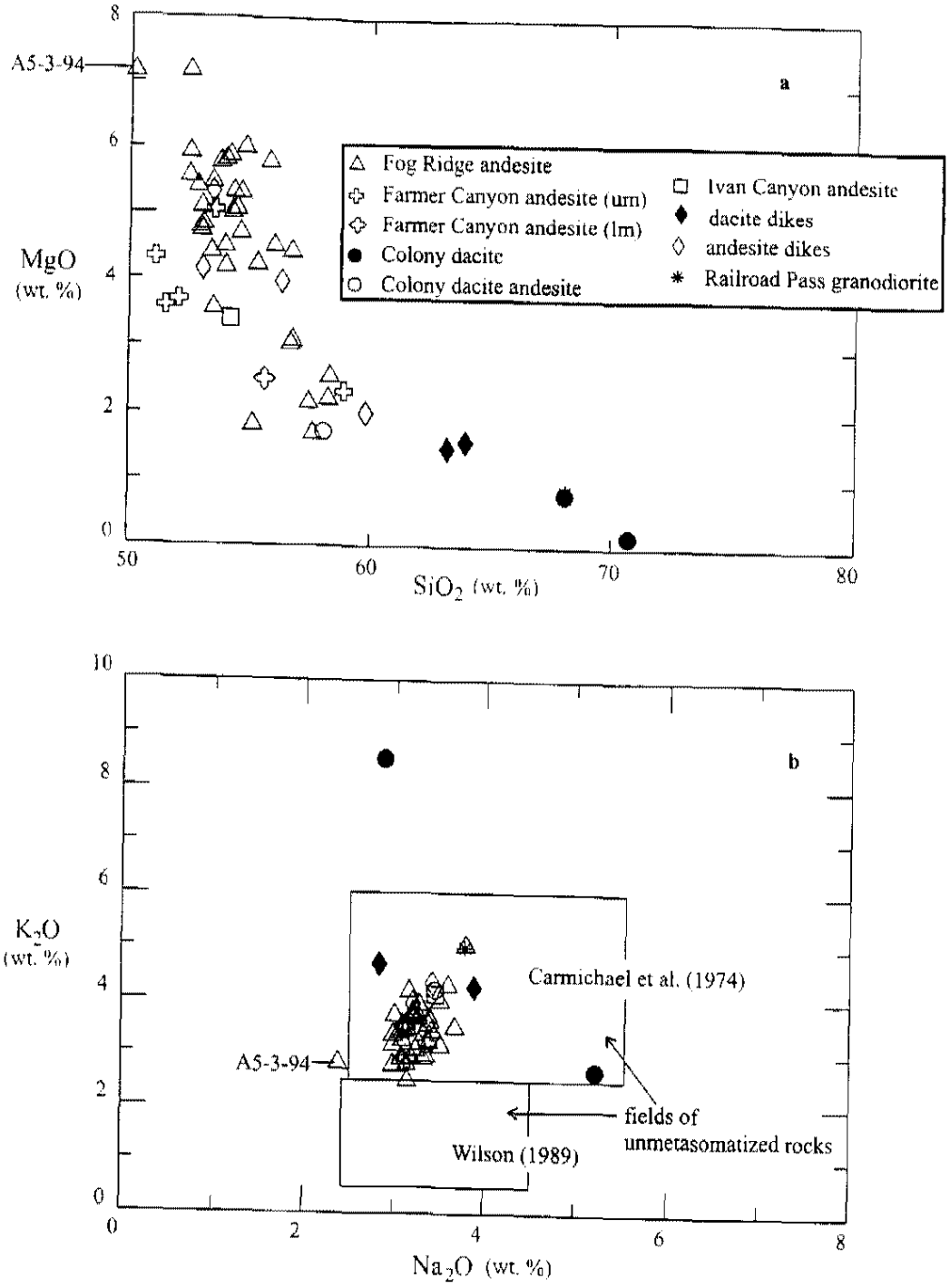

Figure 9. (a) Plot of SiO_2 (wt. %) vs. MgO (wt. %). (b) Plot of Na_2O (wt. %) vs. K_2O (wt.%) showing where the northern McCullough Range rocks fall relative to fields of unmetasomatized igneous rocks defined by Carmichael et al. (1974) and Wilson (1989). Inset key applies to both plots.

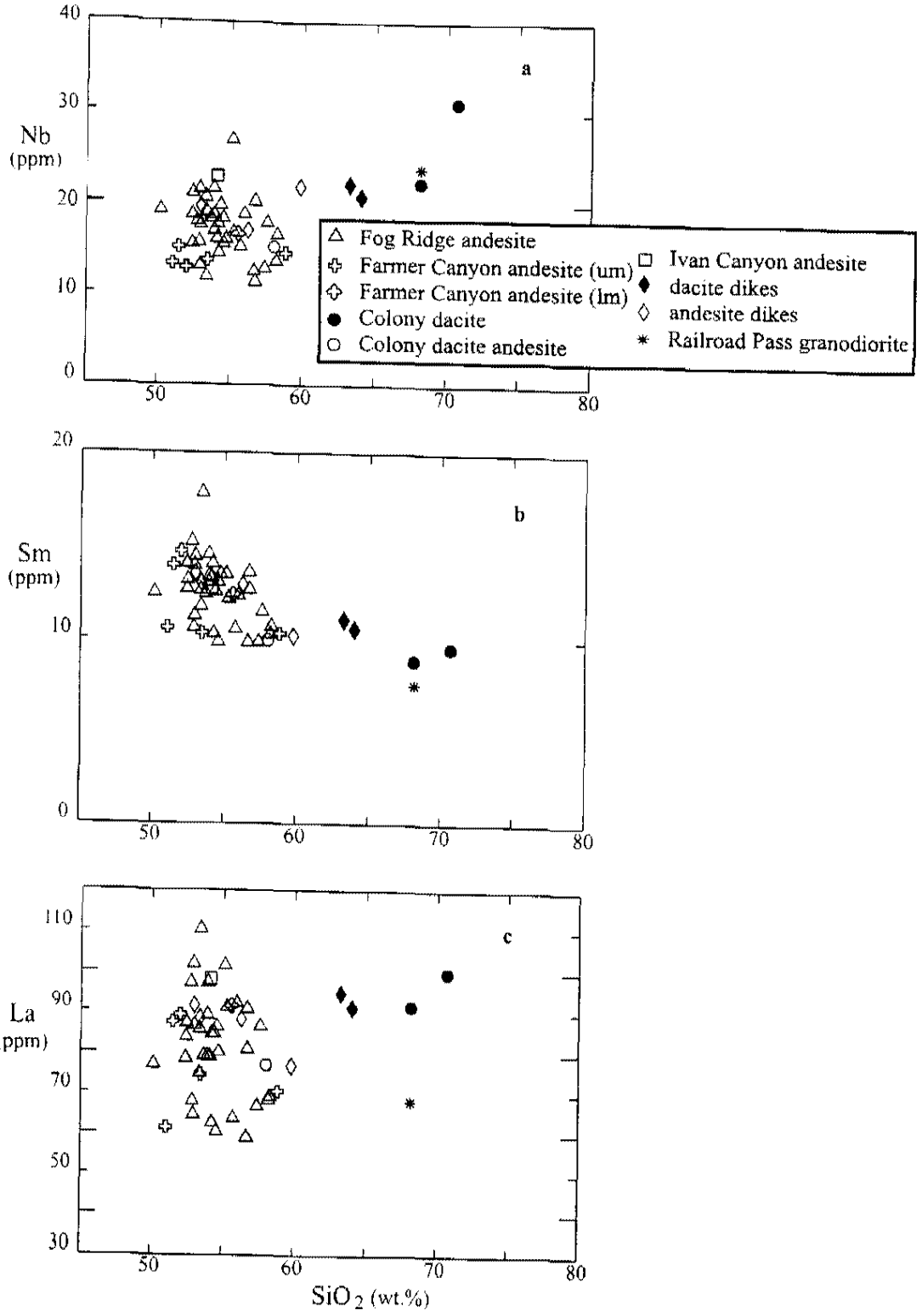

Figure 10. Harker diagrams of incompatible elements plotting SiO_2 (wt. %) vs. incompatible trace elements Nb, Sm, and La (ppm). Note the lack of increase in incompatible trace element concentrations for the andesites with increasing SiO_2.

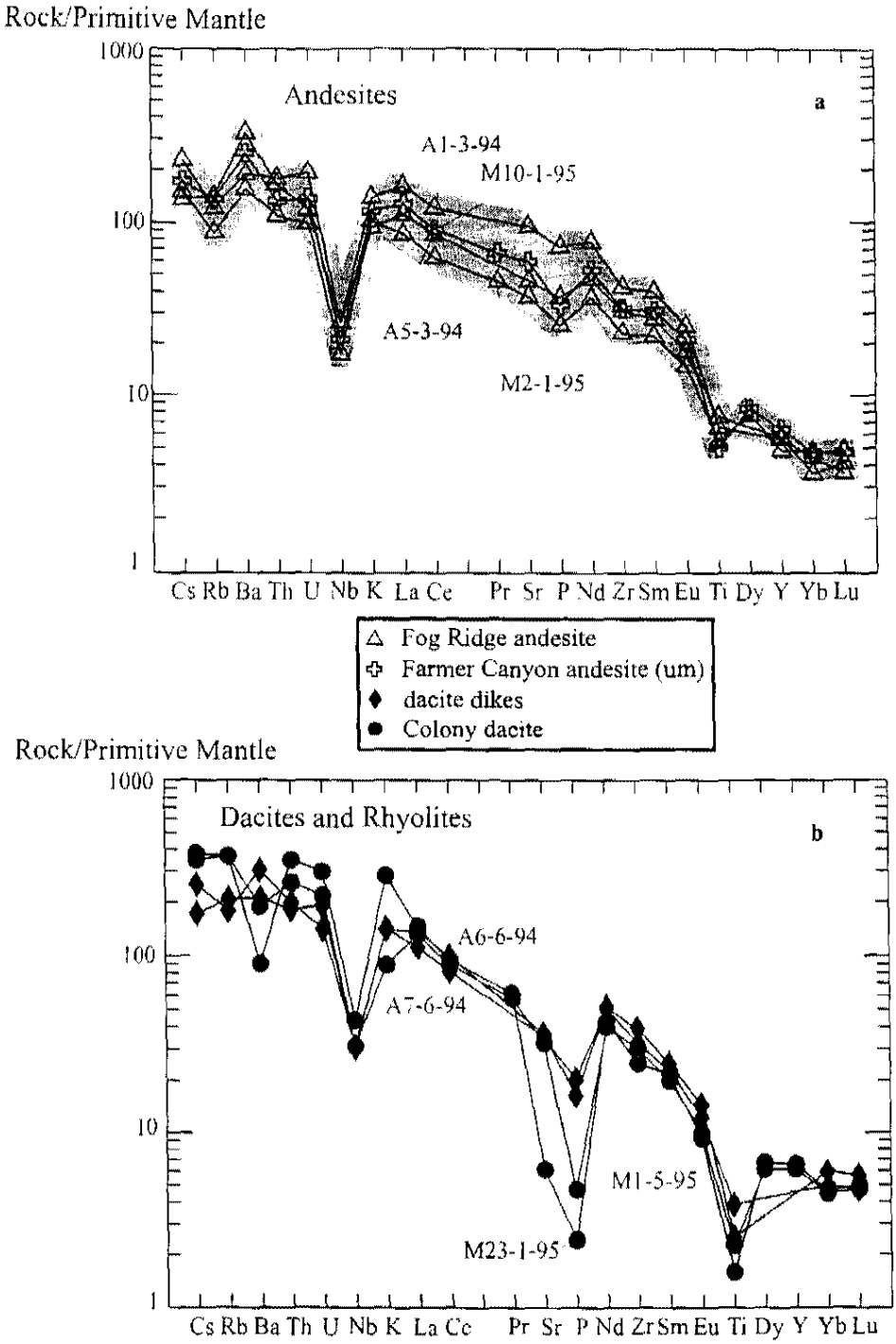

Figure 11. Primitive mantle normalized diagrams using abundances from Sun and McDonough (1989). (a) Andesites from the northern McCullough Range. Shaded region represents the overall range of compositions of andesites analyzed in this study. Four samples are plotted to show details of element distribution. Andesites in the northern McCullough Range are enriched in LIL and LREE relative to HFSE and HREE. Note Nb trough and Ti depletion. (b) Dacites and rhyolites in the northern McCullough Range are more enriched in LIL and LREE and more strongly depleted in P and Ti compared to primitive mantle.

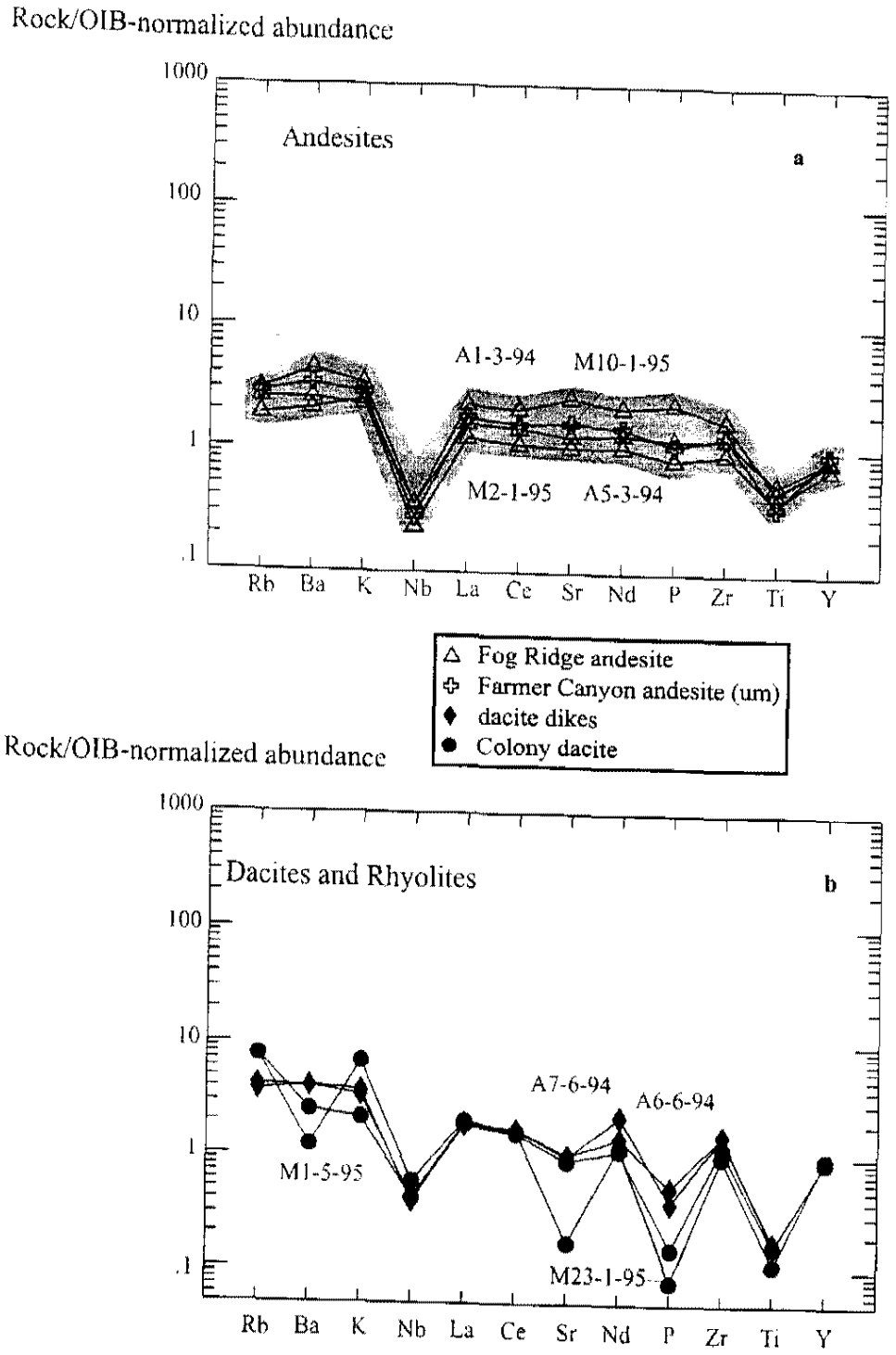

Figure 12. OIB normalized diagrams using abundances from Fitton et al. (1991). (a) Andesites from the northern McCullough Range are similar to OIB except for troughs at Nb and variable depletion of Ti. Shaded region represents the overall range of andesites analyzed in this study. Four samples are plotted to show details of element distribution. (b) Dacites and rhyolites from the northern McCullough Range are more enriched in LIL than OIB but also exhibit a trough at Nb and depletion of Ti. Also, note the variable depletion in P.

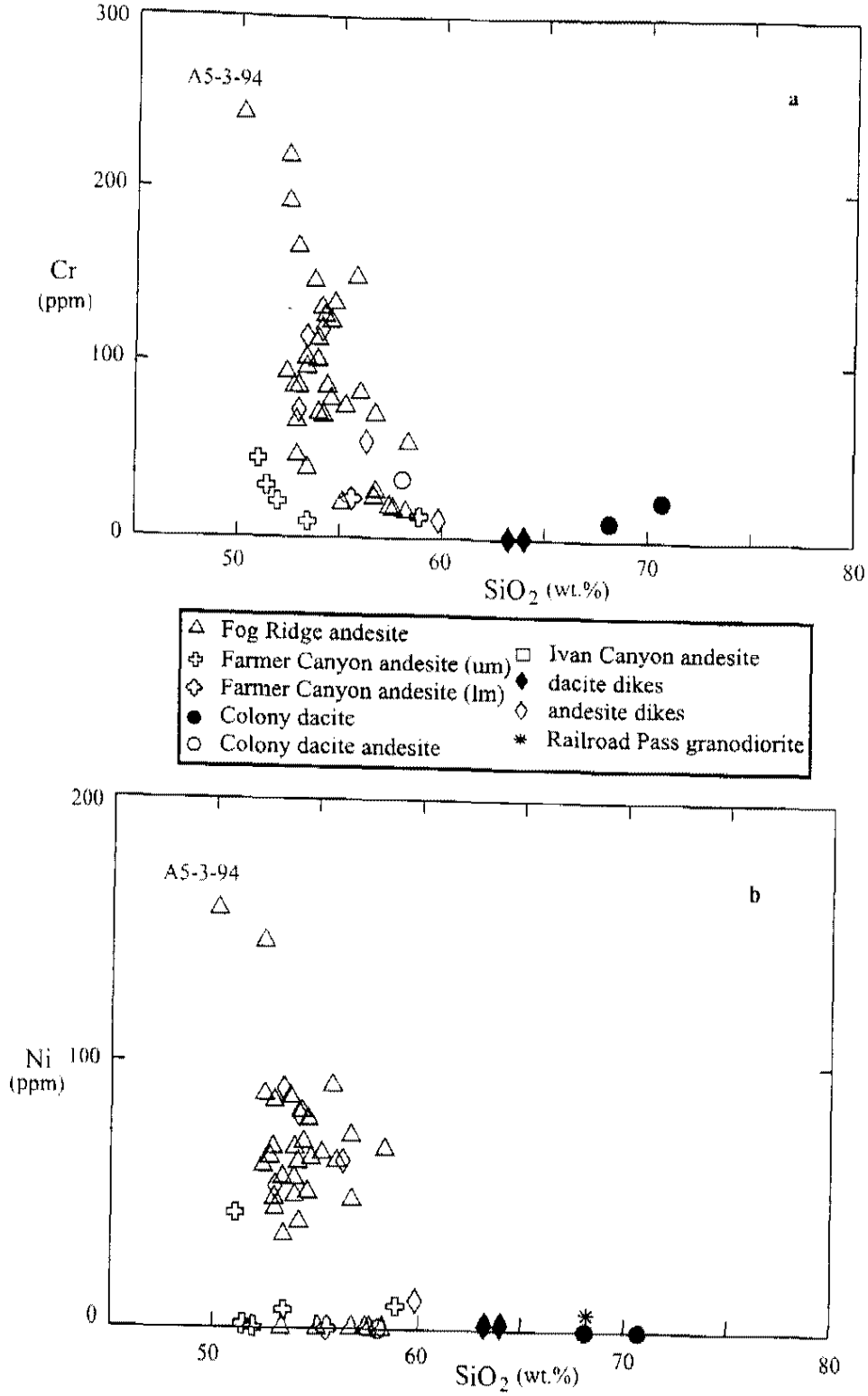

Figure 13. Harker diagrams plotting SiO_2 (wt.%) vs. compatible trace elements Cr and Ni (ppm). Sample A5-3-94 from the Fog Ridge andesite is the least evolved andesite sample from the northern McCullough Range. (a) Cr decreases with increasing SiO_2. (b) Ni also shows a decrease in the range of abundance with increasing SiO_2.

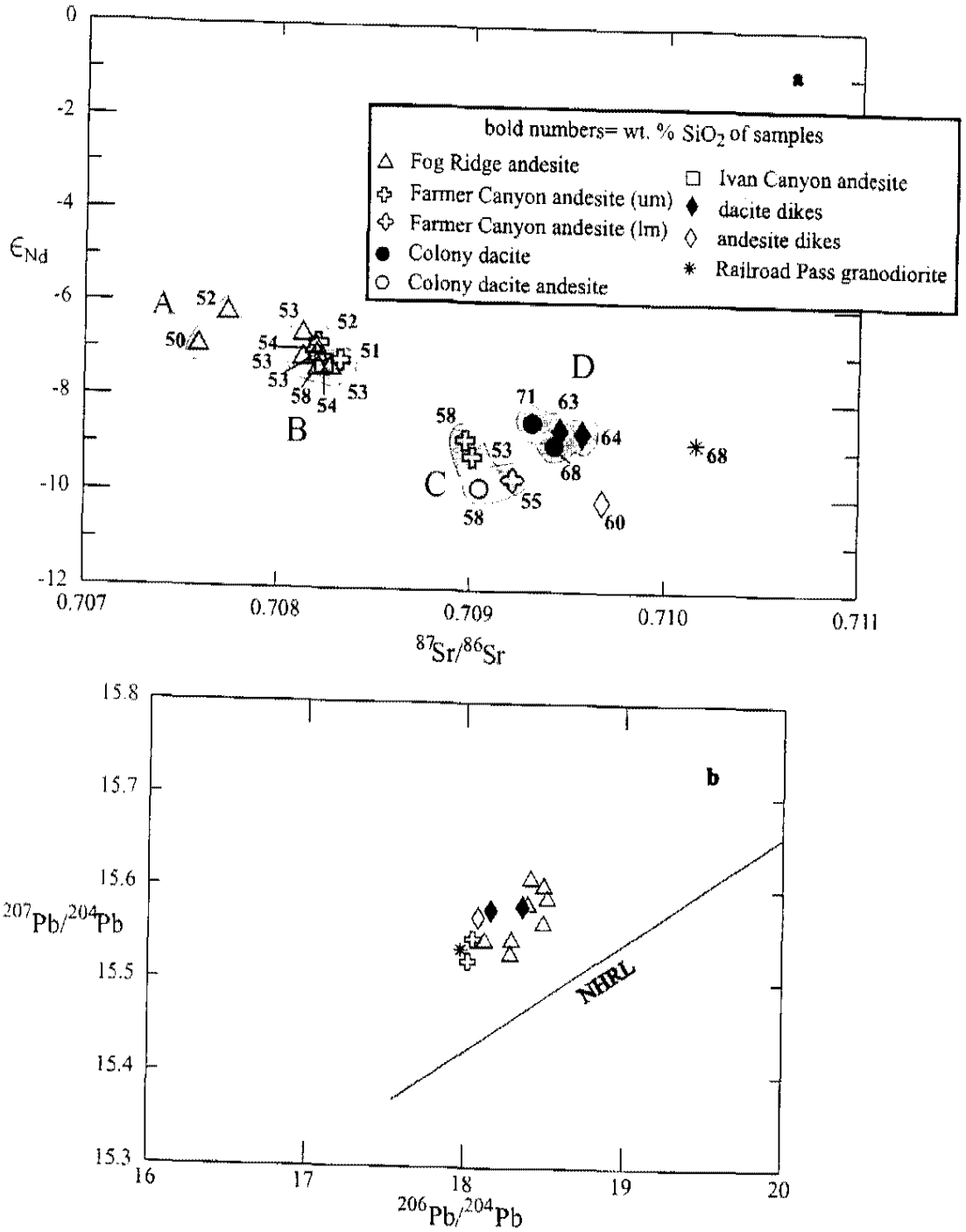

Figure 14. Isotope plots for rocks in the northern McCullough Range. (a) $^{87}Sr/^{86}Sr$ vs. Epsilon Nd shows four isotopic groups: A, B, C, and D. Bold numbers are SiO_2 concentrations for each sample. SiO_2 values between groups A, B, and C do not vary significantly. Note the gaps between groups, especially between groups B and C. (b) Rocks plot above the Northern Hemisphere Reference Line (NHRL) on a $^{207}Pb/^{206}Pb$ diagram. Isotopic ratios of the northern McCullough Range rocks are typical of pre-9 Ma rocks in the NCREC (Feuerbach et al., 1993) (Also, see Figure 16). um=upper member; lm=lower member

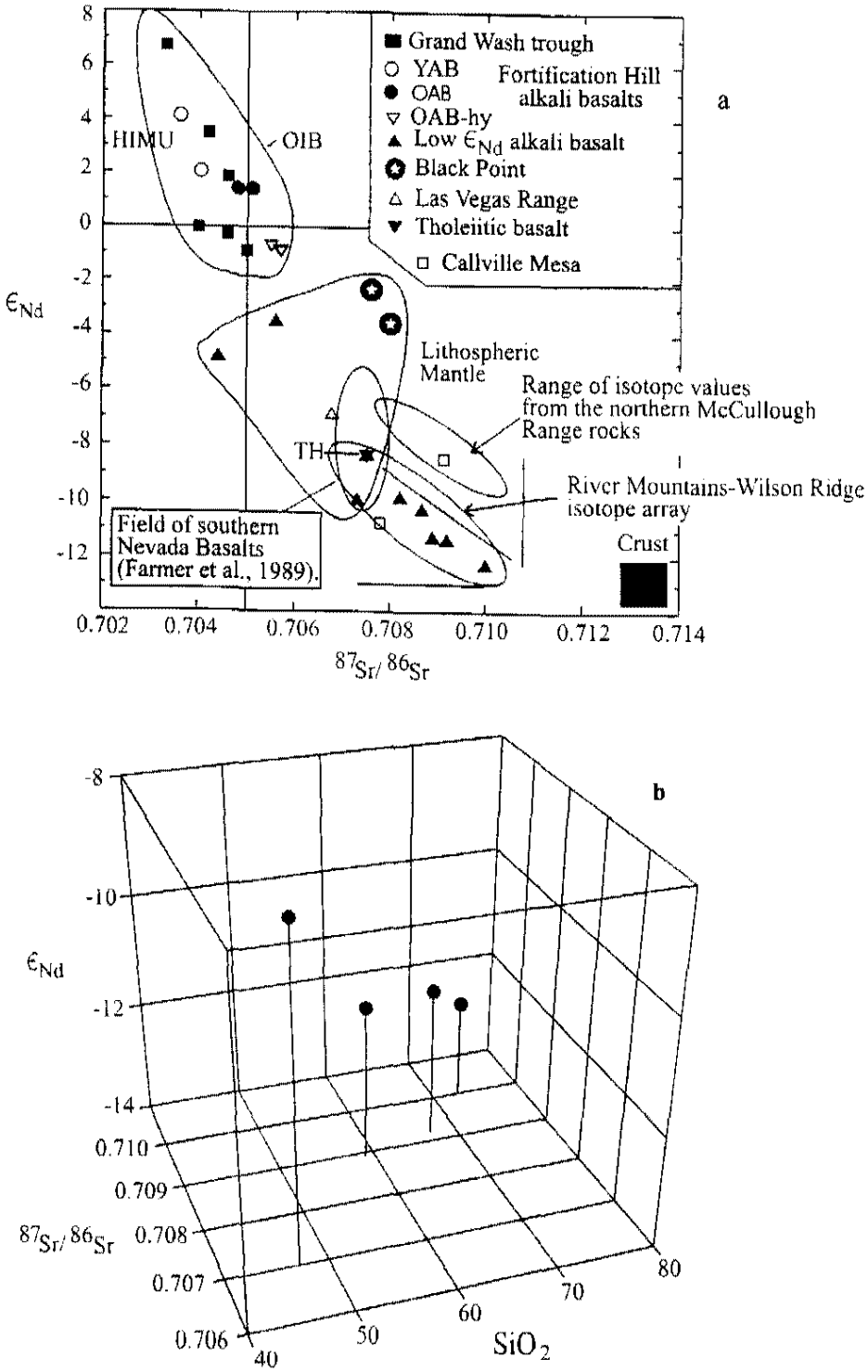

Figure 15. Isotopic data for the River Mountains-Wilson Ridge system from Feuerbach et al. (1993). (a) $^{87}Sr/^{86}Sr$ vs. ϵ_{Nd} demonstrates that in this system a mafic mantle component may have mixed with a crustal component to form the linear data array observed. The McCullough Range data array is shown for comparison. (b) The increase in SiO_2 with increasing $^{87}Sr/^{86}Sr$ and decreasing ϵ_{Nd} reflects the addition of a crustal component in the River Mountains system.

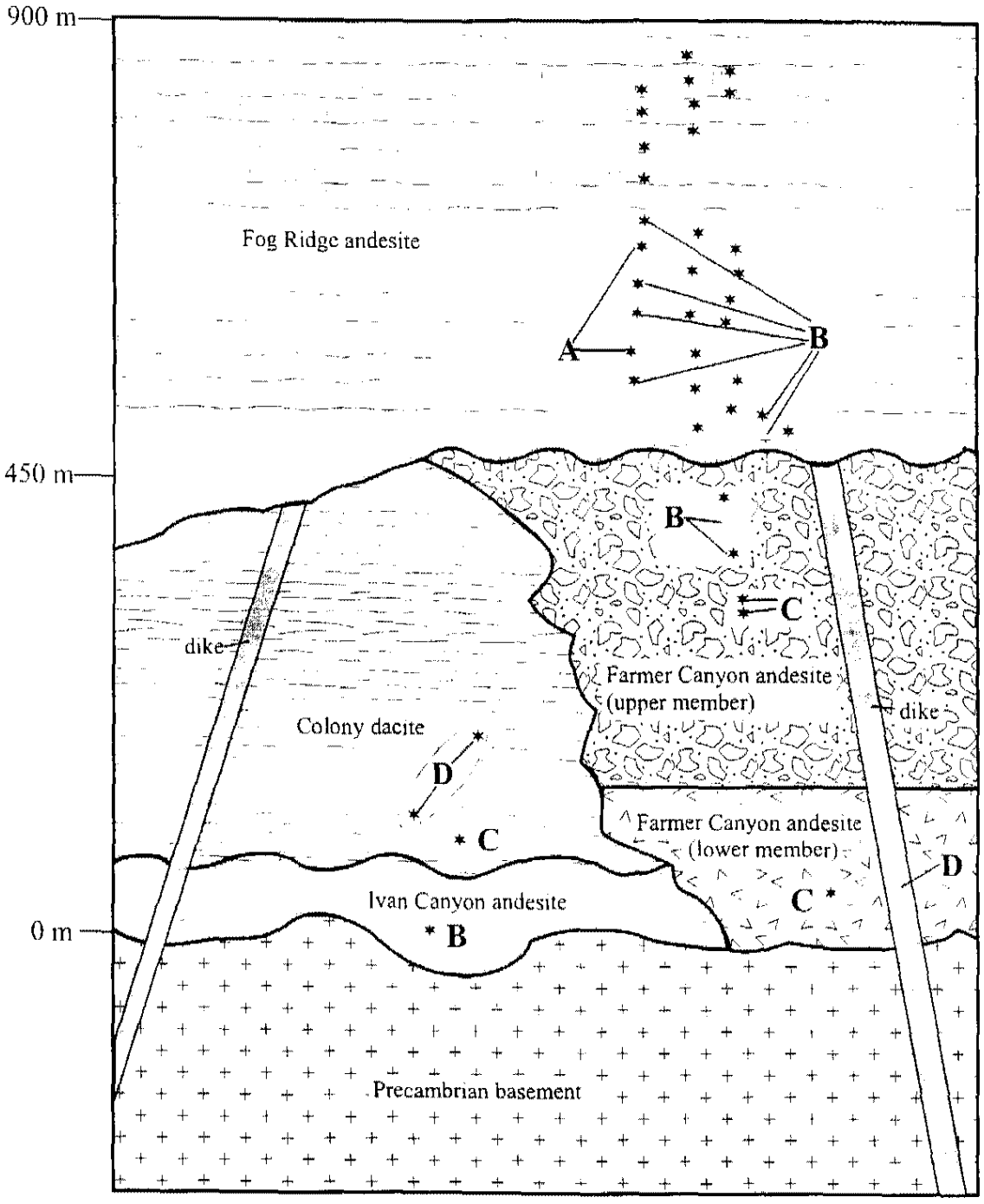

Figure 16. Diagrammatic stratigraphic column of the northern McCullough Range showing correlation of isotopic groups (shown in bold letters A,B,C,and D) to position in the section. Unit thicknesses are variable and estimated from calculations on map (see Plate 1). Black stars represent approximate location of rock samples within the section. Dikes shown are diagrammatic and do not represent true orientation.

Chapter 5

Geochemical Modeling

Introduction

Any proposed model for the petrogenesis of andesites in the northern McCullough Range must honor the geochemical observations described in the previous chapter. These observations include the lack of increase of incompatible elements with increasing SiO_2 (Figure 10), the wide variation in trace element chemistry among the andesites, the existence of four isotope groups (Figure 14a), significant gaps between groups and the change in slope of the isotope array between isotopic groups B and C, the fact that rocks of three isotopic groups (A, B, and C) have similar SiO_2 values, the lack of correlation between SiO_2 and isotopic ratio, and the evolved chemistry of parental andesites as indicated by low Mg #'s, Cr, and Ni (Figures 9a and 13).

Before modeling the petrogenesis of the andesites, it is important to discuss the significance of the four isotope groups. I suggest that isotope groups A, B, and C represent three distinct andesitic end member magma types. The following observations support this hypothesis. Crystal fractionation alone will not change isotope ratios and therefore, can not be used to explain the variation between the four isotope groups. Assimilation of felsic crustal rock or mixing of

a felsic component with isotope group A to produce the isotopic and chemical signatures of isotope groups B, C, and D is unlikely due to the nature of the gap between groups B and C and the lack of correlation of SiO_2 and isotope ratios. If the addition of an upper crustal component or mixing with a felsic magma produced the differences between isotope groups, a correlation should exist between isotope ratios and SiO_2 content as observed in the River Mountains system (Figure 15b). An important assumption of the petrogenetic models is that isotopic groups A and B are cogenetic. Similar trace element concentrations and isotopic ratios for isotopic groups A and B support this assumption.

This chapter is divided into two sections which describe a three stage model for the origin, evolution, and interactions of the andesitic magmas represented by isotopic groups A, B, and C. Note that the numbering of the stages (1,2, and 3) is intended to reflect the chronology of events that resulted in the production of the andesites of the northern McCullough Range. The first section describes the petrogenetic models used to evaluate the evolution and interactions of these isotopically distinct andesitic magmas and their role in producing the andesites in the northern McCullough Range (stage 3). The second section describes the possible origin and history of the primitive magmas and the evolutionary processes that may have occurred to produce the resulting parental andesitic magma types represented by isotopic groups A, B, and C (stages 1 and 2). While the discussion of stages 1 and 2 are based on literature review, the petrogenetic models developed to describe stage 3 are original and an important contribution of this thesis.

Petrogenetic Models (Stage 3)

The following section describes stage 3, the evolution and interactions of the andesite magmas types. Stage 3 is the focus of this study and presents a new petrogenetic model that explains the evolution of volcanic systems dominated by andesite magma. The following sections evaluate fractional crystallization (FC), recharge, assimilation and fractional crystallization (AFC), and magma mixing models.

Fractional Crystallization

FC models tested the chemical variation among the upper Farmer Canyon and Fog Ridge andesites associated with isotopic groups A and B. Because all isotopically analyzed samples of the Fog Ridge andesite belong to isotopic group A or B, it is assumed that the Fog Ridge andesite samples that lack isotopic data belong to groups A and B. FC models use sample A5-3-94 as the parent because A5-3-94 is the most mafic and least evolved of all the samples based on SiO_2 (50.2 wt. %), MgO (7.2 wt. %), Ni (158 ppm), and Cr (243 ppm) contents (Figures 9a and 13). Distribution coefficients (D) for the models are primarily from a compilation by Larsen and Smith (1990) and are listed in Table 1. Refer to Table 2 for a summary and details of models.

FC models compare the behavior of various incompatible elements (Rb, Sm, La, and Ba) with compatible elements and oxides such as MgO, Cr, and Sr. During differentiation processes such as fractional crystallization, incompatible elements will preferentially partition into the melt while compatible elements remain in the mineral phases. MgO and Cr are very compatible in clinopyroxene and olivine which are the dominant phenocryst phases fractionated from the andesites. Removal of these phases, therefore, will result in a decrease in

abundance MgO and Cr with increasing amounts of fractionation. Sr is compatible in plagioclase and will behave in a similar manner provided plagioclase is fractionated.

Model 1 shows that any combination of plagioclase (plag), olivine (ol), and clinopyroxene (cpx) fractionation can not successfully produce most of the andesites (Figure 17, plots 1-1 through 1-6; Table 2). FC will increase incompatible element concentrations in the evolved liquid. This trend is not observed. Only 100% fractionation of cpx approaches and contains some of the andesite samples. The few samples that consistently fall within the fractionation field are A1-3-94, A2-3-94, and A3-3-94, all from the Fog Ridge andesite (Figure 17). However, the difference in Sr and Nd isotopes between the parent (A5-3-94 of isotopic group A) and A1-3-94 and A3-3-94 (isotopic group B) rules out fractionation alone from A5-3-94 to produce these two samples (Figure 14a). A2-3-94, however, does lie within isotope group A along with A5-3-94 and may be explained by fractionation. In conclusion, based on trace element modeling and isotopic evidence, FC can not explain the chemical variation among the andesites.

Modeling also determined if fractionation was a significant process in producing variations in rock compositions within each isotopic group (Figure 18, Models 2, 3, and 4; Table 2). SiO_2, MgO, and Cr contents identified the least evolved sample within each group to use as the parent. Previous FC modeling showed that within isotope group A, fractionation of A5-3-94 may have produced A2-3-94 (Figure 17). However, this is the only successful FC model. Models 2, 3, and 4 demonstrate that within isotope groups B, C, and D respectively, fractionation vectors point away from the more chemically evolved

samples (Figure 18). FC, therefore, does not explain intragroup chemical variation.

Table 1. Distribution coefficient (D) values used in modeling.

	plagioclase	clinopyroxene	olivine	biotite
La	0.2†	0.12†	0.03†	0.7†
Ce	0.12	0.15	0.03†	0.9
Sm	0.067	0.5	0.0013*	0.6
Rb	0.031	0.031	0.04†	4
Ba	0.23	0.026	0.03†	8
Yb	0.067	.62	0.0015*	0.45
Sr	1.88	0.1	0.02†	0.15
Cr	0.01	8.4	2.8†	10
MgO	0.04†	5.4†	9.5†	35†

Values from Table 5, Larsen and Smith, 1990
† values from Villemant et al., 1981
* values from Bradshaw, 1991

Recharge

Recharge of a magma chamber serves to increase incompatible element concentrations in the melt. In fact, the increase in incompatible elements due to magma recharge is even more pronounced than from crystal fractionation (O'Hara, 1977). The enhancement of incompatible element abundances occurs because new magma containing incompatible elements is added to a liquid that was previously enriched in incompatible elements by crystal fractionation. O'Hara's equations predict the increase of incompatible element concentrations for a series of recharge steps based on the concentration of the elements in the parent magma, the amount of recharge vs. fractionation, and the amount of magma erupted from the chamber (overall volume remains constant). Recharge

models for the andesites of the McCullough Range used the composition of sample A5-3-94 (isotopic group B from the Fog Ridge andesite) as the least evolved magma (Figures 9a and 13). Plots of La′ and Th vs. MgO show results of the recharge model for 10% and 50% recharge (relative to fractionation and total amount erupted) (Figure 19, plots 5-1 and 5-2; Table 2). La′ is an enrichment factor calculated by dividing the La concentrations of all the samples by the La concentration of the parent magma. The plots show that the incompatible element concentrations of the McCullough Range samples do not increase at the rate predicted by a recharge process. Recharge models, therefore, can not explain chemical variations in the McCullough Range samples.

Assimilation and Fractional Crystallization (AFC)

The first step in the (AFC) modeling process (DePaolo, 1981) is to choose the proper felsic end member to mix with a mafic component. Potential felsic end members from within the northern McCullough Range (e.g., A8-6-94 from the Railroad Pass Pluton) do not produce reasonable models to explain intragroup or intergroup variation because trace element concentrations and $^{87}Sr/^{86}Sr$ ratios (Figure 14a) are too low. Felsic rocks, therefore, from nearby areas in the (NCREC) were evaluated as possible end members. Metcalf et al. (1993a) point out that although parental mafic magmas in the NCREC vary significantly in chemistry, felsic end members are quite similar; rhyolites and granites from the NCREC have similar trace element patterns and isotopic signatures. It is acceptable, therefore, to use a felsic end member composition from a nearby area for modeling. Felsic rocks that may be suitable end members crop out in the Mt. Perkins Pluton, the Wilson Ridge Pluton, the Aztec Wash

Pluton, and the Dolan Springs volcanic field (Metcalf et al., 1993a; R.V. Metcalf, personal commun.) (Figure 1).

A suitable felsic end-member must lie roughly on trend with the McCullough Range data array and have a high $^{87}Sr/^{86}Sr$ value. A granite from the Mt. Perkins Pluton (sample 922-10) satisfies this criterion. This sample contains 73.97 wt. % SiO_2, has a $^{87}Sr/^{86}Sr$ of 0.71267, and an ε_{Nd} of -12.5 (Metcalf et al., 1995) (Figure 20a). Adding even a small amount of this magma type to a mafic magma would increase the $^{87}Sr/^{86}Sr$ values of the mafic magma significantly. Sample 922-10 is an example of the type of felsic end member required to produce variations in the McCullough Range volcanic rocks and may not be the actual assimilant.

To evaluate the chemical variation among and within isotope groups, the same fractionation models described above were modified to include varying amounts of the Mt. Perkins (922-10) felsic end member (plots are not shown). AFC models using 922-10, however, can not explain variation among groups A, B, or C because adding even a small amount of a felsic component such as 922-10 with 74 wt. % SiO_2 would result in a significant increase (5-10 wt. %) in the silica content of the andesites. The SiO_2 content of the andesites does not increase with increasing $^{87}Sr/^{86}Sr$ or decreasing ε_{Nd} (Figure 20a). For this reason, AFC models using the Mt. Perkins felsic end member are not successful in producing compositional variations within isotope groups.

AFC models 6 and 7 using the felsic end member from the Mt. Perkins Pluton, however, were acceptable in producing group D dacite dikes from a basaltic andesite in group C (Figure 20b and Figure 21; Table 2). Twenty percent fractionation of 50% cpx and 50% plagioclase from a group C andesite (A1-6-94) and addition of 922-10 (4-8%) with an r value (r=ratio of mass assimilated to

mass crystallized) between 0.2-0.4 produced samples A6-6-94 and A7-6-94 (dacite dikes) of group D.

Other felsic rocks of group D (Colony dacite M5-1-95 and rhyolite M23-1-95), however, are not a result of assimilation, mixing or commingling of group C with a felsic end member such as 922-10. These samples fall between group C and the Mt. Perkins sample, however, the SiO_2 contents are too high for their position on the plot (Figure 20a). If samples M5-1-95 and M23-1-95 were part of this mixing trend, the higher SiO_2 contents should correspond to higher $^{87}Sr/^{86}Sr$ values. These Colony samples, therefore, are not part of this mixing trend and may represent an independent felsic component. AFC models 6 and 7 using felsic component 922-10, therefore, can explain some of the variation between groups C and D, but AFC can not explain variation between A and B, B and C, or variations within groups.

Magma mixing

Evaluation of magma mixing as a process in the northern McCullough Range included models with a felsic end member and those that involved mixing isotopically distinct andesitic magmas. A felsic mixing component, however, is not viable for the following reasons. Recall that the silica values among the isotope groups, particularly groups A, B, and C, do not vary much, and do not correlate well with initial Sr (Figure 14a and 20a). Mixing a felsic component with an andesitic magma would increase the initial Sr values, as is observed, however, mixing even small amounts of a felsic component to these andesitic magmas with moderately high Nd and Sr contents would also increase the silica values significantly. This trend is not observed, thus effectively ruling out models that involve felsic end members. Because most of the andesites are from

the upper Farmer Canyon and Fog Ridge andesite sections where isotopic groups A and B are prevalent, models were created to evaluate mixing between andesitic magmas of groups A and B.

End members are difficult to identify for this type of model because the andesites have a limited range of chemistry and isotope values. Models, therefore, are qualitative and mixing fields are created rather than typical mixing curves. End members for each group were chosen by selecting samples that are representative of the chemical range within the isotope group. Samples A1-3-94 and A4-6-94 were chosen as end members to represent isotope group B. These samples are intermediate in silica content (~ 53 wt. %) relative to the rest of the group (51-58 wt. %) and representative of the range of incompatible trace element content (for example, La values are 110 ppm for A1-3-94 and 67.9 ppm for A4-6-94). Incompatible elements were chosen rather than compatible elements because their analytical uncertainties are smaller (for example 0.63 % for La and 4.90 % for the compatible element Cr; see Appendix III) and they probably better represent differences in source compositions. Isotopic group A is defined by only two samples; sample A5-3-94 with the highest Cr, Ni, and MgO concentrations was chosen as the end member. Lines were drawn between the end member compositions of isotopic groups A and B to define a mixing envelope. These lines are not intended to represent unique mixing curves. The lines represent boundaries of a mixing envelope that contains permissible mixing models. The exact number of mixing end members is unknown. It is possible that the hybrid samples within the envelope were produced by 2, 3, or multi-component mixing. Mixing processes may also involve 1 or more stages.

A Cr vs. La/Yb plot shows the envelope created by mixing isotopic groups A and B (Figure 22a and b; Table 2). All samples analyzed for isotopes

are included on this figure. Figure 22b includes the upper Farmer Canyon and Fog Ridge andesites with and without isotope data. Many of the andesite samples fall within or close to the field created by mixing of groups A and B. The dimensions of this mixing envelope, however, are based entirely on the positions of isotopically analyzed samples. It is possible that obtaining further isotopic data for andesites outside of the mixing envelope might change the shape of the envelope and enlarge the mixing field (Figure 22b). Similar results are obtained by plotting other elements such as Zr vs. Nb (Figure 22c).

Although these mixing models are permissive, several problems exist. First, there is considerable trace element variation within isotope group B samples. This variation was evaluated and can not be explained by FC or AFC (see previous explanation and Figures 17 and 18). Additionally, the model appears to contradict the isotope data which display a gap between groups A and B (Figures 14a and 20a). If mixing occurred between groups A and B, hybrids of this mixing should be observed on the isotope plot between groups A and B, rather than a gap. Instead of calling upon a sampling bias to explain the gap, it is possible that the gap has physical significance and no mixing occurred between groups A and B. An alternative explanation is that mixing occurred between isotopically distinct magma types within isotopic group B. A Cr vs. La/Yb plot was also used to test possible mixing within isotopic group B (Figure 23a; Table 2). End members were selected to represent the range of trace element and isotopic variation within group B. Samples A3-3-94 (Cr=248 ppm, La=101 ppm, Zr=415 ppm, $^{87}Sr/^{86}Sr$=0.70819, ε_{Nd}=-7.10) and A4-6-94 (Cr=116 ppm, La=67.9 ppm, Zr=315 ppm, $^{87}Sr/^{86}Sr$=0.70812, ε_{Nd}=-7.17) were selected as end members. Although the fit is poor, many (6 of 9) of the upper Farmer Canyon and Fog Ridge andesites of isotopic group B fall around and near to this mixing

line. Using these same end members on a plot of Zr vs. Nb also demonstrates mixing of different andesitic magma types within group B (Figure 23b). Most of the group B samples (7 of 9) and many of the upper Farmer Canyon and Fog Ridge andesites that lack isotopic data also fall along this mixing line. In these examples, mixing is occurring entirely within group B, and isotopic group A is not a mixing component. This model has the advantage of explaining the gap in the values of isotopic ratios between groups A and B and the range of trace element concentrations within group B.

Although the choice of end members is somewhat subjective, the models that mix isotopically distinct andesitic magmas to produce the chemical variations observed among the andesites in the northern McCullough Range are compelling. In summary, magma mixing between isotopically distinct andesitic magmas represented by groups A and B or mixing of different isotopic types within group B is the preferred petrogenetic model to explain andesite formation in the northern McCullough Range. Group C andesites are probably not cogenetic with group A and B magmas and represent an independent andesitic magma type that co-existed but did not mix with either group A or B magmas.

Table 2. Summary of petrogenetic models.

Model number	Type of model	Elements used	Details (*=minerals fractionated at 100%)	Corresponding figure number in text
1-1	FC	MgO vs. Ce	plag, cpx, ol *	Figure 17
1-2	FC	Cr vs. Rb	plag, cpx, ol *	Figure 17
1-3	FC	Cr vs. Sm	plag, cpx, ol *	Figure 17
1-4	FC	MgO vs. Sm	plag, cpx, ol *	Figure 17
1-5	FC	MgO vs. La	plag, cpx, ol *	Figure 17
1-6	FC	Cr vs. Ba	plag, cpx, ol *	Figure 17
2	FC	MgO vs. Ce	plag, cpx, ol *	Figure 18
3	FC	Sr vs. Yb	plag, cpx, ol, bio *	Figure 18
4	FC	Sr vs. Ce	plag, cpx, bio *	Figure 18
5-1	recharge (10%)	MgO vs. La'		Figure 19
5-2	recharge (50%)	MgO vs. Th		Figure 19
6-1	AFC	Sr vs. Ce	50% cpx, 50% plag; r=0.4	Figure 20b
6-2	AFC	Sr vs. Rb	50% cpx, 50% plag; r=0.4	Figure 21
7	AFC	MgO vs. Ce	50% cpx, 50% plag; r=0.2	Figure 21
8-1	mixing	Cr vs. La/Yb	groups A & B	Figure 22a and b
8-2	mixing	Zr vs. Nb	groups A & B	Figure 22c
9-1	mixing	Cr vs. La/Yb	within group B	Figure 23a
9-2	mixing	Zr vs. Nb	within group B	Figure 23b

Discussion

Conclusions from modeling

The petrogenesis of the andesites in the northern McCullough Range is very complicated and involves fractionation and open system processes such as assimilation and magma mixing. The petrogenetic modeling presented above, however, rules out fractionation, assimilation, and recharge as the dominant processes in explaining the chemical variations (Figures 17, 18, 19, 20,and 21).

Magma mixing of andesitic magmas best explains the observed variation of most McCullough Range andesites. Mixing or assimilating a felsic component, however, would increase SiO_2 contents out of the range observed in isotope groups A, B, and C. Based on the above petrogenetic models, geochemical trends, and isotopic data, I suggest that the andesites of the northern McCullough Range were produced primarily by the mixing of isotopically distinct andesite magmas represented by groups A and B, or mixing of different isotopic types within group B (Figures 22 and 23). Andesites of group C are independent and did not mix with A or B but might have mixed with a felsic component to produce some felsic dikes in group D. An advantage of the model is that it explains the occurrence of andesite dominated systems.

The mixing plots show that a group of andesites falls outside of the mixing field between groups A and B (outlying group on Figure 22b and c). It is possible that this group is more representative of an actual end member group, and the remaining andesites of group B and/or A are hybrids. Unfortunately, isotopic data are not available for any of the samples that fall within the outlying group. Isotopic data, however, would indicate whether this group of andesites is an end member and the other samples hybrids. If so, one would expect the

isotopes of the outlying group to fall along the isotope array but outside of groups A and B. This case would not change the proposed model of mixing different andesitic magmas, but would change the mixing end members.

An alternative model is that the andesites are the product of independent andesitic sources (isotope groups A, B, and C) that have not mixed together. The tapping of separate end members without some component of mixing, however, is not compatible with the variation observed in the trace and REE data. The variation of the trace and REE data is greater than that produced by analytical error (Appendix IV). If no mixing occurred, the trace and REE data should group together as does the isotopic data Based on these observations, I conclude that the alternative model is not valid.

To summarize, four events are responsible for producing the northern McCullough Range volcanic rocks: (1) mixing of andesitic magmas of groups A and B, (2) independent eruption of magma of group C, (3) assimilation of Mt. Perkins-type felsic end member with C to produce dikes of group D, and (4) independent eruption of felsic magmas of group D.

Mixing styles in volcanic systems in the southern Basin and Range

During the eruption of the Ivan Canyon andesite and the Colony dacite, mixing of mafic and felsic magmas was a dominant petrogenetic process, and isotopic groups B, C, and D were produced (Figure 16). The McCullough Range magmatic system, therefore, was initially similar to that at Mt. Perkins and in the River Mountains/Wilson Ridge magmatic system (Weber and Smith, 1987; Larsen and Smith, 1990; Smith et al., 1990). By the time that the upper member of the Farmer Canyon andesite was emplaced, there is no longer any evidence of a felsic end member or the presence of isotope group D. Mixing of andesitic end

members became the dominant process. Towards the end of the eruption of the upper member of the Farmer Canyon andesite, only isotope group B was present. Finally, the formation of the Fog Ridge andesite introduced isotope group A into the section. Isotope groups A and B remain throughout the evolution of the Fog Ridge andesite (Figure 16).

The development of the northern McCullough Range volcanic section, therefore, was dominated first by mixing of andesitic and felsic magma and later by mixing of different andesitic magmas. The formation of the volcanic section involved two styles of magma mixing; the Mt. Perkins style where a felsic magma mixes with a mantle-derived mafic magma and the McCullough style where different andesitic magmas mix without the participation of a felsic component. The Mt. Perkins process produces a wide range of rock compositions (basalt to rhyolite), whereas the McCullough Range process primarily produces a narrow range of rock compositions (andesite to basaltic-andesite).

The McCullough Range type magmatic system has not previously been documented and is a viable explanation for andesite petrogenesis in extensional terranes. The proposed model should be tested in other thick sections of andesite in the southern Basin and Range, such as those in the Piute Range and the Eldorado Range, and possibly extensional environments in other areas of the world.

Source and Evolution of Andesitic Magma Types (Stages 1 and 2)

The following section provides possible explanations for the origin of calc-alkaline andesitic magmas, such as those found in the northern McCullough

Range magmatic system represented by isotopic groups A, B, and C (Figure 14a). The first step, stage 1, involves the partial melting of a compositionally heterogeneous lithospheric mantle to produce primary mafic magmas. Stage 2 describes processes that result in the chemical evolution of primary magmas of stage 1 to produce the parental magmas of isotopic groups A, B, and C.

Stage 1

Nb and Ti troughs on spider diagrams and radiogenic isotopic ratios suggest that andesites of the northern McCullough Range are partial melts of a lithospheric mantle source. Nb and Ti troughs suggest a lithospheric mantle component because high field strength elements (Nb, Ti) are depleted in the lithospheric relative to the asthenospheric mantle (Figures 11a and 12a) (Menzies, 1989; Kempton, 1991; Wilson, 1989). This pattern with troughs at Nb and Ta for northern McCullough Range samples is similar to trace element patterns for other andesites in the NCREC (Figure 24a and b). Radiogenic Sr and Nd isotopic ratios also indicate that the rocks contain a significant lithospheric mantle component ($^{87}Sr/^{86}Sr$ >0.706 and ε_{Nd} <-1) (Figure 14a and 20a) (Farmer et al., 1989).

The mantle source was probably not garnet bearing because HREE concentrations in the McCullough Range rocks are too high (Figure 12a). Garnet retains HREE during partial melting resulting in concentration/chondrite values of Yb and Lu < 1. The McCullough Range rocks have concentration/chondrite values of Yb and Lu > 10 which are too high to be explained by the melting of a garnet bearing source (Wilson, 1989 p. 18,51). The lithospheric mantle source, therefore, is more likely spinel peridotite.

Stage 1 involves partially melting the lithospheric mantle to produce basaltic magmas. What material in the lithospheric mantle melts, and by what mechanism is very controversial. Two different models from previous studies are presented to explain the possible derivation of magmas from a lithospheric mantle source.

Leeman and Harry (1993) presented a model that explains the production of basaltic melts by partially melting veins or pods in the lithospheric mantle. Rather than decompression melting of peridotitic lithospheric mantle to produce large volumes of magma, the authors suggest that synextensional mid-Tertiary magmatism in the Basin and Range resulted from decompression melting of mafic veins or pods contained within the peridotitic lithospheric mantle. These veins and pods formed during either Precambrian or Mesozoic melting events. A Precambrian melting event is more likely because the mafic pods and veins must be isolated from the convecting asthenosphere for at least 1.5 Ga to allow the isotopic system to evolve to values observed in the andesites in the McCullough Range. Pods and veins near the base of the lithosphere would be near their melting point (1475°C at 120 km) and would begin to melt by decompression at the onset of extension (Leeman and Harry, 1993).

In contrast, Perry et al. (1987), Bradshaw et al. (1993), and Hawkesworth et al. (1994) discuss a mechanism by which at a certain temperature, pressure, and volatile content, partial melting of the continental lithospheric mantle produces basaltic melts during extension. For example, Bradshaw et al. (1993) and Gallagher and Hawkesworth (1992) calculate that at 100% extension, partial melting of the continental lithospheric mantle can occur with no increase in mantle potential temperature (T_p) if the source contains small amounts of H_2O and CO_2 (~0.3-0.4% and ~0.7% respectively). The introduction of H_2O and other

volatiles lowers the temperature of the peridotite solidus producing a greater opportunity for lithospheric melting. These calculations take into account mantle viscosities, amount of extension, T_p, mechanical boundary layer (MBL) or lithospheric source region thickness, pre-extension crustal thickness, and final crustal thickness. Hawkesworth et al. (1994) refined this model and suggested that the thinning of the lithosphere raised temperatures throughout the lithospheric mantle. This increase in temperature results in melting of zones in the lithospheric mantle enriched in volatiles during previous partial melting events.

Stage 2

The basaltic magma generated during stage 1 is a primary magma. Andesites of the northern McCullough Range, however, do not represent primary magmas. The andesites are chemically evolved suggesting that a differentiation process such as fractionation occurred. Evidence includes the low to moderate Mg #'s (36.6-61.1), MgO (<7.2 wt. %), and Cr concentrations (<243 ppm) (Figures 9a and 13a). For comparison, a primitive magma should have Mg#>71, MgO>10 wt. %, and Cr>500 ppm. FC affects Mg #'s more than other processes (contamination, mixing) because Mg is more compatible than Fe early during crystallization. The resulting liquid dramatically increases in Fe relative to Mg with the removal of Mg-rich crystals. The relatively low Mg numbers are most probably a sign that fractional crystallization has occurred. The andesitic parental magmas that produced the andesites in the northern McCullough Range, therefore, were probably formed by FC of basaltic primary magmas of stage 1.

Stage 2 involves fractional crystallization (FC) of the basaltic magma produced in stage 1 to produce calc-alkaline andesite magmas. FC occurred in the middle to upper crust or at the base of the crust. Grove and Kinzler (1986) demonstrated that calc-alkaline andesites can form by FC of a tholeiitic, olivine-normative basalt parent magma under anhydrous conditions and elevated pressures (2.5 to 8 kb) (Figure 25). Elevated pressure produces a calc-alkaline trend rather than a tholeiitic trend for two reasons. First, high pressure reduces the plagioclase phase volume so plagioclase is not an early crystallizing phase. Instead, olivine and clinopyroxene crystallize early and remove Fe, therefore, Fe enrichment is not observed as in tholeiitic rocks. Second, the invariant point does not control liquid composition (point A, Figure 25) as it does at lower pressures. Liquids are free to evolve to higher values of SiO_2.

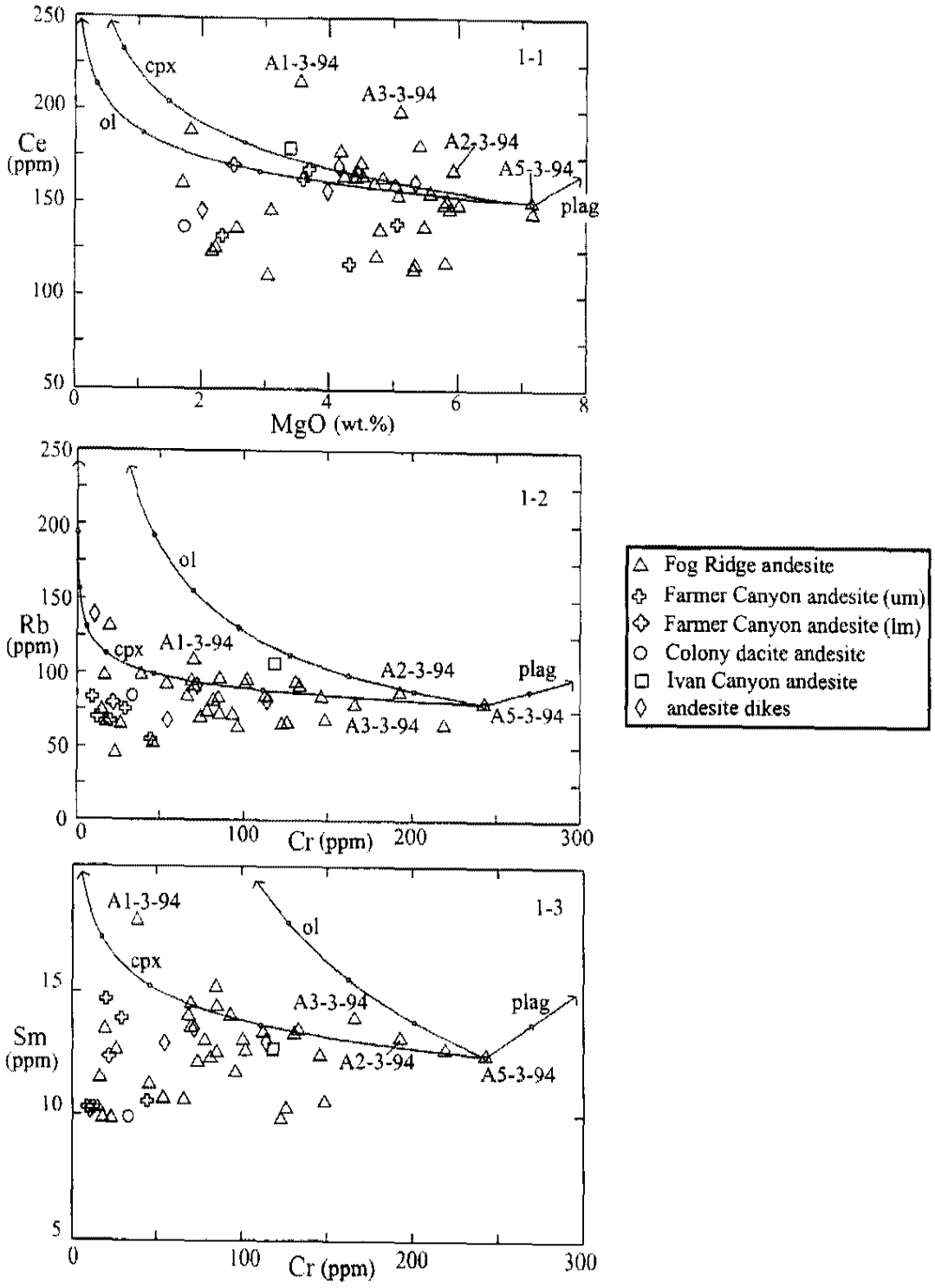

Figure 17. Fractional crystallization plots (Model 1; plots 1-1, 1-2, and 1-3) for andesites of the northern McCullough Range. Vectors represent fractionation of olivine (ol), clinopyroxene (cpx), and plagioclase (plag) from parent andesite sample A5-3-94 (tick marks at 10% fractionation). Most samples fall outside of the field defined by the vectors with the exception of A1-3-94, A2-3-94, and A3-3-94. Refer to Table 2 for details of each model. um=upper member; lm=lower member

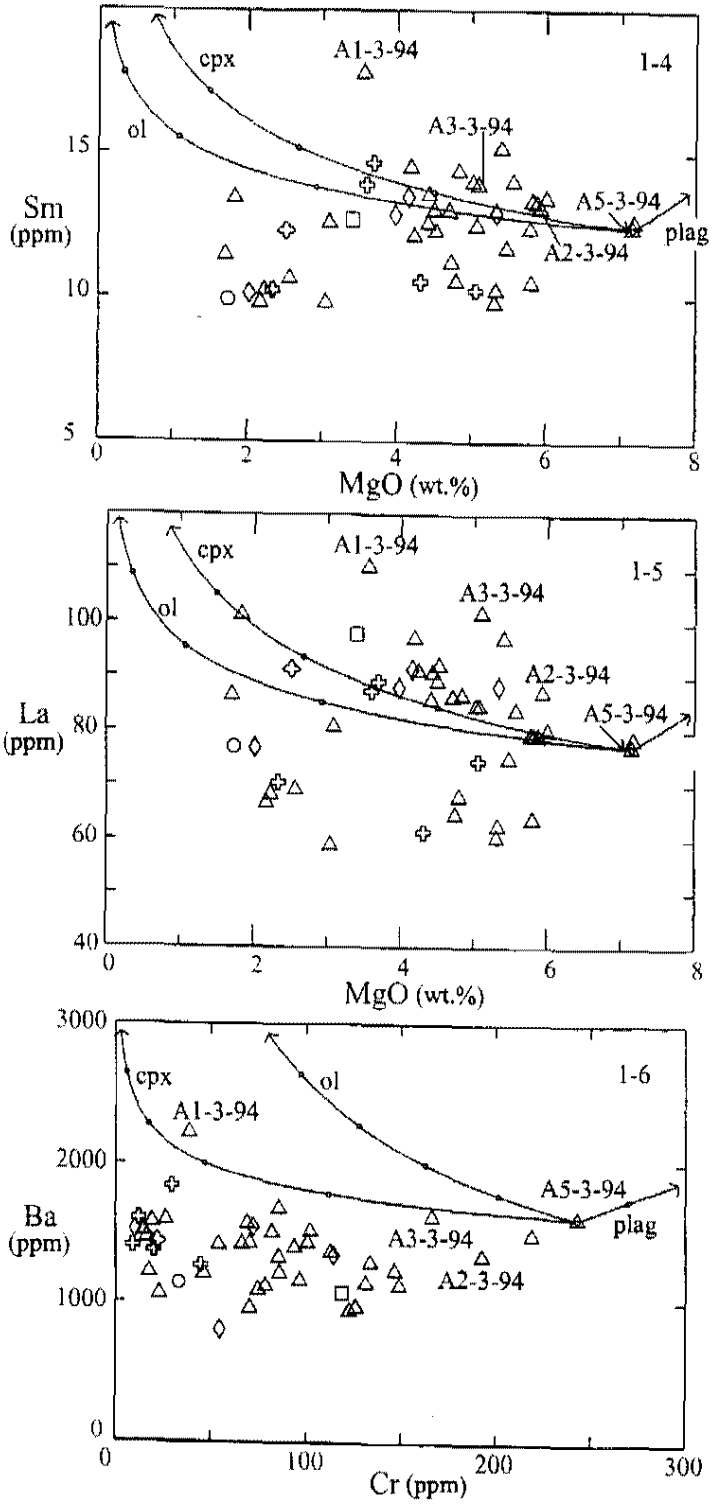

Figure 17 (cont.). Fractional crystallization plots (Model 1; plots 1-4,1-5, and 1-6) for northern McCullough Range andesites. Vectors represent fractionation of olivine (ol), clinopyroxene (cpx), and plagioclase (plag) from parent sample A5-3-94 (tick marks at 10% FC). Most samples fall outside of the field defined by the vectors with the exception of A1-3-94, A2-3-94, and A3-3-94. Refer to Table 2 for details of model.

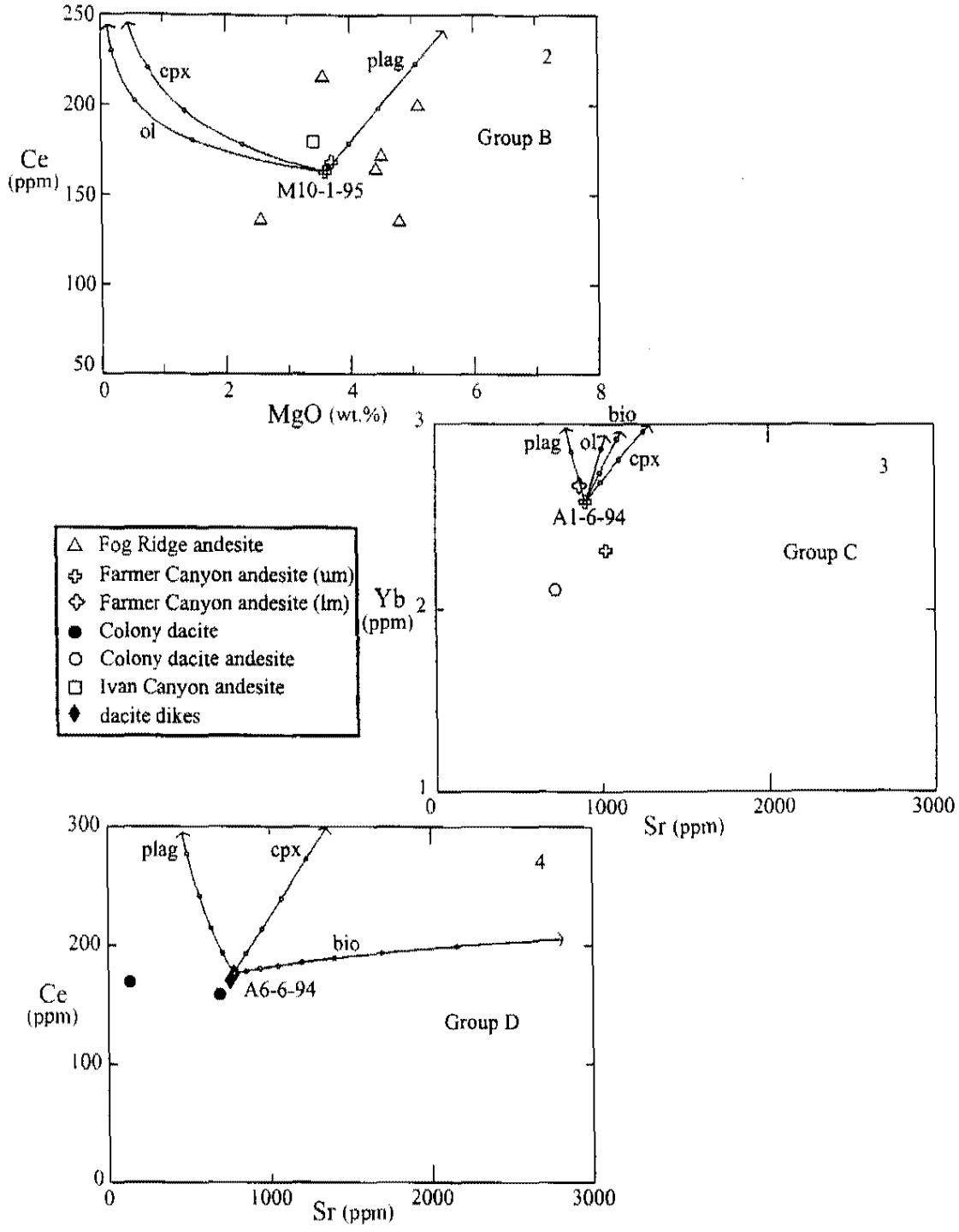

Figure 18. Fractional crystallization models within isotopic groups B (Model 2), C (Model 3), and D (Model 4). The most mafic sample in each group was chosen as the parent rock: M10-1-95, A1-6-94, and A6-6-94. Fractionation vectors trend away from the more chemically evolved samples in each group. Vectors represent 100% fractionation of olivine (ol), clinopyroxene (cpx), plagioclase (plag), and biotite (bio). Refer to Table 2 for details of each model. um=upper member; lm=lower member

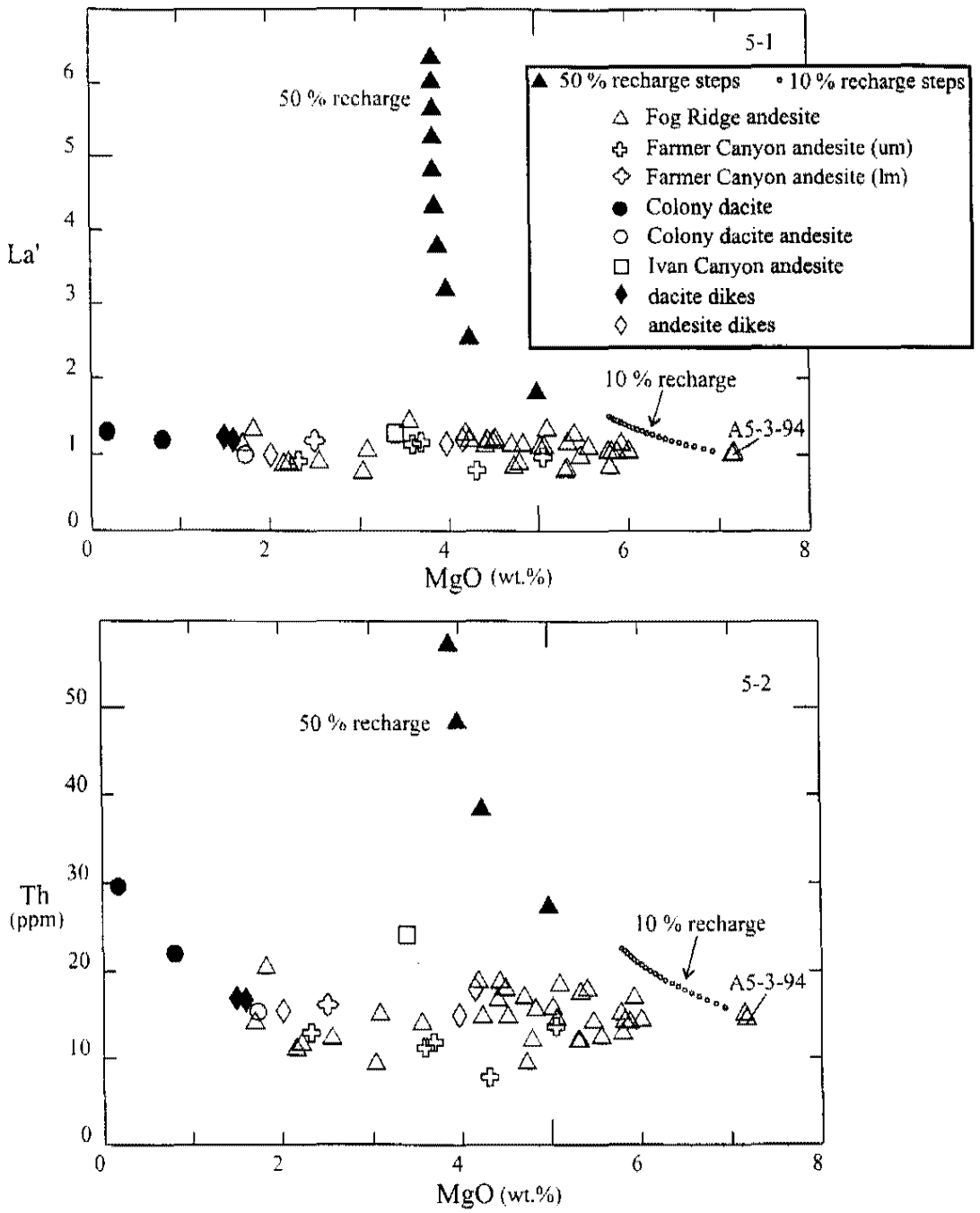

Figure 19. Recharge models for rocks of the northern McCullough Range. Andesite A5-3-94 is the least evolved sample and was used as the parent magma. Models predict the increase of incompatible element concentrations for a series of recharge steps based on the concentration of the elements in the parent magma, the amount of recharge vs. fractionation, and the amount of magma erupted from the chamber. Models show predicted incompatible element increases for 10 % and 50 % recharge plotting MgO vs. La' (5-1) and MgO vs. Th (5-2). La' is an enrichment factor calculated by dividing the La concentrations of the samples by the La concentration of the parent magma. um=upper member; lm=lower member

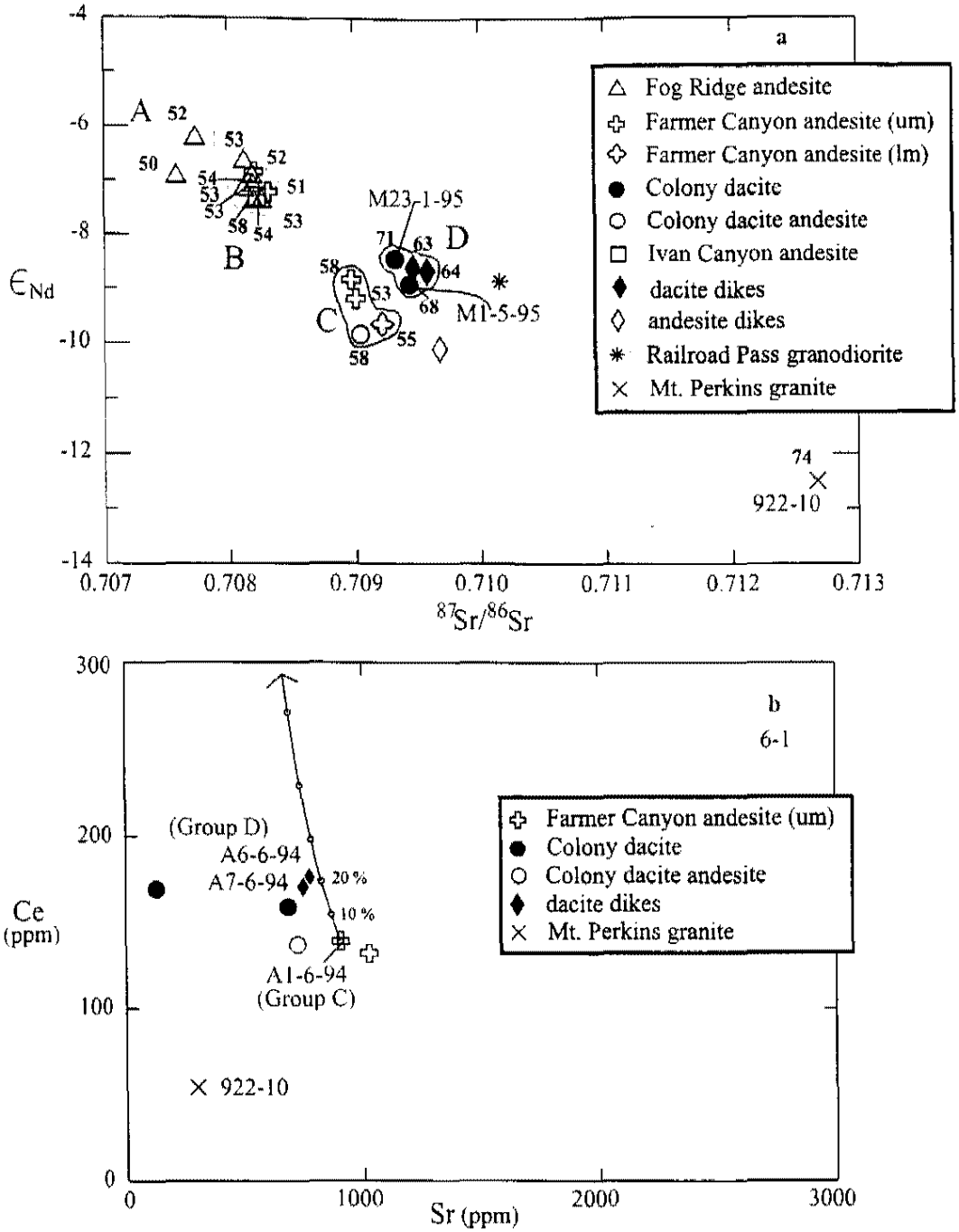

Figure 20. Isotope plot and AFC model. (a) Mt. Perkins granite 922-10 lies roughly on trend with the northern McCullough Range data array and has the initial Sr and SiO_2 required for a felsic end member in AFC models. Note that silica values (bold numbers adjacent to symbols) do not vary much in isotopic groups A, B, and C. (b) Sr vs. Ce plot (AFC Model 6-1) demonstrates that 20% fractionation of 50% cpx and 50% plag from a group C andesite (A1-6-94) and addition of 4-8% of 922-10 produces dacite dikes of group D (A6-6-94). Refer to Table 2 for details of model. Other samples in group D can not be explained by assimilation or mixing models and may represent an independent felsic component. um=upper member; lm=lower member

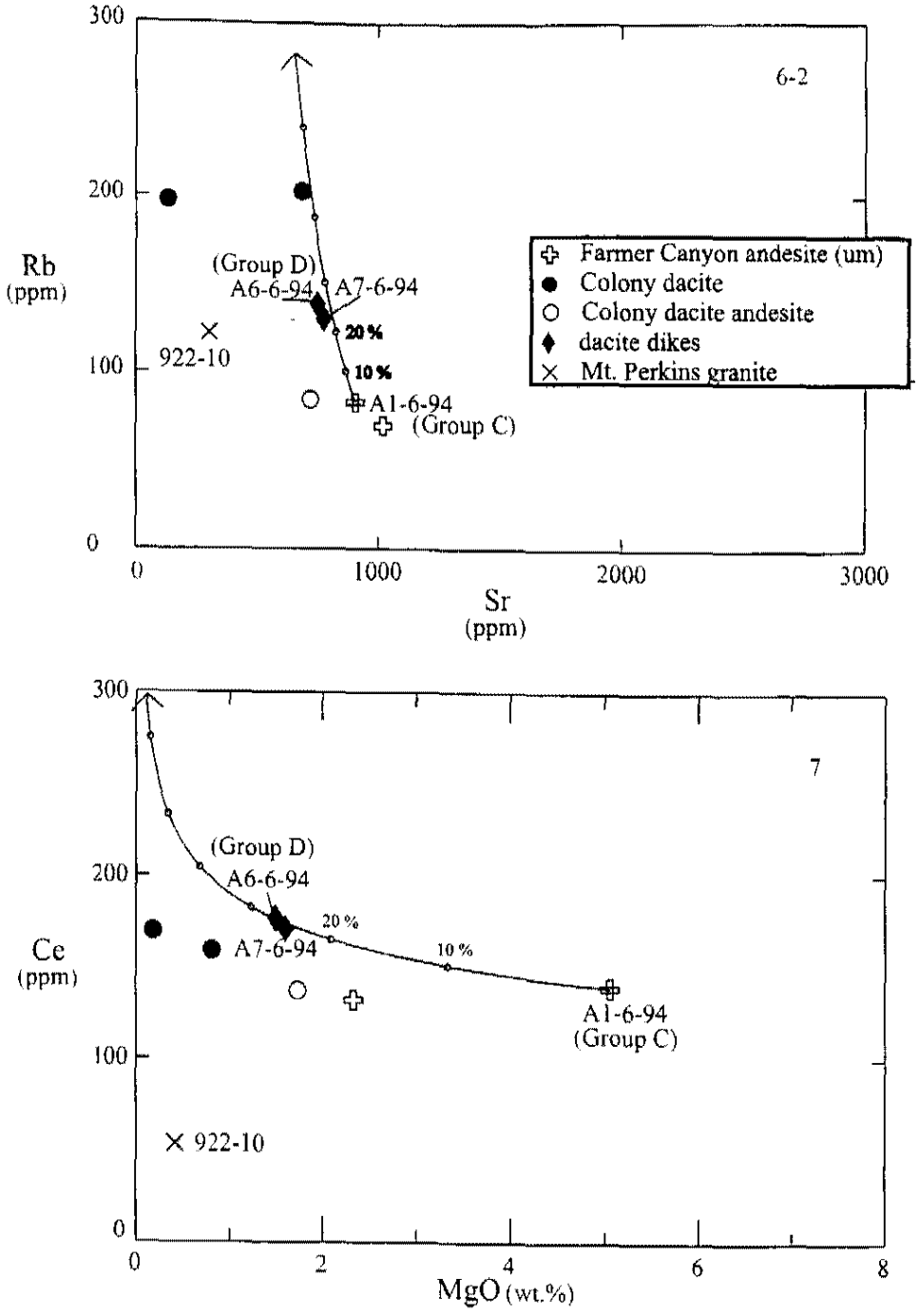

Figure 21. AFC Models 6-2 and 7 suggest that 20% fractionation of 50% cpx and 50% plag from a group C andesite (A1-6-94) and addition of 4-8% of 922-10 produces dacite dikes of group D (A6-6-94 and A7-6-94). Refer to Table 2 for details of each model. um=upper member

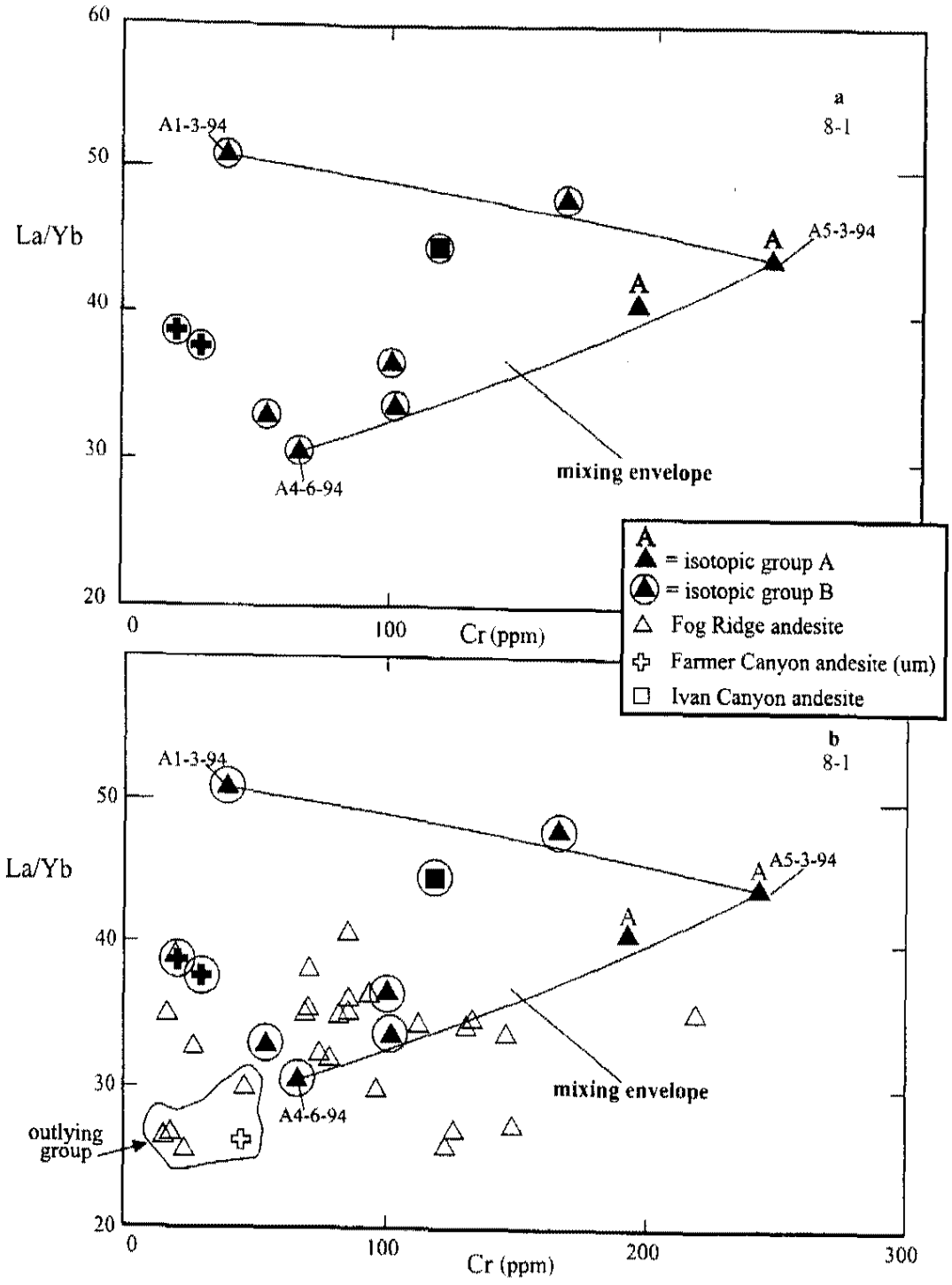

Figure 22. Cr vs. La/Yb plots show mixing between isotopic groups A and B (Model 8-1). End members are representative of the chemical ranges within isotope groups. (a) Only samples with isotopic data are plotted. (b) Many of the andesites from the upper Farmer Canyon and Fog Ridge sections fall within or near the mixing field. A few samples consistently fall outside of the mixing field; this outlying group may represent another mafic end member. um=upper member

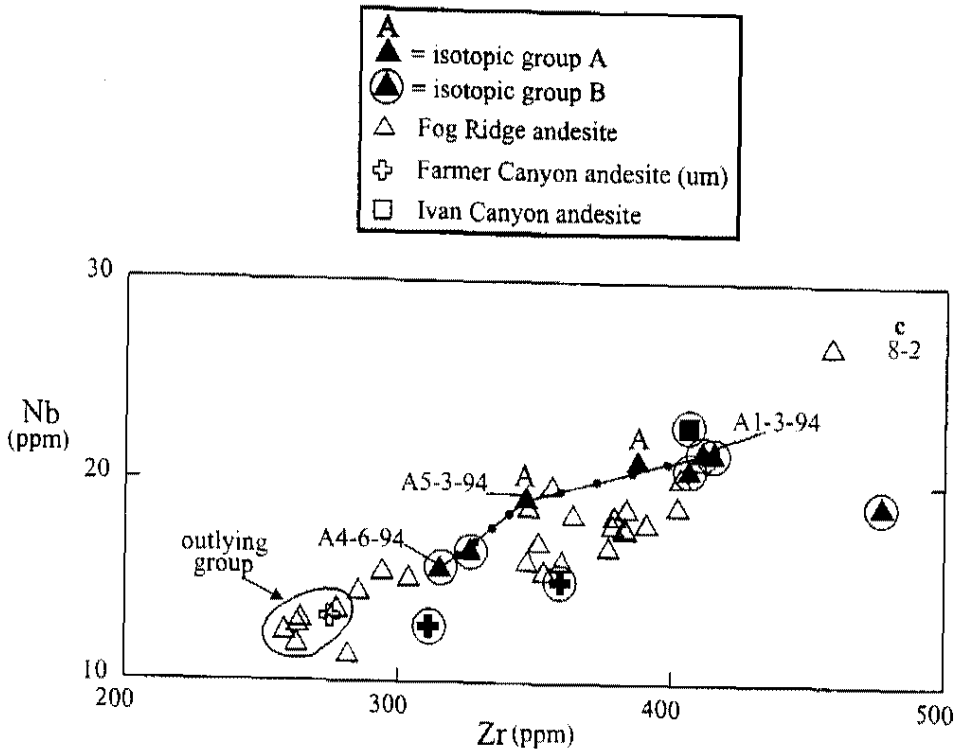

Figure 22 (cont.). (c) Zr vs. Nb plot shows mixing between isotopic groups A and B (Model 8-2). Many group B samples and andesites from the upper Farmer Canyon and Fog Ridge section fall in or near the mixing field. A few samples consistently fall outside of the mixing field; this outlying group may represent another andesitic end member. um=upper member

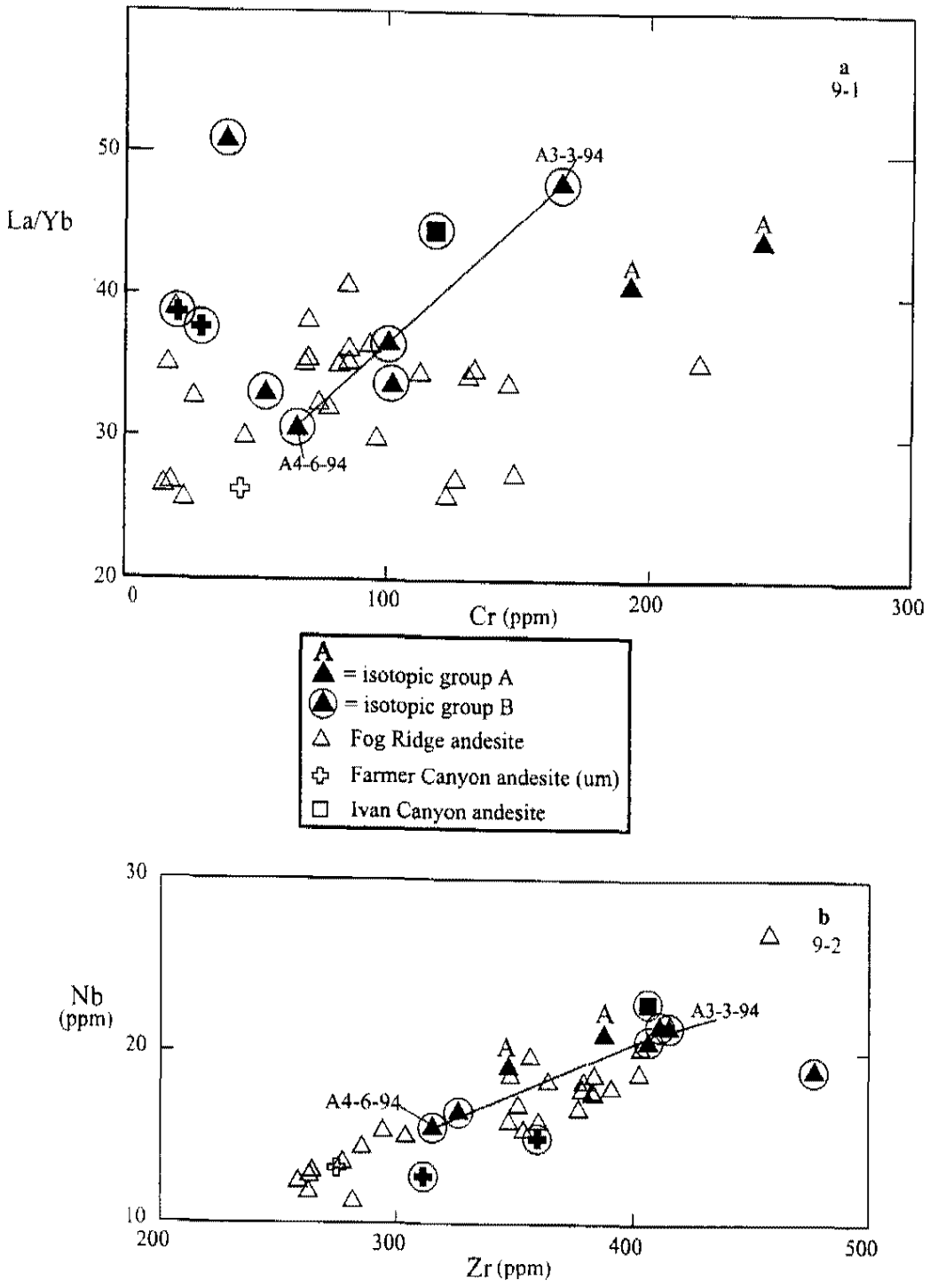

Figure 23. Plots of (a) Cr vs. La/Yb and (b) Zr vs.Nb show mixing between different isotope types within group B using samples A3-3-94 and A4-6-94 as end members to create a mixing line (Model 9). Many of the andesites from isotopic group B, as well as samples from the upper Farmer Canyon and Fog Ridge sections fall along and around this mixing line. um=upper member

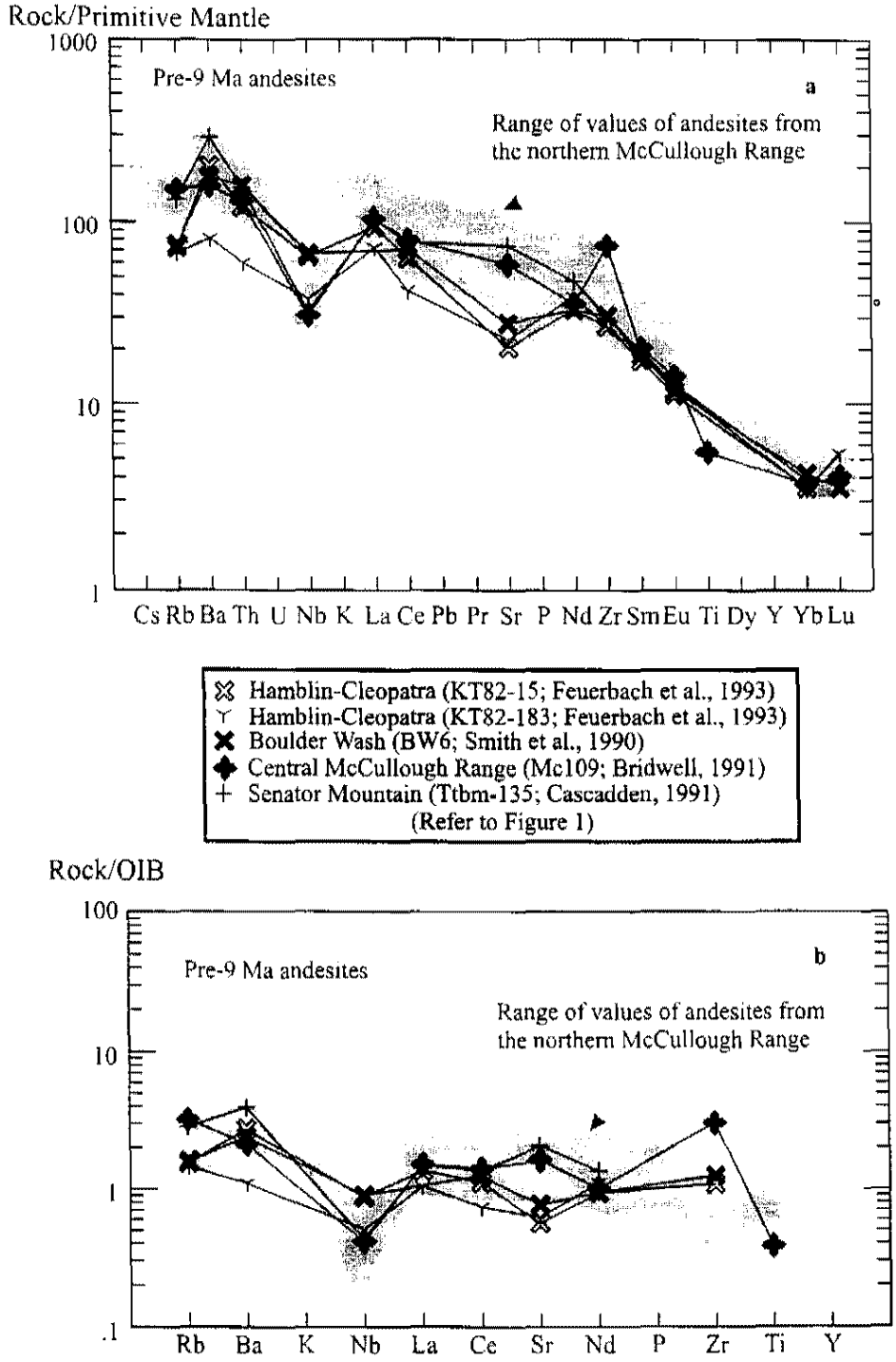

Figure 24. Pre-9 Ma andesites from other areas in the NCREC normalized to (a) primitive mantle abundances from Sun and McDonough (1989) and (b) OIB abundances from Fitton et al. (1991). The ratio Ta=Nb/17 (atomic abundance ratio) was used to calculate Nb or Ta when either Nb or Ta data were unavailable. Pre-9 Ma andesites from the NCREC have similar trace element distribution to andesites in the northern McCullough Range. Patterns are typical of rocks formed by melting of a lithospheric mantle source.

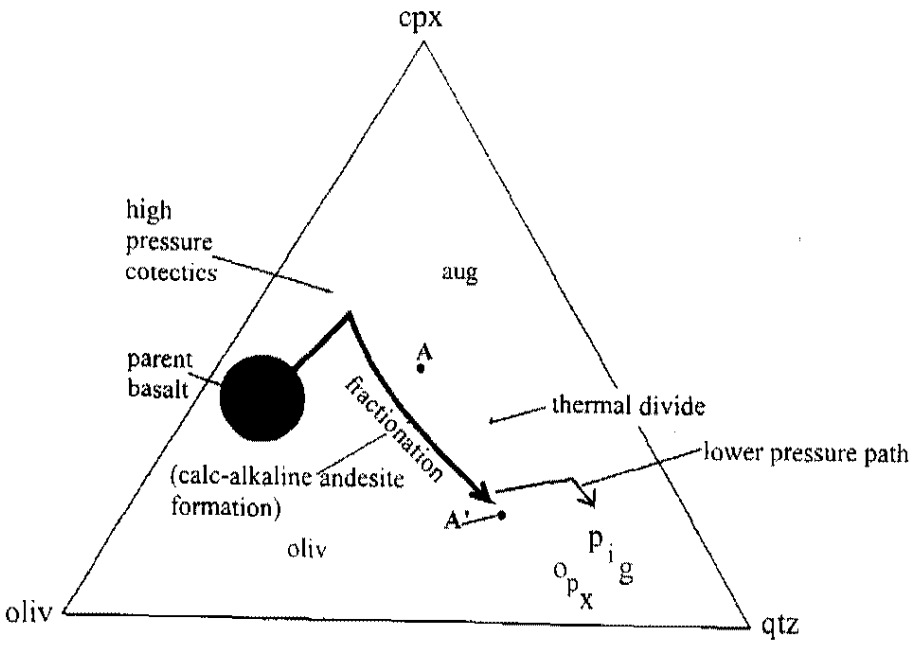

Figure 25. Ternary phase diagram from Grove and Kinzler (1986) demonstrates how calc-alkaline andesites can form from tholeiitic basalt magmas at high pressures. At pressures above 2.5 kb the peritectic point shifts from A to A' and reduces the plagioclase phase volume in plagioclase, olivine, quartz, and clinopyroxene space. As a result, clinopyroxene and olivine crystallize first, thus preventing later iron enrichment. This crystallization sequence produces a calc-alkaline rock series. At higher pressures, liquids are not constrained by an invariant point and are free to evolve to higher values of SiO_2.

Chapter 6

Xitle Volcano, Mexico

Geologic Background

To test the applicability of the model developed in the northern McCullough Range, a preliminary study was done at Xitle volcano, Mexico. Xitle volcano was chosen because it is similar to the northern McCullough Range in tectonic setting and in basic rock chemistry. Xitle volcano lies in the central part of the Trans-Mexican Volcanic Belt (TMVB), a complex volcanic arc that extends from the mouth of the Gulf of California across central Mexico to El Chicon, near the Guatemalan border (Sheridan and Macias, 1992) (Figure 26). The TMVB is a result of subduction of the Cocos and Rivera plates beneath the North American plate. Subduction continues today as the Cocos and Rivera plates, separated by the Rivera Fracture Zone, move away at varying rates from the East Pacific Rise. This complex plate reorganization produced an extensional terrane superimposed on the volcanic arc (Sheridan and Macias, 1992). Workers documented this tectonic regime particularly well in the western TMVB (Allan, 1981; Allan and Carmichael, 1984; Luhr et al., 1985; Wallace et al., 1992), as well as in the Central American Volcanic Arc (Busby-Spera, 1988). The possible influence, however, of extensional overprinting of a subduction complex on the

development of the central and eastern parts of the TMVB is not well documented.

Xitle volcano in the central TMVB, 20 km southwest of Mexico City (Figure 26), formed in an area of the TMVB that is being simultaneously influenced by extension and subduction. A cinder cone associated with andesite flows, scoria and ash deposits, and a lava dome (Xicontle) which lies just west of the main cone compose Xitle volcano. Xitle is about 2000 years old and erupted over a period of less than 100 years (Delgado, ^{14}C dates, personal commun.). Preliminary mapping by Delgado and students at the National University of Mexico (UNAM) documented six andesite flows extending radially from the cone (Figure 27). Most flows followed paths to the north and northeast toward Mexico City (Delgado, unpublished data). Much of the southern part of Mexico City, including UNAM, are built on Xitle lava flows. Samples for this study were collected from flows I-VI according to the mapping of Delgado and his students. Figure 27 shows the location of Xitle flows, Xicontle lava dome, and sample locations. The presence of lava tubes and tube-fed flows however, may complicate the stratigraphy (Lillian Martin, personal commun.). Lillian Martin does not believe that all the flows erupted from the Xitle cinder cone. Instead, Lillian Martin suggested that the flows closest to the vent, as well as Xicontle, the lava dome, are the oldest flows and erupted from the Xitle cinder cone. Lillian Martin further suggested that the more distal flows are younger and were tube fed, possibly through fissures. It is also possible that Xitle flows bury older volcanic vents and/or flows.

Geochemical Descriptions and Petrography

Major elements

Lava flows from Xitle volcano, and the Xicontle lava dome, are calc-alkaline basalts and basaltic-andesites (Figure 28a, b, and c). Xitle lavas range in SiO_2 concentration from 50.1 to 55.8 wt.%. Although samples are very similar in chemistry, they fall into two groups on Harker variation diagrams. Group 1 includes samples X4-10-94, X5-10-94, X6-10-94, X8-10-94, X9-10-94, X10-10-94, and X13-10-94 whereas group 2 includes samples X7-10-94, X11-10-94 and X14-10-94 through X19-10-94 (Figure 29). Both groups show increases in Al_2O_3, FeO, CaO, P_2O_5, and Na_2O with increasing SiO_2. Group 2 shows an increase in TiO_2 and K_2O while group 1 shows little variation of these elements with increasing SiO_2. MgO increases in group 1 and decreases or is scattered in group 2 with increasing SiO_2. Figure 29 shows group 1 and 2 variations as plotted on SiO_2 vs. MgO, FeO, and Al_2O_3 diagrams. Two samples from one flow (X12-10-94 and X12b-10-94) fall far outside groups 1 and 2. The relation of these samples to Xitle volcano is questionable, therefore, they will be excluded from further discussion.

Trace elements

Cr decreases in group 2 and increases in group 1, while Ni data is scattered with increasing SiO_2 (Figure 30). Zr and Sr (Figure 31a) show considerable scatter while Rb and Ba slightly increase in group 2 and remain constant in group 1 with increasing SiO_2. REE slightly increase in group 2 with increasing SiO_2, yet the overall concentrations are lower than in group 1. Group 1 is similar to the northern McCullough Range andesites in that trace element concentrations vary widely within the group. In addition, group 1 shows a lack

of increase in incompatible element concentrations with increasing SiO_2 (Figure 31b and c).

Elemental abundances were normalized to both primitive mantle (Sun and McDonough, 1989) and OIB (Fitton et al., 1991). On primitive mantle diagrams, Xitle lavas are similar to OIB, but have troughs at Rb, Th, and Ti, and a peak at Pb (Figure 32a). On OIB normalized spider diagrams, Xitle lavas are similar to OIB but are slightly depleted in Rb, Ba, and LREE and exhibit Nb and Ti troughs (Figure 32b). Basalts and basaltic andesites also show a slight increase in K, Sr, P, and Zr relative to OIB. The two groups are indistinguishable on spider diagrams (Figure 32a and b).

Sr and Nd isotopes were obtained for two samples; one from each geochemical group. Group 1 (X4-10-94) exhibits a $^{87}Sr/^{86}Sr$ of 0.70382 and an ε_{Nd} of 3.38. Group 2 (X16-10-94) has a $^{87}Sr/^{86}Sr$ of 0.70352 and an ε_{Nd} of 4.92 (Figure 32c). These differences are small but are greater than that produced from analytical uncertainty (Figure 32c).

Petrography

Basaltic-andesite flows from Xitle volcano contain plagioclase and olivine phenocrysts in a fine-grained groundmass consisting of plagioclase and olivine. Groups 1 and 2 are distinguishable petrographically by differences in the amount and type of phenocrysts. Group 1 flows are fine-grained with phenocrysts (9.6%) of plagioclase (10%; up to 0.75 mm) and olivine (90%; up to 0.5 mm). Flows of the Xicontle lava dome (group 1) contain phenocrysts (14.4%) of olivine (100%). The groundmass contains plagioclase laths, olivine, and devitrified glass.

Group 2 flows are coarser grained than group 1 with 26.6% phenocrysts of plagioclase (58%; up to 2 mm) and olivine (42%; up to 3 mm). The groundmass

contains plagioclase laths, olivine, Fe-Ti minerals, vesicles, and devitrified glass. Refer to Appendix I for point count data.

Geochemical modeling

Geochemistry and isotopic data indicate that groups 1 and 2 may be independent partial melts of the asthenospheric mantle. Modeling of groups 1 and 2, therefore, was done separately. Recharge, fractionation, and magma mixing are the petrogenetic models used to assess the chemical variation of the Xitle rocks within the two chemical groups.

Recharge

Recharge significantly increases incompatible element abundances with increasing SiO_2 (O'Hara, 1977). Variation in trace and REE concentrations is limited among samples in group 1 and increases in incompatible elements in group 2 with increasing SiO_2 are small (Figure 31). Recharge, therefore, is most likely not a dominant process in the production of either group of Xitle flows.

Fractional Crystallization

Models involving the fractionation of olivine, clinopyroxene, and plagioclase were attempted to explain the chemical variation within the two groups. Distribution coefficients for olivine are from Villemant et al. (1981), and the remaining elements are from Table 5 in Larsen and Smith (1990) (Table 1).

Group 1

During differentiation processes such as fractionation, incompatible elements will preferentially partition into the melt while compatible elements remain in the crystallizing mineral phases. As a result, incompatible elements should increase with increasing SiO_2 if fractionation occurred. In group 1, however, most incompatible elements remain constant as SiO_2 increases while the compatible elements Cr and Ni increase with increasing SiO_2 (Figures 30 and 31). Fractionation models, therefore, can not explain the chemical variation in group 1. Petrographic evidence also suggests that the magma from group 1 erupted quickly without undergoing significant fractionation. Thin sections show the rocks to be fine-grained with a trachytic texture suggesting that magma erupted rapidly without ponding in the upper crust.

Group 2

In group 2, however, incompatible element trends indicate fractionation as a possible petrogenetic process. In group 2, the incompatible element plot of Yb vs. Hf, as well as SiO_2 vs. FeO/MgO, shows a positive slope consistent with crystal fractionation (Figure 33a and b). Because MgO is more compatible than FeO in clinopyroxene and olivine, fractionation of these phases should result in an increase in the FeO/MgO ratio with increasing amounts of crystal fractionation and increasing SiO_2.

Group 2 fractionation models use sample X16-10-94 as the parent magma based on its low SiO_2 (50.1 wt.%) and high MgO (9.4 wt.%) and Cr (300 ppm) contents. Other samples such as X14-10-94, X15-10-94 and X17-10-94 could also be used as parents. Plots of incompatible elements La, Sm, and Yb vs. compatible element Cr show that the rocks from group 2 can be fractionated from sample

X16-10-94 (Figure 34). These models require small amounts of fractionation (<15 %) of between 50-90% olivine, 10-50% plagioclase, and 0-10% clinopyroxene. The chemical variation in group 2, therefore, can be explained by fractionation.

Petrographic evidence also suggests that crystal fractionation processes operated within group 2. In contrast to group 1, thin sections from group 2 show phenocryst rich textures suggesting that the magma may have ponded in an upper crustal chamber, thus allowing differentiation processes such as fractionation to occur.

Mixing

The variation in trace and REE elements within group 1 is small, however, the variation in compatible trace elements and major element abundances is greater than can be explained by analytical uncertainty (Appendix IV). The chemical variations in group 1 Xitle flows can possibly be explained by a mixing model similar to that proposed for andesites in the northern McCullough Range. Two or more magmas with similar trace element compositions may have mixed together to produce such trends as are observed in group 1. This model explains the lack of increase in incompatible elements and the increase in compatible elements with increasing SiO_2 within this group. Limited sampling, however, prevents quantitative testing of this model or the determination of possible end members. It is also possible that the variation in chemistry reflects slight variations in the source composition.

Discussion

Stratigraphic implications

The two groups of lavas at Xitle volcano have different distributions. Group 1 lavas crop out in and around the cinder cone and Xicontle vent cluster. Group 2 lavas occur at a distance from the cone and do not seem to have erupted from either the cinder cone or Xicontle (Figure 27). These observations support Lillian Martin's interpretation of temporal separation of local and distal flows, as well as the complicated stratigraphy of tube-fed lava flows. Delgado's model of long flows radiating from the cinder cone is not supported.

Comparisons to the northern McCullough Range

Tectonic setting

Although Xitle volcano and the volcanic section in the northern McCullough Range both formed during extension, the tectonic settings are different. The volcanic rocks in the northern McCullough Range formed in the southern Basin and Range between ~15 and 13 Ma. At this time, subduction off the western margin of the North American Plate had ceased (by around 25 Ma) and been replaced with a transform margin (Severinghaus and Atwater, 1990). The Mendocino triple junction swept through the latitude of Las Vegas around 17 or 16 Ma. While it is possible that the older units in the northern McCullough Range volcanic section (Ivan Canyon andesite, Colony dacite, lower member of the Farmer Canyon andesite) erupted during the waning stages of subduction, the upper units where most samples were collected (upper member of the Farmer Canyon andesite and For Ridge andesite) erupted after subduction ceased and extension was initiated. This observation does not discount the

possibility of a remnant detached slab in the area. In contrast, Xitle volcano formed in the TMVB where complex plate movements produced an extensional terrane that is superimposed on the subduction-related volcanic arc. In this area, extension is occurring synchronously with subduction (see Geologic Background section of this Chapter). The effect of subduction on volcanism or possible contribution of a slab component in either area, however, is not clear.

Petrogenesis

Xitle volcano was thought to be a simple monogenetic volcano, but this study demonstrates the presence of two different magma batches that underwent different petrogenetic processes. In group 1, chemical trends possibly indicate mixing between two similar but separate mafic sources. In this sense, a similarity exists between the petrogenesis of Xitle and McCullough Range volcanoes. Both areas contain multiple magma batches of basaltic-andesitic composition.

In the northern McCullough Range and the Xitle volcano lavas, petrographic evidence does not support magma mixing models. The lack of evidence for magma mixing is expected because the mixing of two andesitic magmas of similar composition will not result in distinct mixing textures, disequilibria mineral assemblages, or other features commonly associated with magma mixing of mafic and felsic end members (e.g. see Koyaguchi, 1986).

This preliminary study demonstrates the possible global applications of the McCullough Range type magmatic system. Andesite dominated systems in the two extensional environments may have been produced in part by the mixing of different mafic magma batches. The importance and existence of different mafic sources in these areas and the possible mixing of these magmas to produce andesites should be evaluated in other areas of regional extension.

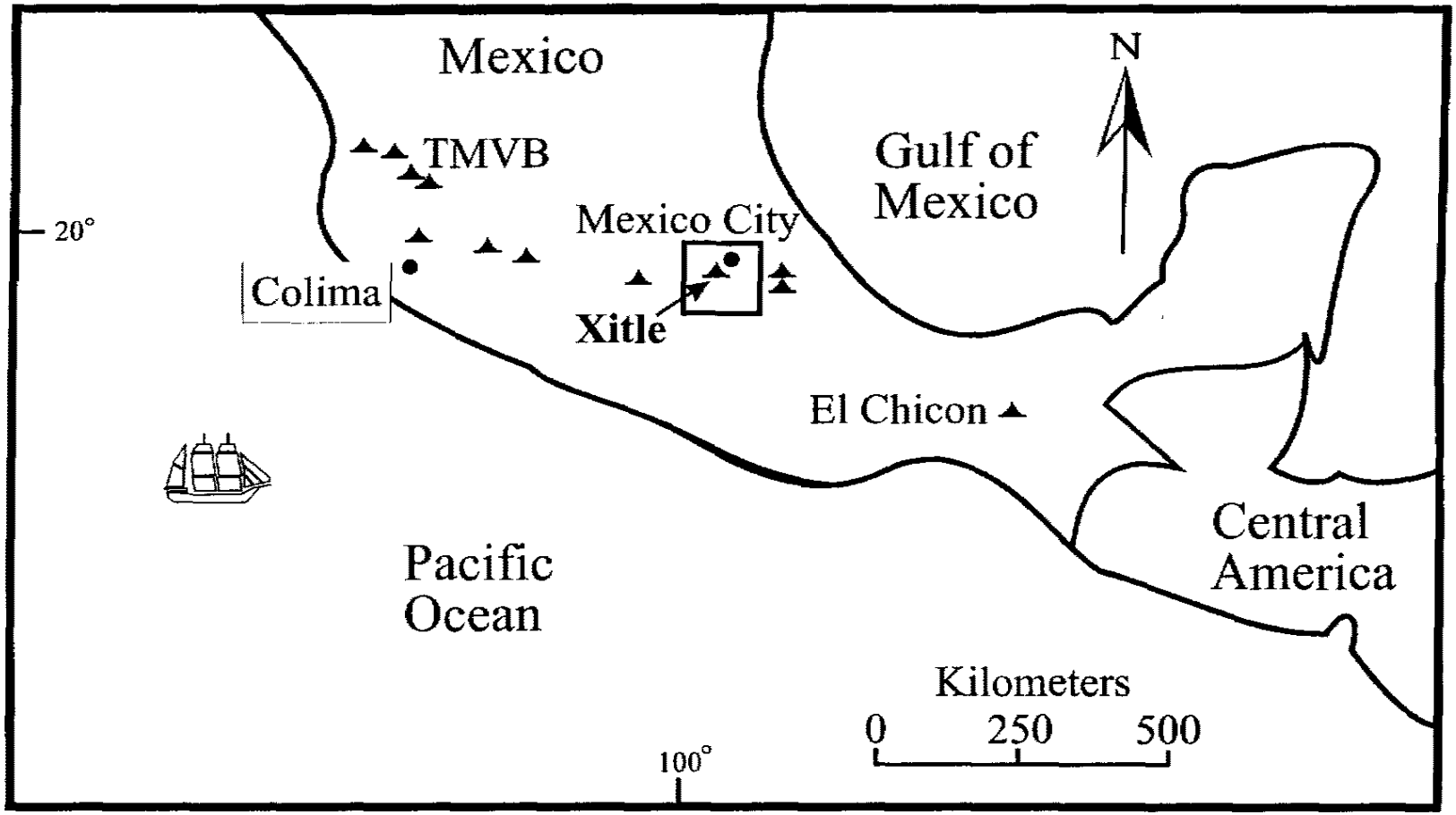

Figure 26. Map of Mexico showing location of the Trans-Mexican Volcanic Belt (TMVB) and Xitle volcano (modified from Sheridan and Macias, 1992).

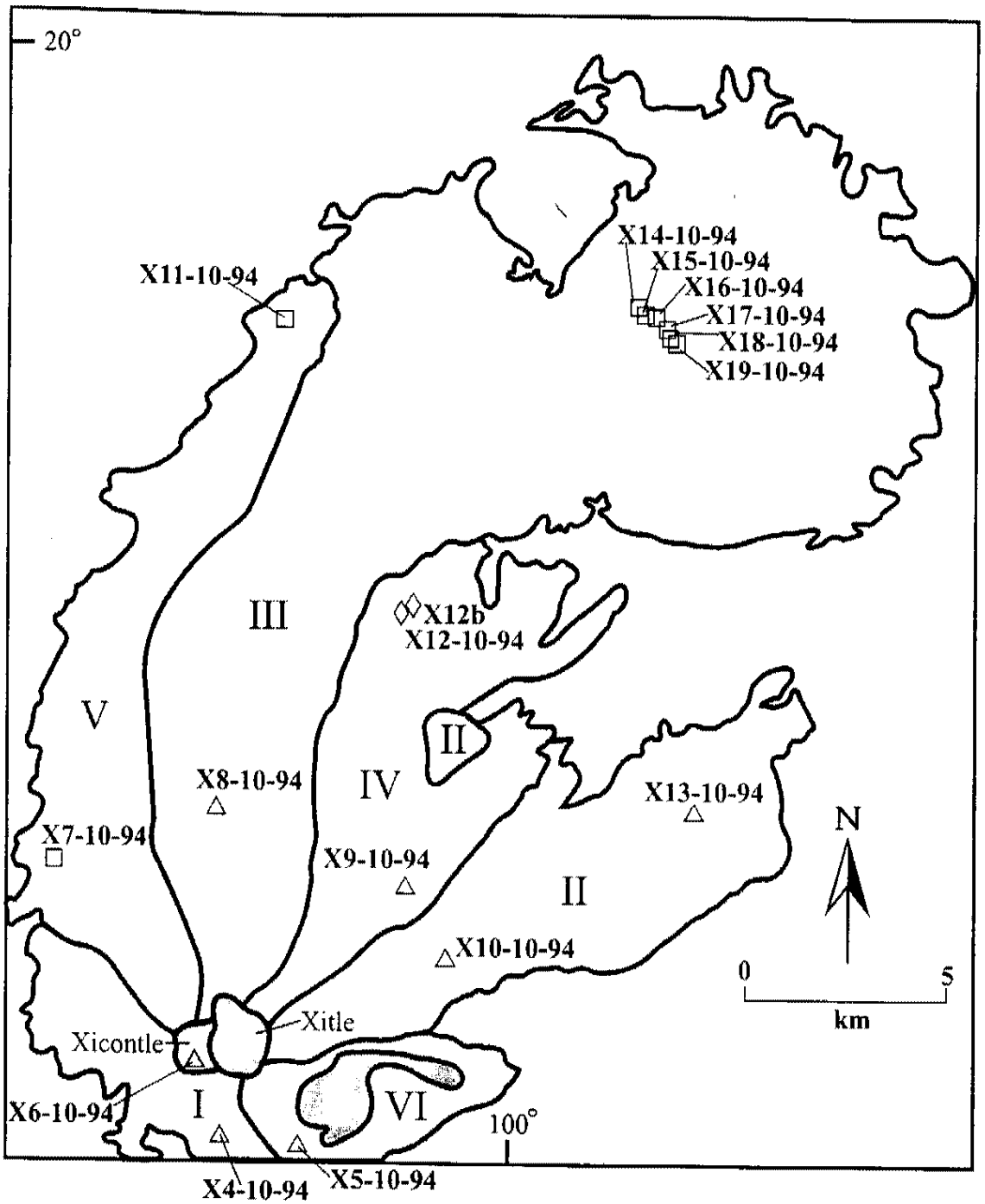

Figure 27. Diagrammatic map of Xitle volcano, Xicontle lava dome and six associated Xitle flows. Flows are labelled with roman numerals from oldest (I) to youngest (VI). Most flows followed paths to the north and northeast toward Mexico City. Bold numbers (ie. X4-10-94) and symbols represent sample locations. Mapping by Delgado and students at the National University of Mexico (UNAM). Lillian Martin, however, suggests a different stratigraphy (see Chapter 6, Geologic Background section).

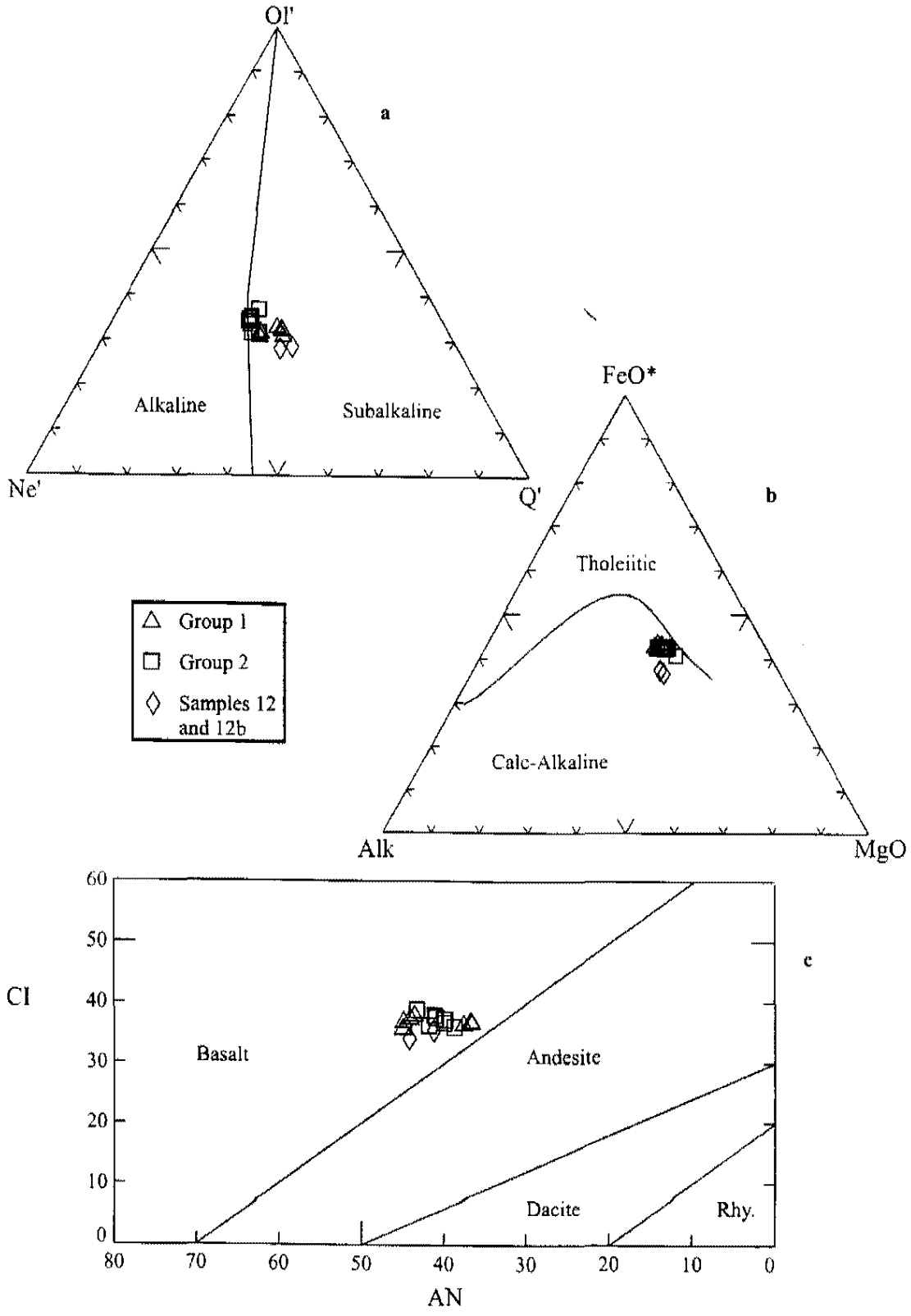

Figure 28. Rock classification diagrams of Xitle volcanic rocks (Irvine and Baragar, 1971). (a) Alkaline vs. subalkaline. (b) Tholeiitic vs. calc-alkaline. (c) AN vs. CI. AN=100 An/(An+Ab+(5/3Ne)), CI-Color Index=normative ol+cpx+mt +il+hm in wt. %.

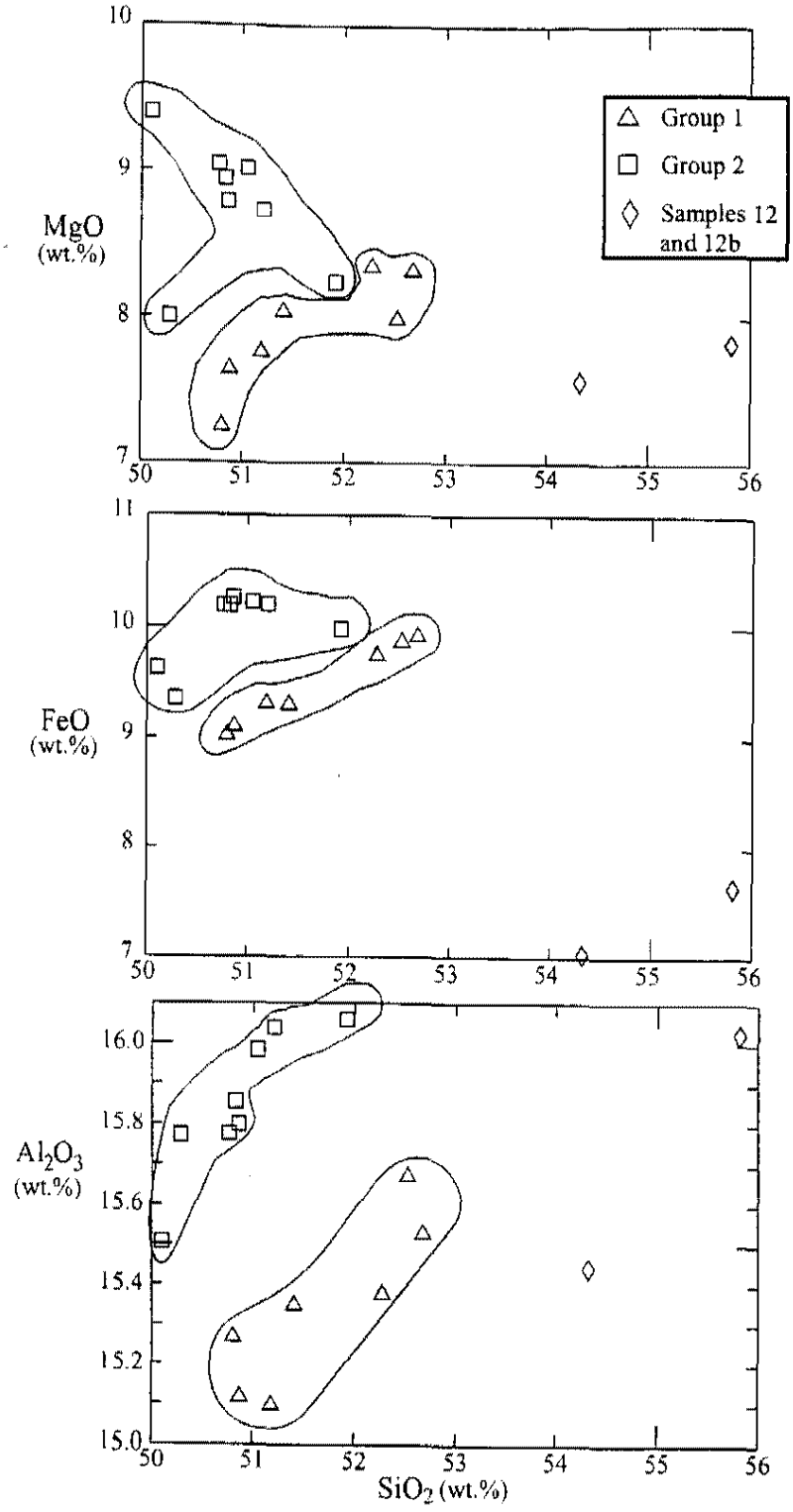

Figure 29. Harker diagrams showing SiO_2 (wt. %) vs. MgO, FeO, and Al_2O_3 (wt. %). Xitle flows fall into two groups, designated groups 1 and 2. Samples 12 and 12b consistently fall far outside groups 1 and 2. Their relationship to Xitle volcano is unclear, so they are excluded from further discussion.

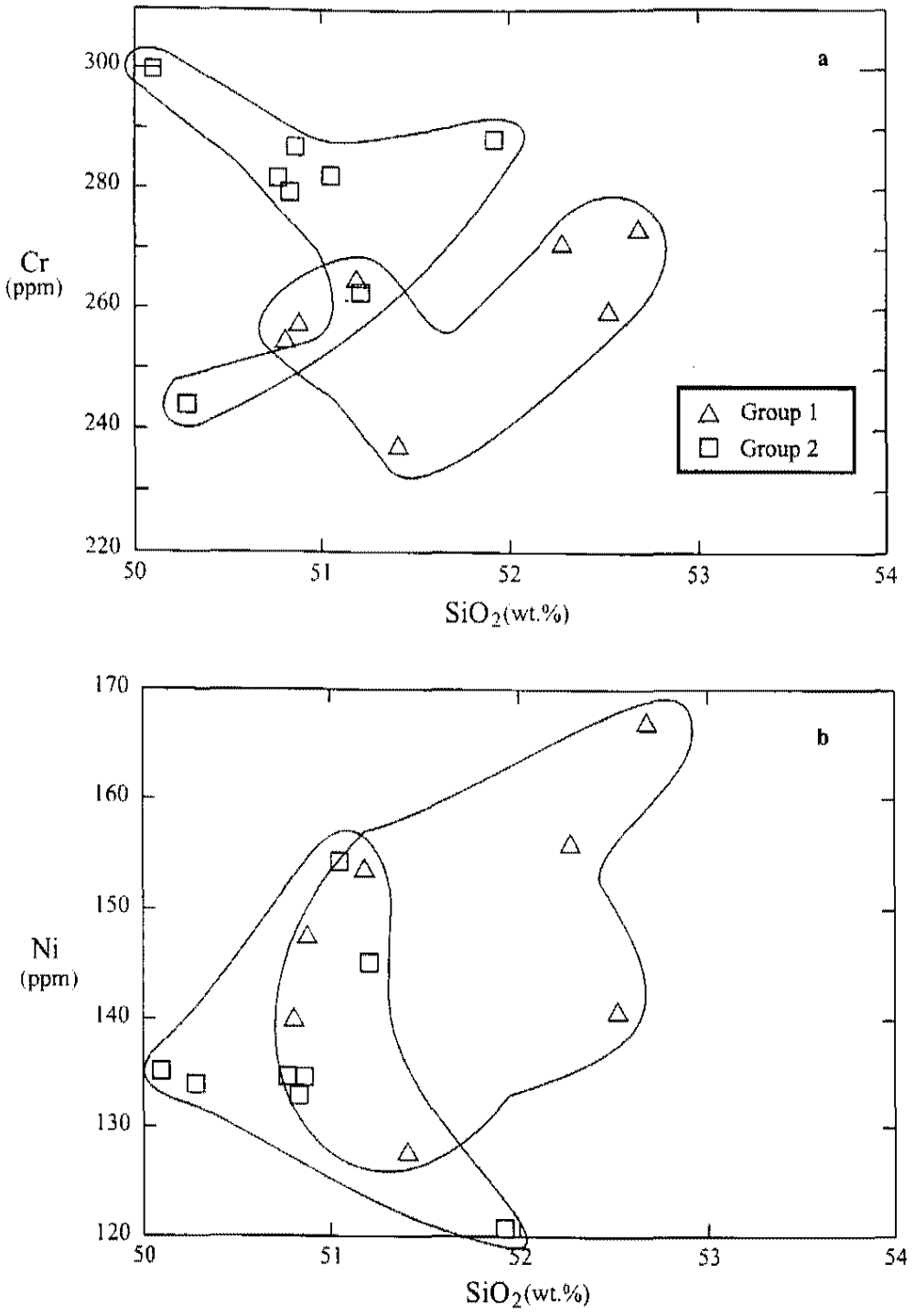

Figure 30. Harker diagrams showing SiO_2 (wt. %) vs. compatible trace elements Cr and Ni (ppm). (a) Cr increases in group 1 and shows scatter in group 2 with increasing SiO_2. (b) Ni data is scattered.

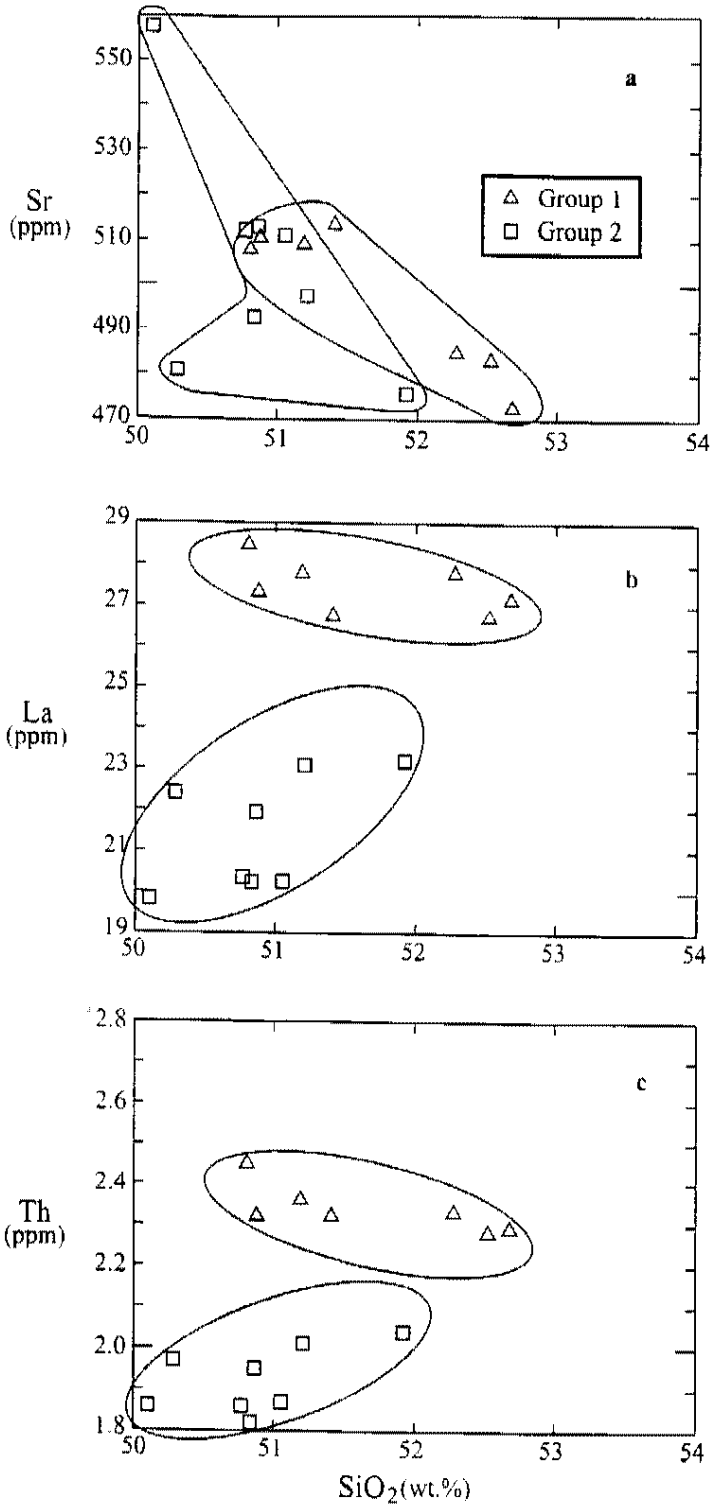

Figure 31. Harker diagrams showing SiO_2 (wt. %) vs. selected trace elements Sr, La, and Th (ppm). Xitle rocks fall into two groups. (a) Sr data is scattered in group 2 and decreases in group 1. (b) and (c) Group 1 decreases in incompatible element concentrations with increasing SiO_2, while group 2 increases in incompatible element concentrations with increasing SiO_2.

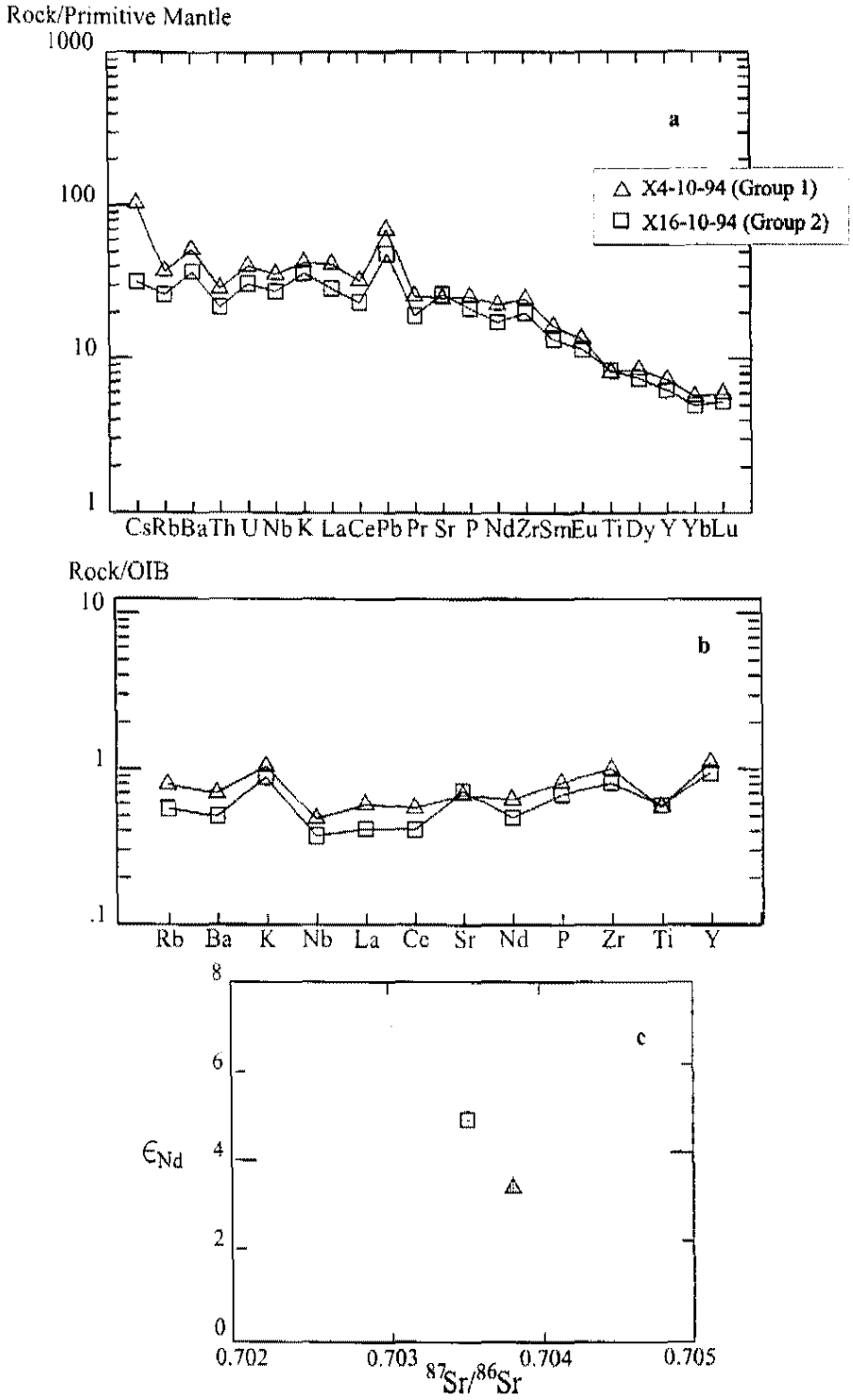

Figure 32. Normalized spider diagrams and isotopic data for Xitle rocks. (a) Rocks normalized to primitive mantle abundances from Sun and McDonough (1989). Note the troughs at Rb, Th, Ti and the peak at Pb. (b) Xitle lavas are similar to OIB but are slightly depleted in Rb, Ba, and LREE and exhibit Nb and Ti troughs. (c) The two Xitle geochemical groups also plot separately on an initial Sr diagram. The differences are small but are greater than that produced from analytical error (error bars shown). Note that error bar for initial Sr is shorter than the width of a symbol.

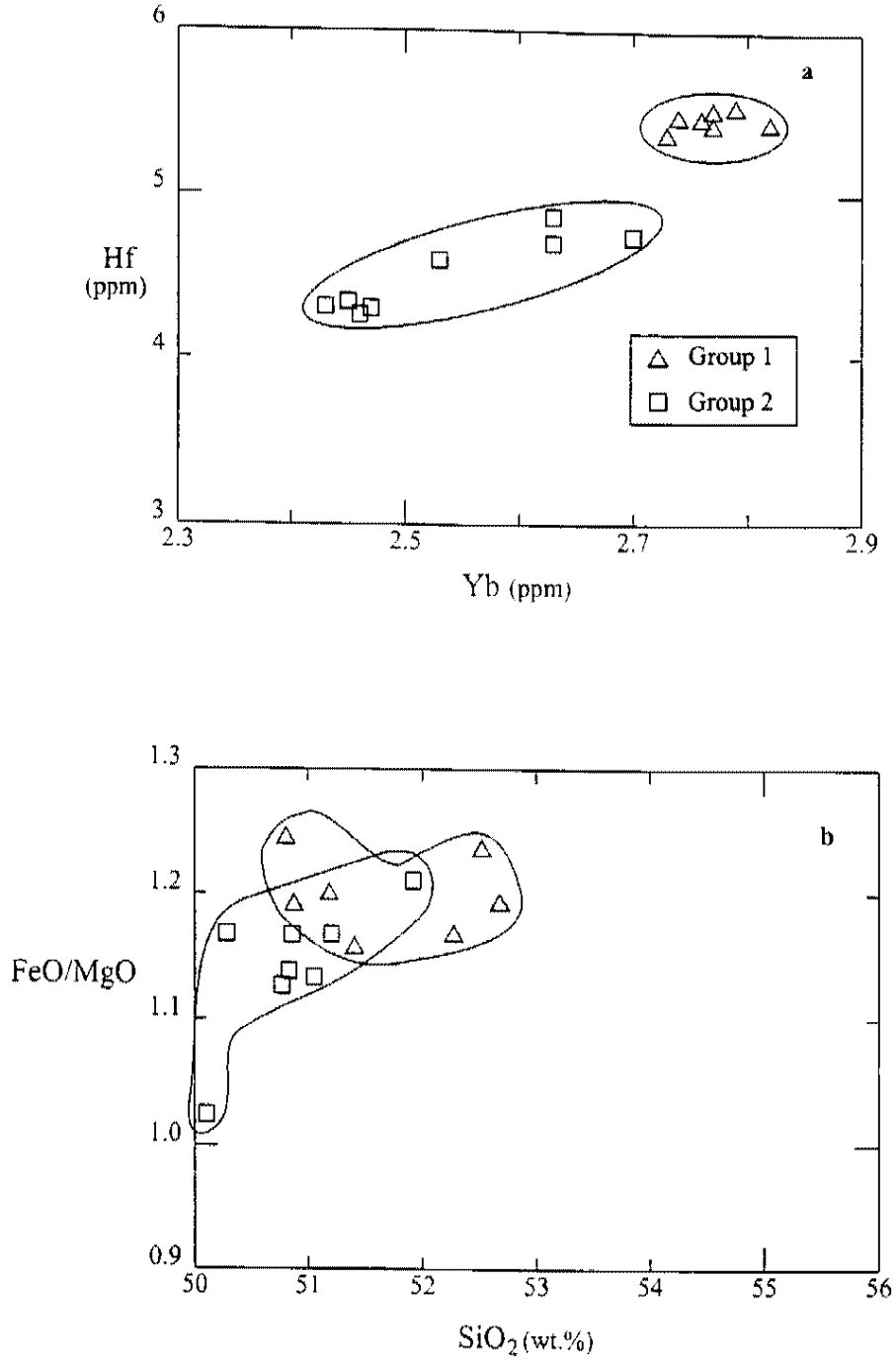

Figure 33. (a) Incompatible element plot of Yb vs. Hf shows that group 2 has a positive slope consistent with fractionation, while group 1 clusters. (b) SiO_2 vs. FeO/MgO plot also shows a positive slope in group 2 consistent with fractionation.

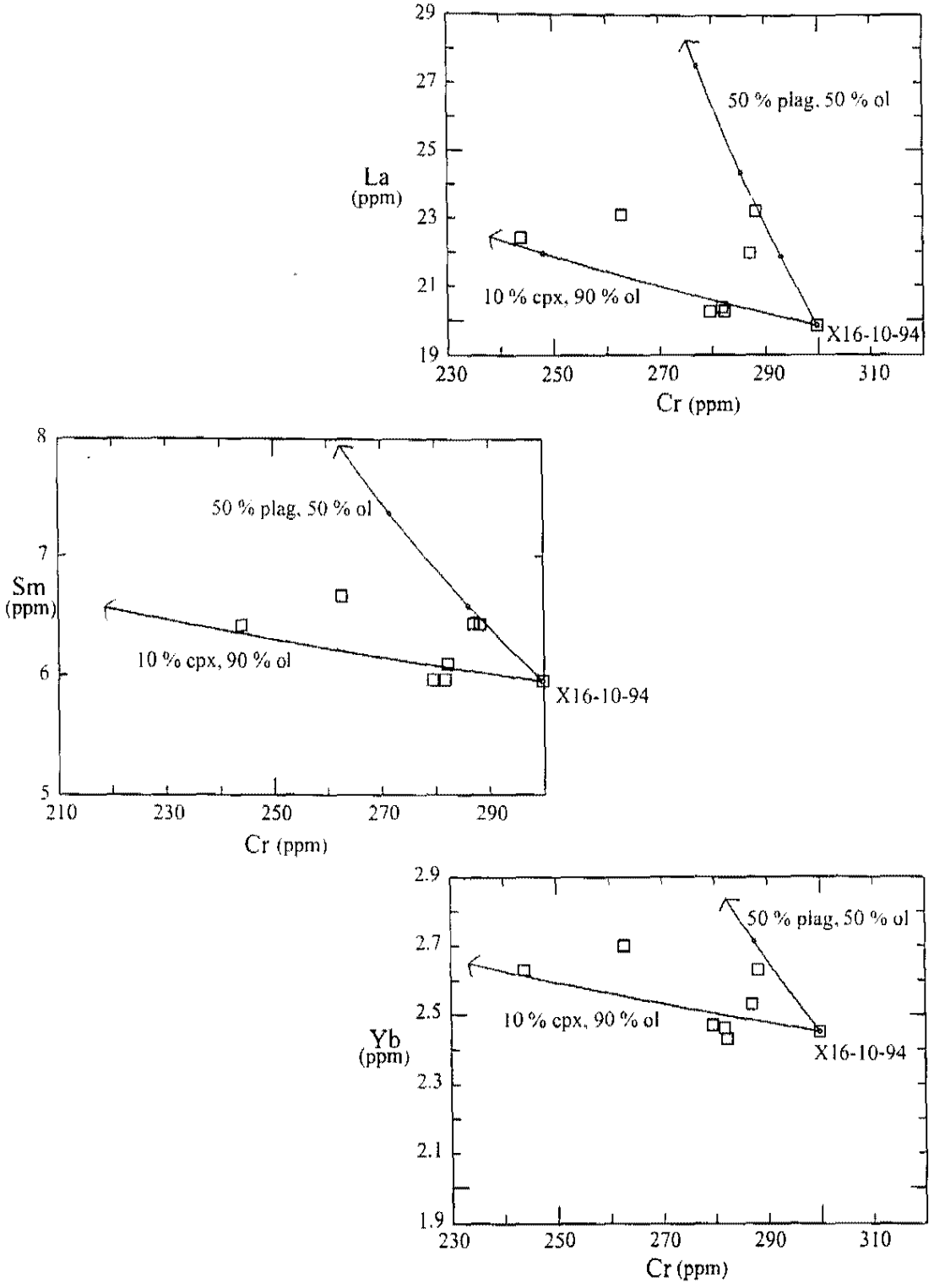

Figure 34. Fractional crystallization models for group 2 Xitle lavas. Models used the least evolved andesite sample X16-10-94 as the parent and require small amounts of fractionation (<15 %) of between 50-90 % olivine, 10-50 % plagioclase, and 0-10 %cpx.

Chapter 7

Conclusions

Important conclusions of this thesis that address the petrogenesis of andesites are:

1. Andesites of the northern McCullough Range are not homogeneous, but instead display a wide range of trace element chemistry and fall into at least 3 isotopic groups: A, B, and C. These isotopic groups represent three distinct andesitic end members.

2. Geochemical data and petrogenetic modeling show that many of the andesites in the northern McCullough Range were produced by mixing of the andesitic magmas represented by isotopic groups A and B.

3. The McCullough Range magmatic process involving mixing of andesitic magmas to produce andesite dominated sections has not been described before and is a significant contribution of this study. It provides a new explanation for andesite petrogenesis in extensional terranes, and may be applied to other andesite dominated sections in the Basin and Range.

4. The preliminary study of Xitle volcano in central Mexico shows similarities to the McCullough Range process. It is possible, therefore, that the petrogenetic model developed in the northern McCullough Range may be applied to extensional environments in other areas of the world.

Other contributions of this thesis include:

5. The volcanic section in the northern McCullough Range consists of a series of andesite flows, breccias, debris flows, as well as dacite domes and flows. These units were assigned informal names in this study and are as follows from oldest to youngest: the Ivan Canyon andesite, the Colony dacite, the Farmer Canyon andesite, and the Fog Ridge andesite. The Ivan Canyon andesite and Colony dacite sections were not described prior to this study.

6. Field observations support Weber and Smith's (1987) suggestion of a stratocone in the northern McCullough Range. This stratocone is most likely associated with eruption of the Farmer Canyon andesite section and possibly the Fog Ridge andesite section. In addition, a vent area for the Colony dacite is described.

7. Westerly dips in the northern McCullough Range may be due to structural tilting related to normal faulting. Dips south of the field area are to the east suggesting that there is a dip reversal in the central and western McCullough Range. The axis of this reversal lies just north of the McCullough Pass Caldera and passes through Hidden Valley.

Appendix I: **Point Count Data**

Whole rock model analyses; counts normalized to 100% (500 counts per section).

sample	**A1-3-94**	**A5-3-94**	**M18-1-95**	**M33-1-95**	**M1-2-95**	**A1-6-94**	**M10-1-95**	**M14-1-95**	**M23-1-95**	**M28-1-95**
	Fog Ridge andesite (Tfra)					*upper member of the Farmer Canyon andesite (Tfau)*			*Colony (Tcd) rhyolite*	*Tcd andesite*
phenocrysts	20.6	23.2	30.8	39.4	30.2	15.4	40.0	34.6	21.0	19.6
plagioclase	75.7	13.8	61.7	63.4	64.2	94.8	72.0	68.2	16.2	70.4
olivine	14.6	45.7	13.0	7.1	3.3		4.5	15.6		
clinopyroxene	9.7	40.5	25.3	29.4	32.4	5.2	19.5	16.2	1.0	
sanidine									71.4	
biotite									4.8	26.5
Fe-Ti oxides							4.0		6.7	3.1
matrix	79.4	76.8	69.2	60.6	69.8	84.6	60.0	65.4	79.0	80.4

*M1-5-95 contains xenoliths of basalt/andesite and A6-6-94 contains xenocrysts of quartz

sample	**M1-5-95**	**M29-1-95**	**M5-1-95**	**A6-6-94**	**M11-1-95**	**X4-10-94**	**X6-10-94**	**X12-10-94**	**X16-10-94**
	Tcd dacite	*Ivan Canyon andesite Tica*	*lower member Tfal*	*dike from Tfal*	*dike from Tfau*	*Xitle flows group 1*	*(lava dome) group 1*		*group 2*
phenocrysts	26.2	21.0	24.4	18.6	34.0	9.6	14.4	13.4	26.6
plagioclase	74.0	49.5	74.6	69.9	59.4	10.4		37.3	57.9
olivine						89.6	100.0	62.7	42.1
clinopyroxene	3.8	46.7	16.4		37.6				
hornblende			trace						
biotite	13.0		trace	16.1					
Fe-Ti oxides	0.8	3.8	9.0	1.1	3.0				
xenocrysts*	8.4			12.9					
zircon				trace					
matrix	73.8	79.0		81.4	66.0	90.4	85.6	86.6	73.4

Appendix II

Regional Structure and Tectonics

Wernicke et al. (1988) defined three zones of Cenozoic extension at the latitude of Las Vegas. These zones consist of a central relatively unextended block and two topographically low, highly extended blocks containing down-to-the-west normal faults. The extended block to the east was labeled the Las Vegas system, and the extended block to the west the Death Valley system (Wernicke et al., 1988). Although the McCullough Range lies within the Las Vegas system, it is a stable block when compared to other ranges in the region (Figure IIa). In the McCullough Range, Tertiary faulting resulted in only 20% extension, and only a few major faults crop out (Weber and Smith, 1987). The Spring Range (see Figure 1) just west of the McCullough Range is also relatively unextended, although some rotation of the range may have occurred during Tertiary extension (Wernicke, 1988). The River Mountains just northeast of the McCullough Range have been extended about 40% (Weber and Smith, 1987). In contrast, the Eldorado Mountains just east of the McCullough Range are highly faulted and were extended over 100% (Anderson, 1971).

Weber and Smith (1987) proposed a model to explain the structural integrity of the McCullough Range. They suggested that the River, Eldorado, and McCullough ranges lie in the upper plate of a west-dipping detachment fault, and that strike-slip and normal faults are transfer structures separating

zones of variable extension in the upper plate (Figure IIa). For example, the Hamblin-Bay fault forms the structural boundary between the River and Eldorado mountains. Weber and Smith (1987) called upon a high-angle, west-dipping normal fault (the Eldorado Valley fault) east of the McCullough Range to account for the 25°-40° east tilt in the central and southern part of the range. They proposed that the Hamblin-Bay fault turns south into the Eldorado Valley and becomes the Eldorado Valley fault which in turn soles into the underlying detachment. The Eldorado Valley fault may serve as the boundary between the McCullough and Eldorado fault-blocks. Weber and Smith (1987) suggested that the difference in the magnitude of extension between these two blocks is due to differences in the thickness of the hanging wall of this detachment structure. The hanging wall is thick beneath the McCullough Range, so the range was carried to the west in a coherent block without being internally faulted. In contrast, the Eldorado Range sits on a thin, easily deformed slice of the upper plate and therefore, was tilted and faulted during extension.

A model by Duebendorfer and Wallin (1991) refined the model of Weber and Smith (1987) and described temporal and spatial relations among the three main Tertiary structures in the Lake Mead area: the Lake Mead fault system, the Las Vegas Valley shear zone, and the Saddle Island Detachment (Figure IIb). The authors note that in the Lake Mead area between 12 and 9 Ma, basin development, normal faulting, stratal tilting, and volcanism occurred coevally with movement along the Las Vegas Valley shear zone and the Saddle Island Detachment. Furthermore, stratigraphic relations of Tertiary sedimentary rocks in Las Vegas Wash suggest that the River Mountains and Frenchman Mountain were part of the same structural block by 13.5 Ma (Bell and Smith, 1980). Movement along the Las Vegas Valley shear zone and the Saddle Island

Detachment at about 12 Ma displaced this block westward (Duebendorfer and Wallin, 1991). Because no structures have been identified separating the River Mountains from the McCullough Range, the McCullough Range is part of the same structural block that contains Frenchman Mountain and the River Mountains. The McCullough Range, therefore, also moved westward (Bridwell, 1991).

A more recent model by Anderson et al. (1994) offers an alternative explanation to the structural development of the Lake Mead area. Instead of detachment faulting, the authors called upon large scale tectonic escape related to structural rafting of fault blocks on top of a "flowing undermass of midcrustal material." They perceived the Lake Mead fault system as a complex zone of crustal flow where large scale upper-crustal blocks underwent horizontal collapse and westerly tectonic escape to accommodate intense north-south shortening. Anderson et al. (1994) suggested that models that view the Lake Mead fault system as a boundary separating regions of differential extension are too simplistic, and that detachment faults accommodated only minor amounts of extension. Although this hypothesis differs from previous models, it also requires that the McCullough Range moved to the west during regional extension.

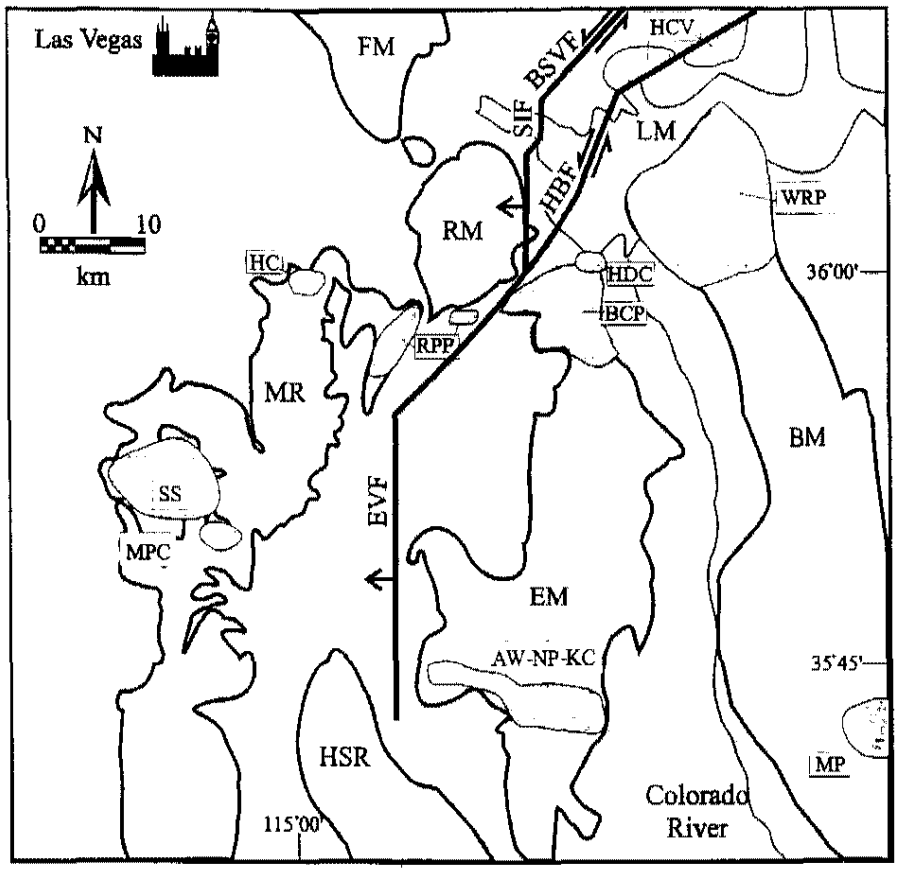

Figure IIa. Simplified geologic map showing major faults in the Lake Mead area as described by Weber and Smith (1987). The McCullough Range is less extended than other ranges in the area and lies in the upper plate of a west-dipping detachment fault. AW-NP-KC= Aztec Wash, Nelson, and Keyhole Canyon plutons; BM=Black Mountains; BCP=Boulder City pluton; EM=Eldorado Mountains; FM=Frenchmen Mountain; HCV=Hamblin-Cleopatra volcano; HC=Henderson caldera; HSR=Highland Spring Range; HDC=Hoover Dam caldera; LM=Lake Mead; MPC=McCullough Pass caldera; MR=McCullough Range; MP=Mt. Perkins pluton; RPP=Railroad Pass pluton; RM=River Mountains; SS=Sloan Sag; WRP=Wilson Ridge pluton.

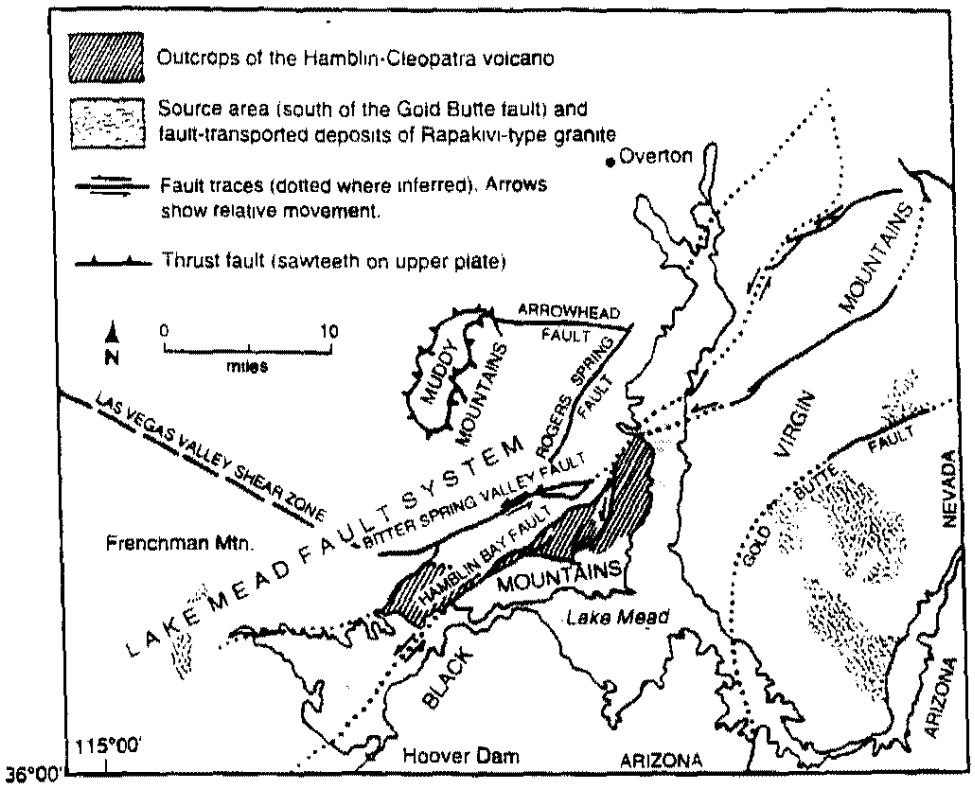

Figure IIb. Map of major fault systems in the Lake Mead area (Purkey et al., 1994)

Appendix III

Geochemical data

Whole rock chemical analyses of samples from the northern McCullough Range are reported by rock units. Totals for major oxides do not include loss on ignition values (LOI). Blank spaces indicate that no analyses were performed. Plate 1 contains a map including sample locations. Samples A1-3-94 through A8-6-94 trace element data was analyzed by INAA. All remaining samples were done by ICP-MS.

bas-and=basaltic-andesite; g-diorite=granodiorite

Tfra=Fog Ridge andesite
Tfau=upper member of the Farmer Canyon andesite
Tfal=lower member of the Farmer Canyon andesite
Tcd=Colony dacite
Tica=Ivan Canyon andesite

Whole Rock Chemical Analyses of the northern McCullough Range rocks. Sample numbers correspond to sample locations found on Plate 1.

Sample #	A1-3-94	A2-3-94	A3-3-94	A4-3-94	A5-3-94	A6-3-94
unit name	Tfra	Tfra	Tfra	Tfra	Tfra	Tfra
rock type	andesite	andesite	andesite	andesite	bas-and	andesite
isotope group	B	A	B	B	A	B
	X-Ray Fluorescence Analysis, wt. %					
SiO_2	53.44	52.46	52.94	53.93	50.17	53.37
Al_2O_3	17.60	15.87	16.12	16.89	14.47	16.76
TiO_2	1.42	1.55	1.45	1.51	1.64	1.44
FeO	7.72	8.10	7.36	7.75	8.77	7.65
CaO	7.16	8.31	7.82	7.30	8.45	7.48
K_2O	4.18	3.17	3.41	3.47	2.81	3.46
MnO	0.12	0.13	0.12	0.12	0.13	0.12
P_2O_5	1.59	0.91	1.00	0.79	0.81	0.76
Na_2O	3.16	2.99	3.06	3.15	2.38	3.12
MgO	3.56	5.93	5.10	4.50	7.15	4.41
Total	99.95	99.41	98.37	99.40	96.78	98.57
	X-Ray Fluorescence Analysis, ppm					
Cr	39	193	166	101	243	102
Zr	477	388	415	411	347	406
Rb	98	87	78	92	80	95
Sr	2005	1090	1133	971	975	1023
Nb	19	21	21	21	19	21
Ni	34	87	85	56	158	56
Y	26	26	26	25	26	26
Ba	2218	1333	1619	1431	1608	1514
	Isotope values calculated from data obtained by Isotope Dilution Analyses					
ε Nd	-6.67	-6.24	-7.11	-6.94	-6.95	-7.39
$^{87}Sr/^{86}Sr_{(i)}$	0.70813	0.70774	0.70820	0.70819	0.70758	0.70827
$^{206}Pb/^{204}Pb$	18.52	18.50	18.40	18.41	18.49	18.13
$^{207}Pb/^{204}Pb$	15.59	15.60	15.58	15.61	15.56	15.54
$^{208}Pb/^{204}Pb$	39.02	38.99	38.88	39.11	38.86	38.96
	Instrumental Neutron Activation Analysis, ppm					
La	110.3	87.1	101.8	89.1	76.9	85.6
Lu	0.3	0.4	0.3	0.3	0.3	0.4
Sm	17.8	13.1	13.9	13.0	12.4	12.6
U	2.5	2.6	3.3	5.3	4.0	3.4
Yb	2.17	2.14	2.12	2.44	1.75	2.55
Ce	215.2	167.6	199.3	171.3	150.8	163.5
Cs	1.08	2.16	1.46	2.06	1.79	2.27
Eu	4.24	2.87	3.07	2.99	3.02	2.67
Hf	8.88	8.41	9.66	9.43	7.55	8.90
Nd	104.78	73.51	74.19	87.87	64.21	62.54
Ta	0.74	1.19	1.34	1.25	1.15	1.09
Tb	1.48	0.93	1.15	1.17	1.13	1.21
Pr						
Dy						
Th	13.99	16.95	18.45	17.96	15.10	16.71
La'	1.4	1.1	1.3	1.2	1.0	1.1

Sample #	A1-6-94	A2-6-94	A3-6-94	A4-6-94	A5-6-94	A6-6-94
unit name	Tfau	Tfau	Tfra	Tfra	dike-Tfau	dike-Tfal
rock type	andesite	andesite	andesite	andesite	andesite	dacite
isotope group	C	C	B	B		D
			X-Ray Fluorescence Analysis, wt. %			
SiO_2	53.46	58.88	58.31	52.90	59.83	63.23
Al_2O_3	16.00	17.05	16.72	15.98	16.19	16.04
TiO_2	1.21	1.05	1.03	1.20	0.84	0.55
FeO	7.58	5.63	5.70	7.77	4.73	3.18
CaO	6.98	5.02	4.86	7.16	4.02	1.94
K_2O	2.92	3.21	3.23	2.81	4.33	4.26
MnO	0.12	0.07	0.09	0.13	0.11	0.11
P_2O_5	0.54	0.50	0.54	0.55	0.44	0.36
Na_2O	3.15	3.38	3.39	3.14	3.42	3.89
MgO	5.06	2.33	2.56	4.79	2.02	1.50
Total	97.02	97.12	96.43	96.43	95.93	95.03
			X-Ray Fluorescence Analysis, ppm			
Cr	9	12	54	66	10	0
Zr	277	300	326	315	364	441
Rb	83	70	92	84	139	130
Sr	906	1023	1101	1046	748	776
Nb	14	14	17	16	22	22
Ni	6	8	67	67	10	0
Y						
Ba	1410	1605	1416	1419	1524	1973
	Isotope values calculated from data obtained by Isotope Dilution Analyses					
ε Nd	-9.19	-8.83	-7.40	-7.18	-10.10	-8.62
$^{87}Sr/^{86}Sr_{(i)}$	0.70901	0.70897	0.70821	0.70813	0.70968	0.70946
$^{206}Pb/^{204}Pb$	18.02	18.05	18.30	18.29	18.08	18.16
$^{207}Pb/^{204}Pb$	15.52	15.55	15.54	15.53	15.57	15.58
$^{208}Pb/^{204}Pb$	38.67	38.67	38.91	38.87	39.26	39.04
			Instrumental Neutron Activation Analysis, ppm			
La	74.4	70.3	69.1	67.9	76.7	94.7
Lu	0.3	0.4	0.3	0.3	0.4	0.4
Sm	10.3	10.3	10.7	10.6	10.2	11.1
U	2.6	2.6	2.6	2.7	4.1	3.0
Yb	2.58	2.32	2.10	2.23	2.44	2.95
Ce	139.2	132.1	136.0	135.3	145.7	176.6
Cs	1.83	0.91	1.47	1.09	1.36	1.99
Eu	2.45	2.48	2.67	2.53	2.05	2.44
Hf	7.06	6.62	7.00	6.84	9.23	11.08
Nd	51.49	92.92	65.71	59.92	69.25	70.17
Ta	1.19	0.85	1.19	0.88	1.38	1.31
Tb	0.95	1.01	1.13	0.93	1.07	0.98
Pr						
Dy						
Th	13.68	12.97	12.26	12.06	15.51	16.91
La'	1.0	0.9	0.9	0.9	1.0	1.2

Sample #	A7-6-94	A8-6-94	M1-1-95	M2-1-95	M4-1-95	M5-1-95
unit	dike-Tfal	Ti	Tfra	Tfra	Tfra	Tfal
rock type	dacite	g-diorite	andesite	andesite	andesite	andesite
isotope group	D					C
	X-Ray Fluorescence Analysis, wt. %					
SiO_2	64.01	68.17	53.39	56.68	52.96	55.60
Al_2O_3	15.57	14.56	15.93	17.08	16.11	16.60
TiO_2	0.53	0.43	1.30	1.18	1.26	0.98
FeO	3.10	2.36	8.20	7.60	7.17	5.58
CaO	3.06	1.70	7.95	6.24	7.12	4.37
K_2O	4.69	5.01	2.50	3.08	2.79	3.68
MnO	0.07	0.05	0.12	0.11	0.10	0.08
P_2O_5	0.26	0.25	0.49	0.56	0.57	0.47
Na_2O	2.84	3.78	3.15	3.24	2.99	3.20
MgO	1.60	0.87	5.48	3.04	4.73	2.51
Total	95.72	97.18	98.50	98.82	95.80	93.06
	X-Ray Fluorescence Analysis, ppm					
Cr	0	10	97	23	46	22
Zr	434	232	263	259	265	345
Rb	139	163	63	46	52	80
Sr	751	340	1089	791	956	871
Nb	21	24	12	12	13	17
Ni	0	6	0	72	48	0
Y			23	22	21	30
Ba	1187	1190	1158	1053	1207	1437
	Isotope values calculated from data obtained by Isotope Dilution Analyses					
ε Nd	-8.68	-8.87				-9.65
$^{87}Sr/^{86}Sr_{(i)}$	0.70958	0.71016				0.70922
$^{206}Pb/^{204}Pb$	18.36	17.98				
$^{207}Pb/^{204}Pb$	15.58	15.54				
$^{208}Pb/^{204}Pb$	38.98	39.05				
	Instrumental Neutron Activation Analysis, ppm; Inductively Coupled Plasma Mass Spectrometer, ppm					
La	91.0	68.1	74.8	58.9	64.5	91.3
Lu	0.4	0.4	0.4	0.4	0.3	0.4
Sm	10.6	7.6	11.7	9.8	11.2	12.4
U	3.6	5.1	3.5	2.1	2.3	2.9
Yb	2.73	2.57	2.51	2.31	2.16	2.67
Ce	170.9	131.3	137.2	111.0	121.0	170.3
Cs	1.57	1.59	2.02	1.18	1.54	0.94
Eu	2.45	1.54	2.91	2.48	2.85	2.84
Hf	11.11	7.62	5.63	5.74	5.81	7.67
Nd	109.98	39.50	63.87	50.21	57.51	71.14
Ta	1.13	2.12	0.80	0.95	0.94	1.09
Tb	0.92	0.74	1.14	1.05	1.09	1.16
Pr			15.97	12.67	14.21	18.65
Dy			6.02	5.72	5.72	6.2
Th	16.74	26.39	14.20	9.31	9.40	16.16
La'	1.2	0.9	1.0	0.8	0.8	1.2

Sample #	M6-1-95	M7-1-95	M8-1-95	M9-1-95	M10-1-95	M11-1-95
unit	dike-Tfal	Tfra	Tfra	Tfra	Tfau	dike-Trau
rock type	andesite	andesite	andesite	andesite	andesite	andesite
isotope group					B	
			X-Ray Fluorescence Analysis, wt. %			
SiO_2	53.40	58.24	57.43	57.62	51.47	52.99
Al_2O_3	15.67	16.57	16.61	17.02	17.22	16.01
TiO_2	1.32	1.03	1.00	0.98	1.09	1.23
FeO	7.34	5.85	5.53	5.25	7.07	6.84
CaO	6.17	5.03	4.94	4.58	7.22	6.74
K_2O	3.51	3.15	3.20	4.28	3.51	3.95
MnO	0.10	0.09	0.09	0.08	0.08	0.10
P_2O_5	0.58	0.48	0.48	0.48	0.73	0.64
Na_2O	3.09	3.51	3.28	3.60	3.14	3.20
MgO	5.33	2.22	2.16	1.70	3.60	4.15
Total	96.51	96.17	94.72	95.59	95.13	95.85
			X-Ray Fluorescence Analysis, ppm			
Cr	114	15	18	16	29	72
Zr	356	278	264	379	360	402
Rb	81	74	66	98	76	91
Sr	849	855	817	843	1257	945
Nb	19	13	13	18	15	20
Ni	90	0	0	0	0	53
Y	27	30	26	29	29	32
Ba	1344	1516	1215	1466	1839	1543
			Isotope values calculated from data obtained by Isotope Dilution Analyses			
ε Nd					-7.21	
$^{87}Sr/^{86}Sr_{(i)}$					0.70832	
$^{206}Pb/^{204}Pb$						
$^{207}Pb/^{204}Pb$						
$^{208}Pb/^{204}Pb$						
			Instrumental Neutron Activation Analysis, ppm; Inductively Coupled Plasma Mass Spectrometer, ppm			
La	88.4	68.2	66.7	86.4	87.4	91.4
Lu	0.4	0.4	0.4	0.4	0.4	0.4
Sm	13.0	10.3	9.9	11.5	13.9	13.5
U	4.0	2.4	2.4	3.3	2.9	4.2
Yb	2.35	2.58	2.50	2.47	2.32	2.41
Ce	161.7	125.3	123.6	160.0	162.7	170.0
Cs	2.02	1.91	1.64	1.46	1.35	1.35
Eu	2.97	2.49	2.49	2.55	3.55	3.00
Hf	8.48	6.13	5.87	8.70	7.26	8.91
Nd	69.67	53.49	52.79	65.32	72.41	73.32
Ta	1.52	1.02	1.01	1.34	0.89	1.34
Tb	1.16	1.09	1.05	1.10	1.25	1.21
Pr	17.85	13.92	13.7	17.58	18.41	19.02
Dy	6.28	5.91	5.84	5.89	6.18	6.39
Th	17.49	11.60	11.02	14.06	11.20	17.93
La'	1.1	0.9	0.9	1.1	1.1	1.2

Sample #	M12-1-95	M13-1-95	M14-1-95	M15-1-95	M16-1-95	M17-1-95
unit	Tfau	Tfau	Tfau	Tfra	dike-Tfau	Tfra
rock type	andesite	andesite	andesite	andesite	andesite	andesite
isotope group		B				
			X-Ray Fluorescence Analysis, wt. %			
SiO_2	51.15	52.01	51.06	55.14	56.29	53.72
Al_2O_3	17.06	16.83	16.97	18.03	16.00	15.46
TiO_2	1.12	1.13	1.26	1.16	1.13	1.17
FeO	7.56	7.57	7.65	5.40	6.47	7.31
CaO	7.28	7.14	7.58	4.68	5.87	7.40
K_2O	3.31	3.54	2.85	5.04	3.63	3.36
MnO	0.11	0.09	0.12	0.09	0.10	0.11
P_2O_5	0.74	0.73	0.58	0.57	0.55	0.60
Na_2O	3.08	3.12	3.09	3.80	3.39	2.99
MgO	3.77	3.69	4.32	1.83	3.98	5.78
Total	95.18	95.85	95.47	95.73	97.41	97.90
			X-Ray Fluorescence Analysis, ppm			
Cr	24	20	45	19	55	146
Zr	369	311	275	458	328	364
Rb	56	67	55	131	68	84
Sr	1335	1141	858	861	752	888
Nb	15	13	13	27	17	18
Ni	0	0	42	0	62	87
Y	29	23	25	35	24	27
Ba	2276	1375	1270	1579	803	1226
			Isotope values calculated from data obtained by Isotope Dilution Analyses			
ε Nd		-6.84				
$^{87}Sr/^{86}Sr_{(i)}$		0.70821				
$^{206}Pb/^{204}Pb$						
$^{207}Pb/^{204}Pb$						
$^{208}Pb/^{204}Pb$						
			Instrumental Neutron Activation Analysis, ppm; Inductively Coupled Plasma Mass Spectrometer, ppm			
La	88.7	89.1	61.4	101.3	88.0	79.1
Lu	0.4	0.4	0.4	0.4	0.4	0.4
Sm	14.6	14.7	10.6	13.5	12.9	12.4
U	3.0	3.2	1.8	5.4	3.1	3.7
Yb	2.35	2.30	2.34	2.60	2.54	2.35
Ce	167.1	168.2	117.2	188.8	156.9	148.9
Cs	2.22	2.05	0.89	2.51	1.45	2.45
Eu	3.66	3.68	2.72	3.05	2.91	2.97
Hf	7.38	7.01	5.92	10.48	8.74	7.83
Nd	75.51	77.03	54.41	76.38	69.36	66.96
Ta	0.89	0.85	0.85	1.77	1.34	1.27
Tb	1.32	1.31	1.11	1.21	1.18	1.21
Pr	19.34	19.26	13.61	20.38	17.95	17.15
Dy	6.73	6.51	5.92	6.24	6.57	6.21
Th	12.26	11.82	7.77	20.43	14.97	15.12
La'	1.2	1.2	0.8	1.3	1.1	1.0

Sample #	M18-1-95	M19-1-95	M20-1-95	M21-1-95	M22-1-95	M23-1-95
unit	Tfra	Tfra	Tfra	Tfra	Tfra	Tcd
rock type	andesite	andesite	andesite	andesite	andesite	rhyolite
isotope group						D
			X-Ray Fluorescence Analysis, wt. %			
SiO_2	54.58	54.27	55.76	52.43	54.58	70.70
Al_2O_3	15.74	15.82	16.07	14.85	16.08	14.60
TiO_2	1.15	1.16	1.15	1.33	1.26	0.35
FeO	7.52	7.48	7.44	8.13	7.46	1.64
CaO	7.55	7.49	7.86	8.08	6.83	1.09
K_2O	2.93	2.91	2.97	2.92	3.53	8.55
MnO	0.11	0.11	0.11	0.12	0.11	0.04
P_2O_5	0.50	0.47	0.52	0.66	0.58	0.05
Na_2O	3.19	3.32	3.35	3.08	3.38	2.87
MgO	5.31	5.33	5.80	7.17	4.70	0.18
Total	98.58	98.36	101.03	98.78	98.51	100.07
			X-Ray Fluorescence Analysis, ppm			
Cr	123	126	149	219	78	23
Zr	294	286	304	348	379	281
Rb	65	66	68	65	74	198
Sr	759	741	790	962	850	130
Nb	15	14	15	19	18	31
Ni	78	81	91	146	50	0
Y	23	22	24	26	29	30
Ba	936	958	1117	1486	1119	276
			Isotope values calculated from data obtained by Isotope Dilution Analyses			
ε Nd						-8.46
$^{87}Sr/^{86}Sr_{(i)}$						0.70932
$^{206}Pb/^{204}Pb$						
$^{207}Pb/^{204}Pb$						
$^{208}Pb/^{204}Pb$						
			Instrumental Neutron Activation Analysis, ppm; Inductively Coupled Plasma Mass Spectrometer, ppm			
La	60.4	62.5	63.7	78.5	86.2	99.9
Lu	0.4	0.4	0.4	0.3	0.4	0.4
Sm	9.8	10.3	10.5	12.7	13.0	9.6
U	3.6	2.9	3.2	3.4	4.0	6.3
Yb	2.34	2.32	2.33	2.23	2.70	2.27
Ce	114.1	116.6	117.8	144.6	160.1	169.5
Cs	1.99	1.79	2.09	1.86	1.13	2.75
Eu	2.35	2.44	2.54	3.06	2.91	1.55
Hf	6.17	6.45	6.55	7.32	8.58	8.52
Nd	52.77	52.40	54.31	66.19	69.81	58.12
Ta	1.00	1.04	1.06	1.23	1.30	2.48
Tb	1.01	1.04	1.05	1.23	1.27	0.88
Pr	13.44	13.43	13.56	16.53	17.74	17.1
Dy	5.57	5.65	5.89	6.4	6.83	4.96
Th	11.95	11.99	12.83	14.51	16.99	29.64
La'	0.8	0.8	0.8	1.0	1.1	1.3

Sample #	M24-1-95	M25-1-95	M26-1-95	M27-1-95	M28-1-95	M29-1-95
unit	Tfra	Tfra	Tfra	Tfra	Tcd	Tica
rock type	andesite	andesite	andesite	andesite	andesite	andesite
isotope group					C	B
	X-Ray Fluorescence Analysis, wt. %					
SiO_2	54.39	55.27	55.98	53.96	58.07	54.15
Al_2O_3	15.86	16.02	16.04	15.59	15.84	15.06
TiO_2	1.13	1.06	1.08	1.15	0.80	1.28
FeO	7.10	6.86	6.96	6.29	4.81	6.26
CaO	7.07	6.04	6.47	6.50	6.28	7.58
K_2O	3.43	3.50	3.61	3.70	4.20	4.12
MnO	0.11	0.12	0.11	0.10	0.09	0.20
P_2O_5	0.58	0.60	0.61	0.64	0.45	0.57
Na_2O	3.43	3.68	3.40	3.20	3.45	3.45
MgO	5.07	4.24	4.52	4.19	1.73	3.40
Total	98.16	97.39	98.78	95.32	95.73	96.08
	X-Ray Fluorescence Analysis, ppm					
Cr	86	74	82	70	33	119
Zr	357	377	402	384	278	406
Rb	72	70	81	91	85	107
Sr	948	840	939	907	722	836
Nb	20	17	19	19	15	23
Ni	69	65	62	49	0	80
Y	24	29	32	27	18	23
Ba	1209	1090	1505	954	1145	1066
	Isotope values calculated from data obtained by Isotope Dilution Analyses					
ε Nd					-9.84	-7.30
$^{87}Sr/^{86}Sr_{(i)}$					0.70905	0.70823
$^{206}Pb/^{204}Pb$						
$^{207}Pb/^{204}Pb$						
$^{208}Pb/^{204}Pb$						
	Instrumental Neutron Activation Analysis, ppm; Inductively Coupled Plasma Mass Spectrometer, ppm					
La	84.5	91.0	92.0	97.2	76.9	98.1
Lu	0.4	0.4	0.4	0.4	0.3	0.3
Sm	12.5	12.2	12.3	14.5	9.9	12.7
U	3.2	2.8	3.0	4.4	3.3	5.6
Yb	2.34	2.82	2.63	2.55	2.11	2.20
Ce	154.0	164.1	164.0	177.6	137.1	179.5
Cs	1.78	1.24	2.02	2.32	1.92	1.65
Eu	2.92	2.72	2.79	3.16	2.38	2.76
Hf	7.82	8.60	8.50	9.08	6.37	10.08
Nd	67.33	66.02	67.47	76.68	55.37	73.96
Ta	1.24	1.26	1.31	1.42	1.16	2.07
Tb	1.16	1.23	1.22	1.31	0.97	1.15
Pr	17.24	17.45	18.01	20.22	14.84	19.91
Dy	6.31	6.56	6.56	6.73	5.12	5.95
Th	14.45	14.75	14.75	18.82	15.37	24.18
La'	1.1	1.2	1.2	1.3	1.0	1.3

Sample #	M30-1-95	M31-1-95	M32-1-94	M33-1-95	M34-1-95	M1-2-95
unit	Tfra	Tfra	Tfra	Tfra	Tfra	Tfra
rock type	andesite	andesite	andesite	andesite	andesite	andesite
isotope group						
	X-Ray Fluorescence Analysis, wt. %					
SiO_2	53.00	54.20	53.95	54.75	54.13	52.76
Al_2O_3	15.62	15.97	15.60	15.60	15.50	15.37
TiO_2	1.11	1.16	1.25	1.22	1.19	1.30
FeO	6.76	7.28	7.78	7.78	7.60	7.14
CaO	7.25	7.57	8.03	7.76	8.26	7.84
K_2O	3.72	3.93	3.67	3.79	3.77	3.73
MnO	0.11	0.12	0.12	0.12	0.12	0.11
P_2O_5	0.66	0.67	0.66	0.62	0.64	0.69
Na_2O	3.00	3.28	3.27	3.21	3.25	3.20
MgO	4.84	5.02	5.82	6.01	5.88	5.41
Total	96.07	99.20	100.15	100.84	100.32	97.55
	X-Ray Fluorescence Analysis, ppm					
Cr	86	69	113	133	131	85
Zr	383	383	352	360	348	391
Rb	96	94	84	91	93	83
Sr	1005	998	930	936	899	1121
Nb	18	18	17	16	16	18
Ni	44	39	67	63	62	64
Y	29	28	27	26	24	26
Ba	1675	1567	1363	1288	1139	1324
	Isotope values calculated from data obtained by Isotope Dilution Analyses					
ε Nd						
$^{87}Sr/^{86}Sr_{(i)}$						
$^{206}Pb/^{204}Pb$						
$^{207}Pb/^{204}Pb$						
$^{208}Pb/^{204}Pb$						
	Instrumental Neutron Activation Analysis, ppm; Inductively Coupled Plasma Mass Spectrometer, ppm					
La	86.5	84.5	79.0	80.0	78.9	97.1
Lu	0.4	0.4	0.4	0.4	0.4	0.4
Sm	14.4	14.0	13.4	13.5	13.3	15.2
U	3.9	3.9	3.5	3.6	3.8	4.5
Yb	2.46	2.41	2.30	2.31	2.31	2.39
Ce	163.0	159.6	150.8	148.7	146.5	181.0
Cs	2.39	2.30	1.96	2.06	2.89	1.95
Eu	3.43	3.32	3.20	3.19	3.13	3.44
Hf	8.57	8.22	7.73	8.00	7.92	8.71
Nd	73.81	72.83	67.91	68.65	68.81	81.26
Ta	1.32	1.30	1.24	1.26	1.22	1.36
Tb	1.38	1.33	1.27	1.26	1.25	1.30
Pr	18.68	18.34	17.26	17.22	17.05	20.91
Dy	7.05	6.72	6.58	6.52	6.54	6.65
Th	15.57	15.77	14.22	14.37	14.08	17.85
La'	1.1	1.1	1.0	1.0	1.0	1.3

Sample #	M2-2-95	M3-2-95	M4-2-95	M1-5-95	922-10
unit	Tfra	Tfra	Tfra	Tcd	
rock type	andesite	andesite	andesite	dacite	granite
isotope group					
	X-Ray Fluorescence Analysis, wt. %				
SiO_2	52.42	56.72	56.77	68.14	73.97
Al_2O_3	15.23	15.97	17.22	14.95	13.84
TiO_2	1.21	1.27	1.19	0.49	0.16
FeO	7.63	7.25	8.03	2.40	1.66
CaO	8.56	6.41	6.51	2.21	1.28
K_2O	3.26	3.98	3.14	2.69	4.24
MnO	0.12	0.11	0.12	0.05	0.04
P_2O_5	0.64	0.56	0.54	0.10	
Na_2O	3.09	3.51	3.52	5.22	4.16
MgO	5.57	4.43	3.09	0.81	0.41
Total	97.72	100.21	100.12	97.05	99.76
	X-Ray Fluorescence Analysis, ppm				
Cr	94	70	26	11	
Zr	354	403	282	340	111
Rb	71	109	65	203	122
Sr	1117	851	1151	687	300
Nb	15	20	11	22	9
Ni	60	48	0	0	
Y	27	31	26	28	
Ba	1395	1426	1590	785	869
	Values calculated from data obtained by Isotope Dilution Analyse				
ε Nd				-8.92	-12.50
$^{87}Sr/^{86}Sr_{(i)}$				0.70943	0.71267
$^{206}Pb/^{204}Pb$					
$^{207}Pb/^{204}Pb$					
$^{208}Pb/^{204}Pb$					
	Instrumental Neutron Activation Analysis, ppm; Inductively Coupled Plasma Mass Spectrometer, ppm				
La	83.7	90.6	80.8	91.5	33.5
Lu	0.4	0.4	0.4	0.4	0.2
Sm	14.0	13.6	12.6	8.9	3.3
U	3.2	4.4	3.6	4.6	
Yb	2.30	2.56	2.47	2.21	1.32
Ce	155.6	167.0	145.9	159.1	54.0
Cs	1.70	3.40	2.11	19.76	
Eu	3.40	2.90	3.06	1.67	0.73
Hf	7.63	9.16	5.89	8.41	
Nd	74.18	70.03	64.24	54.33	16.21
Ta	1.08	1.48	0.85	1.69	1.22
Tb	1.27	1.27	1.12	0.81	0.38
Pr	18.28	18.46	16.01	15.98	
Dy	6.73	6.61	6.13	4.54	
Th	12.40	18.73	15.03	22.01	
La'	1.1	1.2	1.0	1.2	

Whole Rock Chemical Analyses of rocks from Xitle volcano

Sample #	X4-10-94	X5-10-94	X6-10-94	X7-10-94	X8-10-94	X9-10-94
flow	I	VI	lava dome	V	III	IV
rock type	bas-and	bas-and	bas-and	bas-and	bas-and	bas-and
			X-Ray Fluorescence Analysis, wt. %			
SiO_2	50.81	51.19	50.88	51.92	52.52	51.41
Al_2O_3	15.27	15.10	15.12	16.06	15.67	15.35
TiO_2	1.78	1.77	1.78	1.78	1.79	1.79
FeO	9.02	9.30	9.10	9.98	9.87	9.30
CaO	7.32	7.33	7.36	8.41	7.80	7.43
K_2O	1.29	1.29	1.31	1.21	1.31	1.29
MnO	0.15	0.16	0.15	0.15	0.14	0.16
P_2O_5	0.56	0.56	0.57	0.51	0.55	0.53
Na_2O	3.20	3.24	3.17	3.97	3.93	3.34
MgO	7.25	7.76	7.64	8.24	7.99	8.04
Total	96.64	97.69	97.06	102.22	101.56	98.63
			X-Ray Fluorescence Analysis, ppm			
Cr	254	265	257	288	259	237
Zr	278	279	279	233	257	274
Rb	21	21	22	17	20	22
Sr	508	509	511	476	483	513
Nb	23	23	23	16	18	22
Ni	140	153	147	121	141	128
Y	34	33	33	27	30	34
Ba	212	209	247	178	227	247
	Isotope values calculated from data obtained by Isotope Dilution Analyses					
ε Nd	3.38					
$^{87}Sr/^{86}Sr_{(i)}$	0.70382					
	Instrumental Neutron Activation Analysis, ppm; Inductively Coupled Plasma Mass Spectrometer, ppm					
La	28.5	27.8	27.3	23.2	26.7	26.8
Lu	0.4	0.5	0.4	0.4	0.4	0.4
Sm	7.3	7.4	7.1	6.4	7.2	7.3
U	0.9	0.8	0.8	0.7	0.8	0.8
Yb	2.82	2.79	2.77	2.63	2.73	2.76
Ce	57.7	57.4	56.4	47.2	54.7	56.2
Cs	0.81	0.68	0.7	0.6	0.66	0.66
Eu	2.28	2.28	2.27	2.07	2.25	2.26
Hf	5.43	5.53	5.42	4.87	5.36	5.46
Nd	30.65	29.97	30	26.54	28.95	29.43
Ta	1.53	1.55	1.54	1.37	1.53	1.55
Tb	1.08	1.07	1.07	0.97	1.04	1.08
Pr	7.11	7	6.97	5.91	6.67	6.85
Dy	6.3	6.38	6.3	5.82	6.38	6.3
Th	2.45	2.36	2.32	2.04	2.28	2.32

Sample #	X10-10-94	X11-10-94	X12-10-94	X13-10-94	X14-10-94	X15-10-95
flow	II	V	IV	II	III	III
rock type	bas-and	bas-and	bas-and	bas-and	bas-and	bas-and
			X-Ray Fluorescence Analysis, wt. %			
SiO_2	52.68	50.28	54.33	52.28	50.77	50.83
Al_2O_3	15.53	15.77	15.44	15.38	15.77	15.86
TiO_2	1.77	1.80	1.06	1.80	1.84	1.89
FeO	9.92	9.35	7.03	9.74	10.19	10.19
CaO	7.55	8.16	7.30	7.54	8.60	8.53
K_2O	1.32	1.12	1.22	1.30	1.12	1.13
MnO	0.15	0.15	0.12	0.15	0.15	0.15
P_2O_5	0.61	0.50	0.31	0.60	0.49	0.49
Na_2O	3.98	3.63	3.33	3.93	3.70	3.84
MgO	8.32	8.00	7.57	8.35	9.05	8.95
Total	101.83	98.76	97.72	101.07	101.67	101.84
			X-Ray Fluorescence Analysis, ppm			
Cr	273	244	236	271	282	280
Zr	268	225	174	273	220	210
Rb	19	15	21	19	17	15
Sr	473	481	536	485	512	493
Nb	22	18	9	21	17	16
Ni	167	134	156	156	135	133
Y	32	27	19	32	28	26
Ba	177	51	265	197	60	69
			Isotope values calculated from data obtained by Isotope Dilution Analyses			
ε Nd						
$^{87}Sr/^{86}Sr$						
			Instrumental Neutron Activation Analysis, ppm; Inductively Coupled Plasma Mass Spectrometer, ppm			
La	27.2	22.4	20.5	27.8	20.4	20.2
Lu	0.4	0.4	0.3	0.4	0.4	0.4
Sm	7.2	6.4	5.3	7.3	6.0	6.0
U	0.8	0.7	0.9	0.8	0.7	0.6
Yb	2.74	2.63	1.91	2.77	2.46	2.47
Ce	56.5	46.6	41.5	57.5	42.0	42.2
Cs	0.69	0.53	0.8	0.69	0.41	0.3
Eu	2.24	2.08	1.62	2.25	2.02	1.97
Hf	5.47	4.71	3.48	5.51	4.26	4.3
Nd	30.04	25.44	22.5	29.73	23.66	23.91
Ta	1.5	1.38	0.69	1.51	1.2	1.19
Tb	1.07	0.98	0.73	1.06	0.91	0.91
Pr	7.01	5.77	5.18	6.96	5.32	5.33
Dy	6.07	5.84	4.25	6.34	5.55	5.55
Th	2.29	1.97	2.77	2.33	1.86	1.82

Sample #	X16-10-94	X17-10-94	X18-10-94	X19-10-94	X12b
flow	III	III	III	III	IV
rock type	bas-and	bas-and	bas-and	bas-and	bas-and
		X-Ray Fluorescence Analysis, wt. %			
SiO_2	50.10	51.05	50.86	51.21	55.81
Al_2O_3	15.51	15.98	15.80	16.04	16.03
TiO_2	1.81	1.87	1.91	1.94	1.09
FeO	9.63	10.22	10.26	10.20	7.65
CaO	8.28	8.71	8.46	8.51	7.78
K_2O	1.10	1.12	1.15	1.18	1.20
MnO	0.16	0.15	0.15	0.15	0.13
P_2O_5	0.47	0.46	0.52	0.52	0.27
Na_2O	3.45	3.76	3.79	3.85	3.73
MgO	9.39	9.01	8.79	8.73	7.83
Total	99.89	102.34	101.69	102.32	101.52
		X-Ray Fluorescence Analysis, ppm			
Cr	300	282	287	263	213
Zr	225	222	230	235	172
Rb	19	15	15	16	19
Sr	558	511	513	498	517
Nb	17	17	17	18	10
Ni	135	154	135	145	152
Y	29	27	28	28	18
Ba	190	118	117	151	209
	Isotope values calculated from data obtained by Isotope Dilution Analyses				
ε Nd	4.92				
$^{87}Sr/^{86}Sr$	0.70352				
	Instrumental Neutron Activation Analysis, ppm; Inductively Coupled Plasma Mass Spectrometer, ppm				
La	19.8	20.3	22.0	23.1	19.5
Lu	0.4	0.4	0.4	0.4	0.3
Sm	6.0	6.1	6.4	6.7	5.2
U	0.7	0.6	0.7	0.7	0.9
Yb	2.45	2.43	2.53	2.70	1.96
Ce	41.7	41.9	46.1	48.3	39.7
Cs	0.25	0.41	0.38	0.55	0.8
Eu	1.95	2.02	2.08	2.14	1.62
Hf	4.34	4.31	4.6	4.75	3.49
Nd	23.54	23.66	25.3	26.81	21.73
Ta	1.23	1.19	1.28	1.37	0.69
Tb	0.92	0.9	0.98	1.03	0.75
Pr	5.3	5.31	5.75	6.06	5.07
Dy	5.53	5.58	5.86	5.99	4.28
Th	1.86	1.87	1.95	2.01	2.55

Appendix IV

Analytical Techniques: Data Precision and Accuracy

Analytical techniques are described in detail in Chapter 4. Presented here are tables reporting accurracy and precision for major and trace element analyses done by X-ray fluorescence, Instrumental Neutron Activation Analysis, and Inductively Coupled Plasma Mass Spectrometry.

Table 1. Calibration standards used for the Rigaku 3030 X-ray Fluorescence Spectrometer. Standards are from the United States Geological Survey except AL-1 which is a French standard (Govindaraju, 1994).

Major Elements	Trace Elements
SCO-1	G-2
STM-1	W-2
GSP-1	BIR-1
DNC-1	RGM-1
RGM-1	QLO-1
BHVO-1	BHVO-1
PCC-1	PCC-1
AGV-1	SCO-1
QLO-1	AGV-1
AL-1	DNC-1

Table 2. Accuracy for the Rigaku 3030 X-ray Fluorescence Spectrometer. Standard BIR-1 was used as a reference for major elements, Cr, and Ni, while MAG-1 was used for the remaining trace elements.

Element	%error
SiO2	0.23
Al2O3	0.51
TiO2	0.28
FeO	0.37
CaO	0.72
K2O	31.11
MnO	6.02
P2O5	62.83
Na2O	7.04
MgO	0.76
Cr	4.90
Ni	1.02
Zr	2.77
Rb	0.95
Sr	0.42
Nb	30.93
Y	6.09
Ba	5.25

Table 3. Precision for the Rigaku 3030 X-ray spectrometer for major and trace elements. Data is reported for ten replicate analyses using U.S.G.S. standards BIR-1 for major elements, Cr, and Ni, and MAG-1 for the remaining trace elements.

Element wt %	Published value	Mean of 10 replicate analyses	Standard deviation	Mean relative % error
SiO2	47.77	47.66	0.56	1.17
Al2O3	15.35	15.43	0.14	0.93
TiO2	0.96	0.96	0.03	2.91
FeO	11.26	11.30	0.33	2.93
CaO	13.24	13.34	0.21	1.55
K2O	0.027	0.04	0.00	11.62
MnO	0.171	0.16	0.00	3.09
P2O5	0.046	0.07	0.01	19.11
Na2O	1.75	1.87	0.11	5.83
MgO	9.68	9.61	0.20	2.09
Cr	382	400.73	17.70	4.42
Ni	166	167.70	7.55	4.50
Zr	126	129.49	2.09	1.61
Rb	149	147.58	3.78	2.56
Sr	146	146.62	1.24	0.85
Nb	12	15.71	0.97	6.20
Y	28	29.71	1.85	6.21
Ba	479	504.16	25.26	5.01

Table 4. Accuracy for INAA (instrumental neutron activation analyses). U.S.G.S. standard BHVO-1 was used as a reference.

Element	% error
Ba	0.72
La	0.63
Lu	30.00
Sm	4.35
Yb	10.40
Ce	1.03
Cr	1.38
Eu	4.37
Hf	6.85
Sc	2.83
Ta	0.81
Tb	5.21
Th	4.63

Table 5. Precision for INAA of trace elements. Data reported is from four replicate analysis of U.S.G.S standard BHVO-1.

Element ppm	Published value	Mean of 4 replicate analysis	Standard deviation	Mean relative % error
Ba	139	140	16.10	11.5
La	15.8	15.7	0.44	2.8
Lu	0.4	0.28	0.06	19.8
Sm	6.2	6.47	0.15	2.3
Yb	2.02	1.81	0.07	3.8
Ce	39	39.4	4.49	11.4
Cr	289	293	7.33	2.5
Eu	2.06	1.97	0.12	5.9
Hf	4.38	4.68	0.08	1.7
Sc	31.8	30.9	0.37	1.2
Ta	1.23	1.24	0.09	7.6
Tb	0.96	0.91	0.11	12.3
Th	1.08	1.13	0.18	16.3

Table 6. Accuracy for the Inductively Coupled Plasma Mass Spectrometer (ICP-MS). U.S.G.S standard BHVO-1 was used as a reference.

Element ppm	Published value	WSU ICP-MS value	% error
Ba	139	133	4.32
La	15.8	15.65	0.95
Ce	39	37.07	4.95
Sm	6.2	6.2	0
Eu	2.06	2.12	2.91
Tb	0.96	0.96	0
Yb	2.02	2.02	0
Lu	0.29	0.28	3.45
Hf	4.38	4.34	0.91
Ta	1.23	1.25	1.63
Th	1.08	1.25	15.74

Table 7. Precision for the (ICP-MS). Data reported is from twenty-four replicate analysis of Washington State in-house standards BCR-P.

Element ppm	Mean of 24 replicate analysis	Standard deviation	Mean relative % error
Ba	670	13	1.89
La	26.26	0.49	1.86
Ce	51.67	0.62	1.2
Sm	7.03	0.15	2.07
Eu	2.13	0.05	2.48
Tb	1.17	0.01	1.12
Yb	3.36	0.03	0.94
Lu	0.52	0.01	1.9
Hf	4.67	0.07	1.47
Ta	0.82	0.02	2.7
Th	5.13	0.49	9.5

References

Allan, J. F., 1981, The Colima graben, SW Mexico [abs.]: EOS (American Geophysical Union Transactions), v. 62, p. 1034.

Allan, J. F. and Carmichael, I. S. E., 1984, Lamprophyric lavas in the Colima graben, SW Mexico: Contributions to Mineralogy and Petrology, v. 88, p. 203-216.

Anderson, R. E., 1971, Thin skin distension in Tertiary rocks of southeastern Nevada: Geological Society of America Bulletin, v. 82, p. 43-58.

Anderson, R. E., 1973, Large-magnitude late Tertiary strike-slip faulting north of Lake Mead, Nevada: U.S. Geological Survey Professional Paper 794, 18 p.

Anderson, R.E., Barnhard, T.P., and Snee, L.W., 1994, Roles of plutonism, mid-crustal flow, tectonic rafting, and horizontal collapse in shaping the Miocene strain field of the Lake Mead area, Nevada and Arizona: Tectonics, v. 13, p. 1381-1410.

Bell, J.W., Smith, E.I., 1980, Geologic map of the Henderson Quadrangle, Nevada: Nevada Bureau of Mines and Geology Map 67.

Boggs Jr., S., 1987, Principles of Sedimentology and Stratigraphy, Merrill Publishing Company, Columbus, Ohio, 784 p.

Bradshaw, T. K., 1991, Tectonics and magmatism in the Basin and Range province of the western United States [Ph.D. thesis]: Milton Keynes, Open University, 240 p.

Bradshaw, T. K., Hawkesworth, C. J. and Gallagher, K., 1993, Basaltic volcanism in the Southern Basin and Range: no role for a mantle plume: Earth and Planetary Science Letters, v. 116, p. 45-62.

Bridwell, H. L., 1991, The Sloan Sag: A mid-Miocene volcanotectonic depression, north-central McCullough Mountains, southern Nevada [M.S. thesis]: Las Vegas, University of Nevada, 147 p.

Busby-Spera, C. J., 1988, Speculative tectonic model for the early Mesozoic arc of the southwest Cordilleran United States: Geology, v. 16, p. 1121-1125.

Carmichael, I. S. E., Turner, F. J. and Verhoogen, J., 1974, Igneous Petrology, New York, McGraw Hill Book Company, 739 p.

Cas, R. A. F.,. Wright., J.V., 1988, Volcanic Successions, Chapman and Hall, London, 528 p.

Cascadden, T., 1991, Style of volcanism and extensional tectonics in the eastern Basin and Range province, northern Mohave County, Arizona [M.S. thesis]: Las Vegas, University of Nevada, 156 p.

Chapin, C. E. and Glazner, A. F., 1983, Widespread K_2O metasomatism of Cenezoic volcanic and sedimentary rocks in the southwestern United States: Geological Society of America Abstracts with Programs, v. 15, p. 282.

DePaolo, D. J., 1981, Trace element and isotopic effect of combined wallrock assimilation and fractional crystallization: Earth and Planetary Science Letters, v. 53, p. 189-202.

Duebendorfer, E. M. and Christensen, C., 1995, Synkinematic (?) intrusion of the "anorogenic" 1425 Ma Beer Bottle Pass pluton, southern Nevada: Tectonics, v. 14, no.1, p. 168-184.

Duebendorfer, E. M., Sewall, A. J. and Smith, E. I., 1990, The Saddle Island detachment; An evolving shear zone in the Lake Mead area, Nevada *in* B. P. Wernicke eds., Basin and Range extensional tectonics near the latitude of Las Vegas, Nevada: Geological Society of America, Memoir 176, p. 77-97.

Duebendorfer, E. M. and Wallin, E. T., 1991, Basin development and syntectonic sedimentation associated with kinematically coupled strike-slip and detachment faulting, southern Nevada: Geology, v. 19, p. 87-90.

Falkner, C., 1993, History and Petrogenesis of the Aztec Wash Pluton, Eldorado Mountains, Nevada [M.S. thesis]: Nashville, Tennessee, Vanderbilt University, 204 p.

Farmer, G. L., Perry, F. V., Semkin, S., Crow, B., Curtis, D. and DePaolo, D. J., 1989, Isotopic evidence on the structure and origin of subcontinental lithospheric mantle in southern Nevada: Journal of Geophysical Research, v. 94, p. 7,885-7,898.

Faulds, J. E., Feuerbach, D. L., Reagan, M. K., Metcalf, R. V., Gans, P. and Walker, J. D., 1995, The Mt. Perkins Block, northwestern Arizona: An exposed cross section of an evolving, preextensional to synextensional magmatic system: Journal of Geophysical Research, v. 100, p. 15,249-15,266.

Faulds, J. E., Gans, B. and Smith, E. I., 1994, Spatial and temporal patterns of extension in the northern Colorado River extensional corridor, northwestern Arizona and southern Nevada: Geological Society of America Abstracts with Programs, v. 26, no.2, p. 51.

Faulds, J. E., Geissman, J. W. and Mawer, C. K., 1990, Structural development of a major extensional accommodation zone in the Basin and Range Province, northwestern Arizona and southern Nevada; Implications for kinematic models of continental extension *in* B. P. Wernicke ed., Basin and Range extensional tectonics near the latitude of Las Vegas, Nevada: Geological Society of America, Memoir 176, p. 37-76.

Feuerbach, D. L., Smith, E. I., Walker, J. D. and Tangeman, J. A., 1993, The role of the mantle during crustal extension: Constraints from geochemistry of volcanic rocks in the Lake Mead area, Nevada and Arizona: Geological Society of America Bulletin, v. 105, p. 1561-1575.

Fitton, J. F., James, D. and Leeman, W. P., 1991, Basic magmatism associated with Late Cenozoic extension in the Western United States: Compositional variations in space and time: Journal of Geophysical Research, v. 96, p. 13,693-13,711.

Gallagher, K. and Hawkesworth, C. J., 1992, Dehydration melting and the generation of continental flood basalts: Nature, v. 358, p. 57-59.

Gans, P. B., Mahood, G. A. and Schermer, E., 1989, Synextensional magmatism in the Basin and Range Province: A case study from the eastern Great Basin, Geological Society of America Special Paper 233, p. 53.

Gill, J., 1981, Orogenic andesites and plate tectonics, Springer-Verlag, Berlin-Heidelberg, 390 p.

Glazner, A. F., 1990, Recycling of continental crust in Miocene volcanic rocks from the Mojave block, southern California *in* J. L. Anderson ed., The nature and origin of Cordilleran magmatism: Geological Society of America Memoir 174, p. 147-168.

Green, D. H., Edgan, H. D., Beasley, P., Kiss, E. and Ware, N. G., 1974, Upper mantle source for some hawaiites, mugaerites and benmorites: Contributions to Mineralogy and Petrology, v. 48, p. 33-43.

Grove, T. L. and Kinzler, R. J., 1986, Petrogenesis of andesites: Annual reviews, Earth and Planetary Science, v. 14, p. 417-454.

Hawkesworth, C., Bradshaw, T., Gallagher, K., Hunter, A., Rogers, N. and Turner, S., 1994, Calk-alkaline magmatism and extension in the Basin and Range: Journal of Geophysical Research, v. 100, no.B7, p. 10,271-10,286.

Hewett, D. F., 1956, Geology and mineral resources of the Ivanpah Quadrangle, California and Nevada: U.S. Geological Survey Professional Paper 275, p. 172.

Howard, K. A. and John, B. E., 1987, Crustal extension along a rooted system of imbricate low-angle faults: Colorado River extension corridor, California and Arizona *in* M. P. Coward, J. F. Dewey and P. L. Hancock eds., Continental Extensional Tectonics: Geological Society of London Special Publication 28, p. 299-311.

Hughes, S. S., 1990, Mafic magmatism and associated tectonism of the central high Cascade Range, Oregon: Journal of Geophysical Research, v. 95, p. 19,623-19,638.

Kay, S. M., Ramos, V. A. and Marquez, M., 1993, Evidence for Cerro Pampa volcanic rocks for slab-melting prior to ridge-trench collision in southern South America: Journal of Geology, v. 101, p. 703-714.

Kempton, P. D., Fitton, J. G., Hawkesworth, C. J. and Ormerod, D. S., 1991, Isotopic and trace element constraints on the composition and evolution of the lithosphere beneath the Southwestern United States: Journal of Geophysical Research, v. 96, no. B8, p. 13,713-13,735.

Koyaguchi , T., 1986, Textural and compositional evidence for magma mixing and its mechanism, Abu volcanic group, Southwestern Japan: Contributions to Mineralogy and Petrology, v. 93, p. 33-45.

Lange, R. A. and Carmichael, I. S. E., 1991, A potassic volcanic front in western Mexico: The lamprophyric and related lavas of San Sebastian: Geological Society of American Bulletin, v. 103, p. 928-940.

Larsen, L. L. and Smith, E. I., 1990, Mafic enclaves in the Wilson Ridge pluton, Northwestern Arizona: Implications for the generation of a calc-alkaline intermediate pluton in an extensional environment: Journal of Geophysical Research, v. 95, p. 17,693-17,716.

Leeman, W. P. and Harry, D. L., 1993, A binary source model for extension-related magmatism in the Great Basin, western North America: Science, v. 262, p. 1550-1554.

Longwell, C. R., 1974, Measure and date of movement on Las Vegas Valley shear zone, Clark County, Nevada: Geological Society of America Bulletin, v. 85, p. 985-990.

Longwell, C. R., Pampeyan, E. H., Bowyer, B. and Roberts, R. J., 1965, Geology and Mineral Deposits of Clark County, Nevada, Nevada Bureau of Mines and Geology Bulletin 62, 218 p.

Luhr, J. F. and Carmichael, I. S. E., 1985, Jorullo volcano, Michoacan, Mexico (1759-1774): The earliest stages of fractionation in calc-alkaline magmas: Contributions to Mineralogy and Petrology, v. 90, p. 142-161.

Luhr, J. F., Nelson, S. A., Allan, J. F. and Carmichael, I. S. E., 1985, Active rifting in southwestern Mexico: Manifestations of an incipient eastward spreading ridge jump: Geology, v. 13, p. 54-57.

McMillan, N. J. and Dungan, M. A., 1986, Magma mixing as a petrogenetic process in the development of the Taos Plateau Volcanic Field, New Mexico: Journal of Geophysical Research, v. 91, p. 6,029-6,045.

Menzies, M. A., 1989, Cratonic, circum-cratonic and oceanic mantle domains beneath the western United States: Journal of Geophysical Research, v. 94, p. 7,899-7,915.

Metcalf, R. V., Smith, E. I., Martin, M. W., Gonzales, D. A. and Walker, J. D., 1993a, Isotopic evidence of source variations in commingled magma systems: Colorado River extensional corridor: Geological Society of America Abstracts with Programs, v. 25, p. 120.

Metcalf, R. V., Smith, E. I. and Mills, J. G., 1993b, Magma mixing and commingling in the Northern Colorado River Extensional Corridor; Constraints on the production of intermediate magma - Part I *in* M. M. Lahren Trexler, J.H., and Spinoza, C. eds., Crustal evolution of the Great Basin and Sierra Nevada: Cordilleran/Rocky Mountain Section, Geological Society of America Guidebook: Department of Geological Sciences, University of Nevada, Reno p. 35-55.

Metcalf, R. V., Smith, E. I., Walker, D. J., Reed, R. C. and Gonzales, D. A., 1995, Isotopic disequilibrium among commingled hybrid magmas: evidence for a two-stage magma mixing-commingling process in the Mt. Perkins Pluton, Arizona: Journal of Geology, v. 103, p. 509-527.

Mills, J. G., 1985, The geology and geochemistry of volcanic and plutonic rocks in the Hoover Dam 7.5 minute quadrangle, Clark County, Nevada and Mohave County, Arizona [M.S. thesis]: University of Nevada, Las Vegas, 119 p.

Nielson, J. E. and Nakata, J. K., 1993, Tertiary stratigraphy and structure of the Piute Range, California and Nevada *in* D. R. Sherrod and J. E. Nielson eds., Tertiary stratigraphy of highly extended terranes, California, Arizona, and Nevada: U.S. Geological Survey Bulletin 2053, p. 51-53.

Noorish, K. and Hutton, J. T., 1969, An accurate X-ray spectrographic method for the analysis of a wide range of geological samples: Geochimica et Cosmochimica Acta, v. 33, p. 431-453.

O'Hara, M. J., 1977, Geochemical evolution during fractional crystallization of a periodically refilled magma chamber: Nature, v. 266, p. 503-507.

Olsen, E. L. and Faulds, J. E., 1995, Geometry and kinematics of an extensional anticline, Highland Spring Range, southern Nevada: Geological Society of America Abstracts with Programs, Annual Meeting, p. 385.

Perry, F. V., Baldridge, W. S. and DePaolo, D. J., 1987, Role of asthenosphere and lithosphere in the genesis of late Cenozoic basaltic rocks from the Rio

Grande Rift and adjacent regions of the southwestern United States: Journal of Geophysical Research, v. 92, No. B9, p. 9193-9213.

Purkey, B. W., Duebendorfer, E. M., Smith, E. I., Price, J. G. and Castor, S. B., 1994, Geologic Tours in the Las Vegas Area: Nevada Bureau of Mines in Geology Special Publication 16, 156 p.

Reagan, M. K., Gill, J. B., Malavassi, E. and Garcia, M. O., 1987, Changes in magma composition at Arenal volcano, Costa Rica, 1968-1985: Real-time monitoring of open-system differentiation: Bulletin of Volcanology, v. 49, p. 415-434.

Schmidt, C. S., 1987, A mid-Miocene caldera in the central McCullough Mountains, Clark County, Nevada [M.S thesis]: University of Nevada, Las Vegas, 78 p.

Severinghaus, J. and Atwater, T., 1990, Cenozoic geometry and thermal state of the subducting slabs beneath western North America *in* B. P. Wernicke eds., Basin and Range extensional tectonics near the latitude of Las Vegas, Nevada: Geological Society of America Memoir 176, p. 1-22.

Sheridan, M. F. and Macias, J. L., 1992, Colima workshop of volcanic risk: Field guide to Colima Volcano: Universidad de Colima (informal publication, Colima, Mexico).

Smith, E. I., 1982, Geology and geochemistry of the volcanic rocks in the River Mountains, Clark County, Nevada, and comparisons with volcanic rocks in nearby areas *in* E. G. Frost and D. L. Martin eds., Cenozoic tectonic evolution of the Colorado River region, California, Arizona, Nevada: Cordillleran Publishers, p. 41-54.

Smith, E. I., 1986, Geology of the River, Eldorado, and McCullough Ranges, Clark County, Nevada *in* Field trip guide to the geology of southern Nevada: National Association of Geology Teachers, Far West Section meeting, October 3-5, 1986, Las Vegas, Nevada, p. 22-64.

Smith, E. I., Bridwell, H., Schmidt, C., Switzer, T. T. and the UNLV Winter Field Class, 1993, Late Miocene intermediate to felsic volcanism in the McCullough Range, southern Nevada [abs.]: Journal of the Arizona-Nevada Academy of Science, 37th Annual Meeting, University of Nevada, Las Vegas, v. 28, p. 45.

Smith, E. I. and Faulds, J. E., 1994, Patterns of Miocene magmatism in the northern Colorado River extension corridor, Nevada, Arizona, and California: Geological Society of America Abstracts with Programs, v. 26, no.2, p. 93.

Smith, E. I., Feuerbach, D. L., Naumann, T. R. and Mills, J. G., 1990, Mid-Miocene volcanic and plutonic rocks in the Lake Mead area of Nevada and Arizona; Production of intermediate igneous rocks in an extensional environment *in* J. L. Anderson ed., The nature and origin of Cordilleran magmatism: Geological Society of America Memoir 174, p. 169-194.

Smith, E. I., Schmidt, C. S. and Mills, J. G., 1988, Mid-Tertiary volcanoes in the Lake Mead area of southern Nevada and northwestern Arizona *in* D. L. Weide and M. L. Faber eds., This extended land, geological journeys in the southern basin and range: Geological Society of America, Cordilleran section, field trip guidebook, p. 107-122.

Sun, S. S. and McDonough, W. F., 1989, Chemical and isotopic systematics of oceanic basalts: implications for mantle composition and processes *in* Saunders, A.D., and Norry, M.J. eds., Magmatism in the Ocean Basins: Geological Society Special Publication no. 42, p. 313-345.

Thompson, K. G., 1985, Stratigraphy and petrology of the Hamblin-Cleopatra volcano, Clark County, Nevada [Unpubl. M.A. thesis]: The University of Texas at Austin, 306 p

Varga, R. J. and Faulds, J. E., 1995, Grasshopper Junction anticline: an interference segment within the Black Mountains Accommodation Zone, NW, Arizona and S. Nevada: Geological Society of America Abstracts with Programs, Annual Meeting, p. 385.

Villemant, B., Jaffrezic, H., Joron, J.L., and Treuil, M., 1981, Distribution coefficients of major and trace elements; fractional crystallization in the alkali basalt series of Chaine Des Puis (Massif Central, France): Geochemica Cosmochemica Acta, v. 45, p. 1997-2016.

Walker, J. D., Beaufait, M. S. and Zelt, F. B., 1981, Geology of the Devil Peak area, Spring Mountains, Nevada: Geological Society of America Abstracts With Programs, Cordilleran Section, v. 13, p. 112.

Wallace, P., Carmichael, I. S. E., Righter, K. and Becker, T. A., 1992, Volcanism and tectonism in western Mexico: A contrast of style and substance: Geology, v. 20, p. 625-628.

Weber, M. E. and Smith, E. I., 1987, Structural and geochemical constraints on the reassembly of disrupted mid-Miocene volcanoes in the Lake Mead-Eldorado Valley area of southern Nevada: Geology, v. 15, p. 553-556.

Wernicke, B., Axen, G. J. and Snow, J. K., 1988, Basin and Range extensional tectonics at the latitute of Las Vegas, Nevada: Geological Society of America Bulletin, v. 100, p. 1738-1757.

Wilson, M., 1989, Igneous Petrogenesis: A Global Tectonic Approach: London, United Kingdom, Chapman and Hall, 465 p.

Yogodzinski, G. M., Volynets, O. N., Koloskov, A. V., Seliverstov, N. I. and Matvenkov, V. V., 1994, Magnesian andesites and the subduction component in a strongly calc-alkaline series at Piip Volcano, Far Western Aleutians: Journal of Petrology, v. 35, p. 163-204.